INVESTIGATION OF A MULTIPHASE TWIN-SCREW PUMP OPERATING AT HIGH GAS VOLUME FRACTIONS

A Thesis

by

RYAN DANIEL KROUPA

Submitted to the Office of Graduate Studies of
Texas A&M University
in partial fulfillment of the requirements for the degree of

MASTER OF SCIENCE

May 2011

Major Subject: Mechanical Engineering

INVESTIGATION OF A MULTIPHASE TWIN-SCREW PUMP OPERATING AT HIGH GAS VOLUME FRACTIONS

A Thesis

by

RYAN DANIEL KROUPA

Submitted to the Office of Graduate Studies of
Texas A&M University
in partial fulfillment of the requirements for the degree of

MASTER OF SCIENCE

Approved by:

Chair of Committee, Gerald Morrison
Committee Members, Timothy Jacobs
Robert Randall
Head of Department, Dennis O'Neal

May 2011

Major Subject: Mechanical Engineering

ABSTRACT

Investigation of a Multiphase Twin-screw Pump
Operating at High Gas Volume Fractions. (May 2011)
Ryan Daniel Kroupa, B.S., University of Wisconsin – Milwaukee
Chair of Advisory Committee: Dr. Gerald Morrison

The use of twin-screw pumps for moving fluids is not new technology but its application to wet gas compression (high gas volume fraction [GVF]) is still considered relatively new. There are many advantages for using twin-screw pumps for oil field applications; three of the immediate improvements include reducing hardware costs, reducing well bore pressure, and producing a pressure boost to move the product to a central collection facility.

While there are many advantages to using twin-screw pumps in wet gas applications, there are some problems that have been encountered while operating at high GVFs. When operating at high GVF, over 95% twin-screw pumps experience a severe loss of efficiency and an increase of operating temperature. A common way to increase the efficiency while operating in the high GVF range includes adding a liquid recirculation system where a portion of liquid is stored downstream of the pump and is injected into the pump inlet. These systems lower the effective GVF of the multiphase fluid below 95% in order to increase the pump efficiency.

The first objective is to characterize the performance of a twin-screw pump fitted with a liquid recirculation system while operating under high GVF conditions. The second objective is to investigate the transient heat rise associated with high GVF operation.

While traditional twin-screw pumps can be fitted with a liquid recirculation system to allow them to operate under high GVF conditions the pumps themselves are not optimized for wet gas compression and still suffer performance penalties. The results of this investigation show that the liquid recirculation system can allow the pump to operate under high GVF but the heat added to the system reduces the systems efficiency. Without a method of removing the heat generated in the pumping process the pump will not run at its optimal efficiency. The following investigation provides recommendations for further research in area of multiphase pumping using twin-screw pumps based on the characterization and transient studies provided in this thesis.

ACKNOWLEDGEMENTS

I would like to express my sincere gratitude to Dr. Gerald Morrison for his valuable guidance and for making this work possible. I would also like to thank Dr. Timothy Jacobs and Dr. Robert Randall for being on my committee. My thanks also goes to Mr. Eddie Denk and Mr. Ray Matthews for assisting me with guidance for the fabrication and assembly of the laboratory set-up. I also thank my friends and colleagues at the turbomachinery lab that have helped me throughout the project including Shankar Narayanan, Abhay Patil, and Becky Hollkamp for all of their hard work and knowledge. I would also like to offer a special thank you for Dr. Stuart Scott and Dr. Jun Xu at Shell for making this research possible.

NOMENCLATURE

A =	cross-sectional area of volume created by screw
B =	outer screw diameter
BPD =	barrels of oil per day
c =	average clearance
c_c =	circumferential clearance
C_{eff} =	effective clearance
c_f =	flank clearance
c_g =	constant volume specific heat of air
c_l =	constant volume specific heat of water
CFD =	computational fluid dynamics
CJC =	cold Junction Compensation
f_c =	correction factor
GPM =	gallons per minute
GVF =	gas volume fraction
GVF_{eff} =	effective gas volume fraction including the seal flush fluid
H =	distance between screw centerlines
HP_{drive} =	horsepower from electric motor
HP_{gas} =	horsepower required to move gas
$HP_{leakage}$ =	horsepower lost in “re-pumping” slip
HP_{liq} =	horsepower required to move gas
HP_{net} =	horsepower required to move multiphase fluid
$HP_{friction}$ =	horsepower lost to friction
HP_{VFD} =	horsepower recorded from the VFD, also known as the load
L =	screw length
l_h =	helical arc that describes the circumferential gap
$\dot{m}_{flush}$=	mass flow rate of seal flush liquid

$\dot{m}_g$ = mass flow rate of the gas

$\dot{m}_l$ = mass flow rate of liquid

MPP = multiphase pump

n = pump speed

P_{exh} = pump exhaust pressure

P_{in} = pump inlet pressure

PC = personal computer

PID = proportional integral derivative control algorithm

Q = total volumetric flow rate of the fluid entering the pump

Q_{air} = volumetric flow rate of the air at the pump suction

Q_{flush} = volumetric flow rate of seal flush fluid

Q_{liq} = volumetric flow rate of the liquid at the pump suction

Q_{th} = maximum Theoretical Flow Rate

Q_{slip} = slip flow rate

$Q_{slip,cir}$ = slip flow in circumferential gap

$Q_{slip,flank}$ = slip flow in flank gap

$\dot{Q}_{flush}$= heat transfer of seal flush fluid

$\dot{Q}_{HC}$ = heat transfer of gas heat of compression

$\dot{Q}_{loss}$ = heat lost during the pumping process

R_c = clearance Radius

ROV = robotically operated vehicle

RPM = revolutions per minute

s = screw lead

T_{exh} = pump exhaust temperature

T_{flush} = seal flush fluid temperature

V_g = pump displacement per revolution

$\dot{W}_{electric}$ = electrical power delivered to the motor

$\dot{W}_{fluid}$= power required to move the fluid

X = empirical pump factor

α = angle of overlap between screws

ΔP = differential pressure across pump

ΔT = differential temperature across pump

ρ = fluid density

κ = heat capacity ratio of air

$\eta_{calc,VFD}$ = mechanical efficiency calculated using calculated horse power

$\eta_{mech,VFD}$ = mechanical efficiency calculated using actual horsepower from the VFD

η_{vol} = volumetric efficiency

μ = viscosity

TABLE OF CONTENTS

Page

Page

LIST OF FIGURES

Page

Page

Page

Page

LIST OF TABLES

Page

1. INTRODUCTION

Within recent history the demand for energy is experiencing accelerated growth as much of the recoverable oil and gas fields are past their optimal production capacity. Multiphase pumps can answer this call for technology. These systems add pressure to multiphase flow and have the capability to handle wet gas compression (high GVF). While there are many advantages for using a positive displacement pump for oil field applications, three of the immediate improvements include saving time and money by reducing hardware, reducing well bore pressure thus increasing production, and producing a boost to move the product from the wells to a central collection facility. Installing one pump that replaces a separator, gas compressor, and a separate liquid pump significantly reduces the overall capital, physical space, and installation time. Key development issues for MPP include large differential pressures up to 200 bar (for subsea application), broad range of GVF running conditions over the life of an oil field, operation flexibility more important than efficiency, modular designs, innovations to existing implementations, and cheaper more simple design options. MPPs are a proven technology and subsea processing is an expanding business that will focus on the optimization of systems rather than equipment [1].

1.1 General Uses for Multiphase Pumps

The use of positive displacement pumps for moving fluids is not new technology but it is still considered relatively new. The origins of multiphase pumping began in 1957 in the oil and gas literature and for some 30 years the research about the technology was put aside due to “unsolvable tasks” at the time. The late 1980’s saw a resurgence of the multiphase research led by Bornemann Pumps with the Poseidon project. The philosophy behind the project developed with the possibility to boost well production

---

This thesis follows the style of ASME Journal of Turbomachinery.

directly from the subsea well and transfer the product to a processing center many miles away. In 1990 the installation and field trials of the Poseidon project began. Over the two year trial period two major phenomena were observed. Prolonged gas phases with Gas Volume Fractions (GVF) between 90% and 100% occurred frequently leading to excessive heat generation that could render the pump inoperable and if not closely monitored, the possibility of catastrophic damage. Along with the prolonged dry running, the mechanical seals in the early application were exposed to the inlet of the pump and experienced large temperature shocks due to the variation of GVFs that would lead to premature wear or failure of the seals [2].

In the early stages the developmental costs outweighed the benefits of multiphase pumps. The oil fields of the world were booming and while conservation and efficiency were still paramount, the cost of developing the multiphase technology was not considered a viable option until recently. During the current scenario it is becoming more important to increase the productivity of old wells and to reduce the costs of the current operations. A traditional oil field application, whether on or off shore, consists of a gas separator, gas compressor, fluid pump, gas production line, liquid production line, and a particulate handling system. The reduction of equipment and thus capital costs can be obtained by simply using a single MPP along with a single gas/liquid production line that is capable of transporting the multiphase fluid. The proposed multiphase systems reduce system complication and capital costs, require less equipment, reduce footprint on the oil rig, and offer a complete system consisting of a single pumping facility with a single production line.

The MPPs are also easily adaptable to subsea applications that would allow the installation of a MPP without a full oil rig construction. This simplified process could open up many more possibilities for open new wells that were otherwise less accessible to the traditional oil rig facilities.

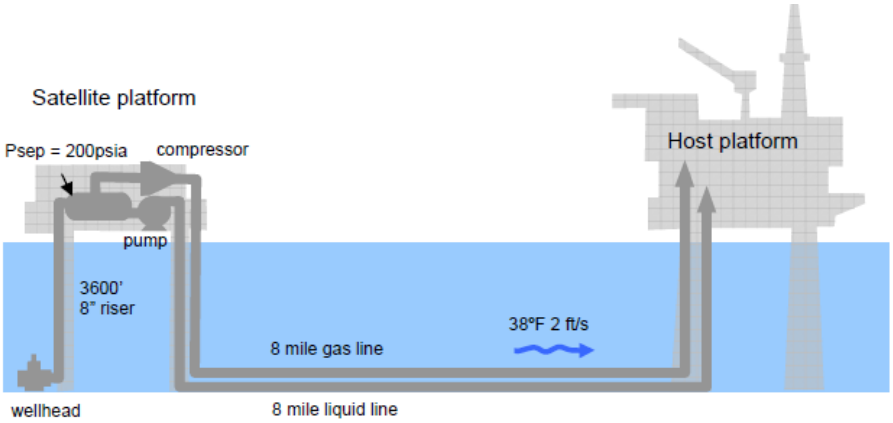

Figure 1.1 System Diagram of a Typical Installation (Shippen 2002)

As Figure 1.1 shows in the typical installation for harvesting oil/natural gas from an oil field. The satellite platform would be installed with a connection to the host platform. Whether the pumping station was placed on the host platform or the satellite platform, a significant footprint is required and more infrastructure is needed to support the equipment. The required separator, gas compressor, and liquid pump takes up considerably more space than a single MPP. The high cost of the current systems makes it impossible to access some wells due to relatively low productivity or remoteness of the well including ultra-deep sea wells. Figure 1.2 shows the MPP placement on the sea floor as opposed to the traditional oil rig set up [3].

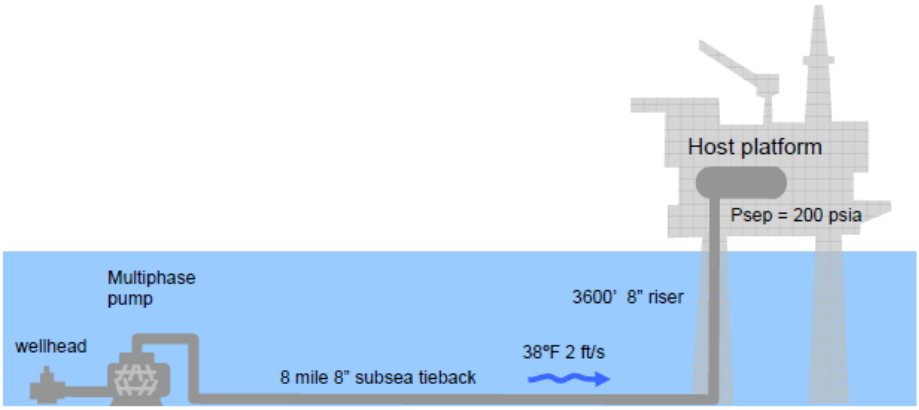

Figure 1.2 System Diagram Utilizing a MPP (Shippen 2002)

With the MPP technology, it would make smaller, less productive, and extremely remote wells accessible where they were previously unavailable due to the high cost of a fully equipped oil rig. Placing a MPP on the seafloor directly on the wellhead frees up space on future oil rigs and can access a network of pipelines. Without the need for extra platforms, including satellite platforms, wells that would not have met the production minimum for a full on traditional oil rig can be economically utilized. The worldwide oil economy has reached a time when these untouched oil pockets cannot afford to be left unused.

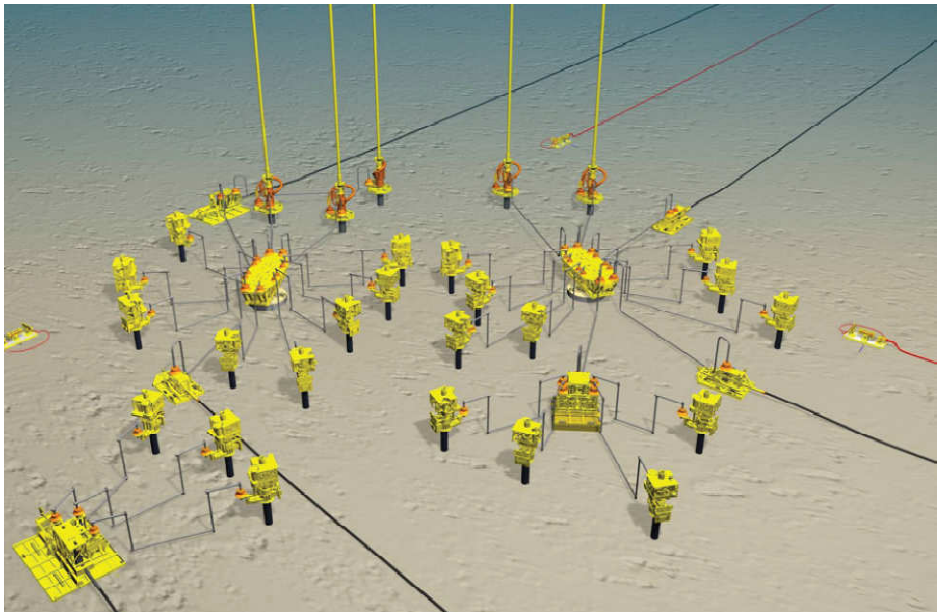

Figure 1.3 Subsea Oil Field (FMC Technologies 2007)

Figure 1.3 is a digital rendering of a current development by FMC Technology for Shell [4]. The use of subsea MPP allows many wells to be accessed with central pumping stations boosting the harvested fluid to central processing centers. The use of these subsea networks is an easy way to tap into the lesser producing wells without the need for a full oil rig installation which significantly reduces costs and access to product that was previously not available.

While the technology exists to implement such a system, the robustness and reliability still needs to be improved before widespread use of such a system is feasible. While topside applications have been installed and utilized across the world, the maintenance required would be too much of a risk for immediate subsea deployment. A failure on land would result with the pump not running for a period of time while a technician was deployed to make the required repairs. The same type of failure on a subsea application would require an array of ROVs being deployed to the bottom of the ocean to service the downed pump. The significantly higher maintenance cost for the subsea

applications is a clear driver for the continued research of the technology. The current issues that are being investigated need to be resolved before any robust solution can be implemented.

1.2 Multiphase Pump Implementation

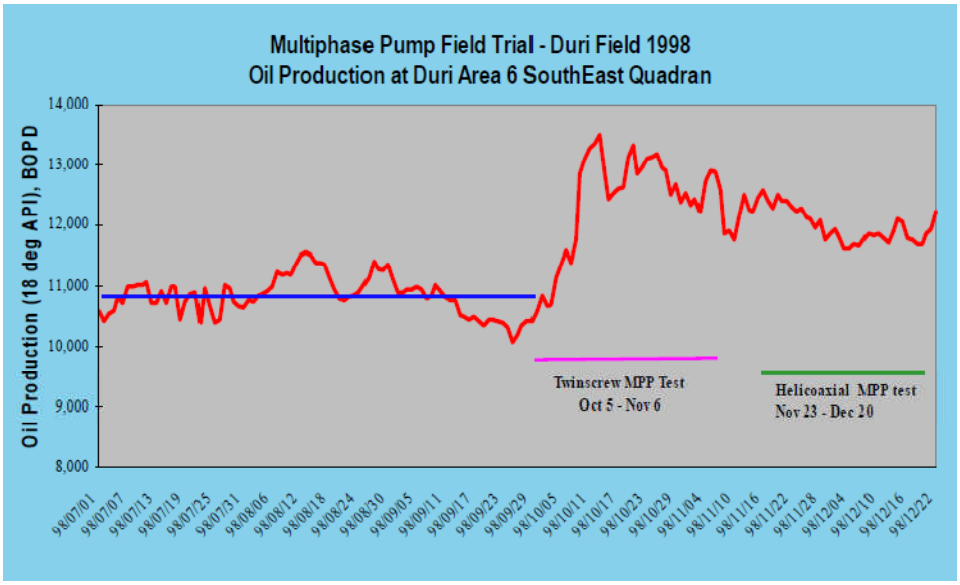

Figure 1.4 Results of Multiphase Boosting (Heyl 2008)

The productivity gained by using multiphase pumps is illustrated in Figure 1.4 where the red line represents the production. In the above figure the red line represents the production of oil from a MPP field test. This study performed in 1998 shows a constant production of nearly 11,000 BPD until the installation of a twin-screw MPP. At that point the production increased to just over ~12,000 BPD with a spike at 13,000+ BPD. A second MPP was then tested and similar results can be seen over the implemented time period. These results are consistent with many other field tests administered around the world.

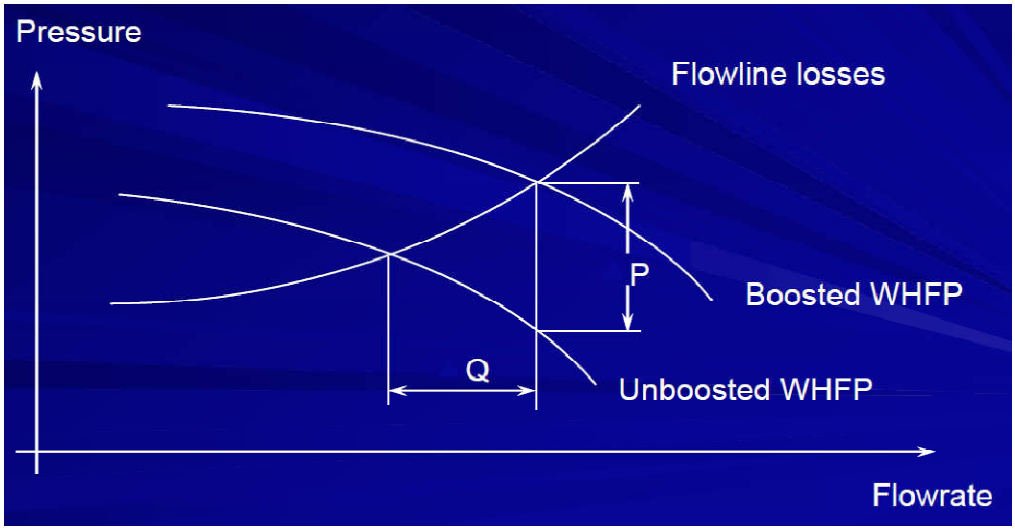

Figure 1.5 Multiphase Boosting (Heyl 2008)

The main advantage of the twin-screw positive displacement pump in well production is the reduced backpressure at the wellhead, which increases the production at the wellhead. Figure 1.5 shows what happens when a MPP is installed at the wellhead of an oil well. The increase in pressure corresponds to the increase of flow in the pipeline. The more volume that is extracted, the higher the back pressure is on the pump. The advantage of the positive displacement pumps is that no matter what the pressure differential of the flow going through them equals the void space of the pump times the speed at which the pump is spinning. This will be described more in-depth in the following section [5].

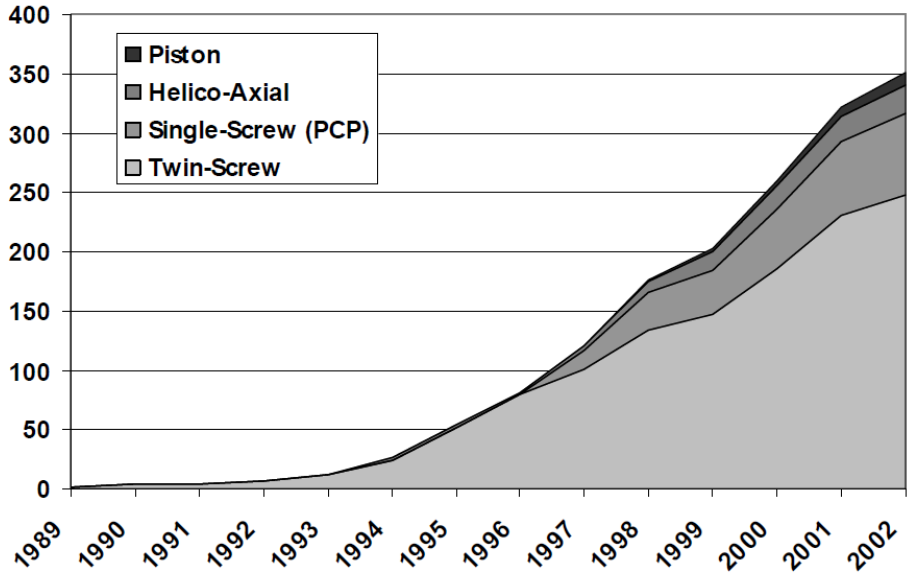

Figure 1.6 Worldwide Usage of MPP (Scott 2002)

Figure 1.6 shows the installations of MPPs around the world. As of 2002, the dominant pump used is the twin-screw. Currently there are 500+ installations of MPPs and after two decades of field testing the technology has been proven to be successful. There is a significant need for more information regarding the performance of these pumps to supply the worldwide demand for this technology.

1.3 Multiphase Fluids

Before understanding how a MMP works, it should be understood what is meant by a multiphase fluid. A multiphase fluid can be any mixture of gas, liquid, or solid particulate. In the simplest case the fluid flow is comprised of only a gas or only a liquid, this is considered single phase flow. Within the oil pipeline the multiphase mixture could contain substances such as crude oil, gas, water, natural gas hydrates, wax, and sand.

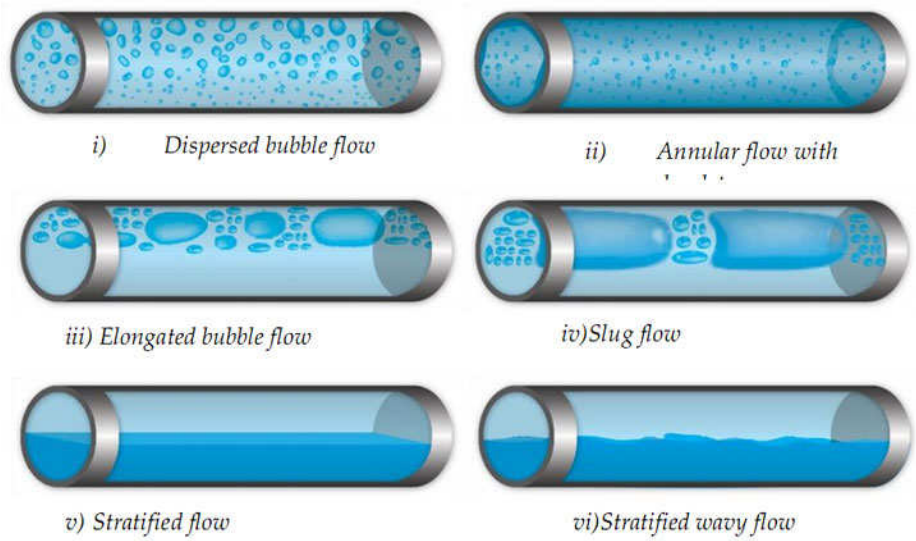

Figure 1.7 Possible Flow Regimes for Mixed Fluid Flow (Bratland 2010)

There are also many flow regimes as can be seen in Figure 1.7 that can be observed in multiphase fluids. The parameters that determine the flow regime depend on the GVF and the relative velocities of the respective single phase fluids. In the current investigation it will be impossible to observe the flow regime or the pump inlet conditions directly since it will not be possible to insert sight glasses into the pump assembly; therefore, only a topical understanding of these flow regimes is required [6].

1.4 Twin-screw Pumps

The twin-screw pump is a unique type of positive displacement pump, shown in Figure 1.8, where the flow along the pump profile is truly axial. The fluid moves along the screw profile while the screw is spinning. In theory as the fluid enters the pump, it splits and equally travels down the axial direction. This action equalizes the forces acting on the screws because the fluid is traveling equally and opposite directions. This also means that the addition of a thrust bearing to counter the axial forces is not explicitly necessary but is included to help dissipate any disturbances in the flow.

Twin-screw pumps have been used in many industrial applications including the petroleum, crude oil, hydraulics, chemical plants, and now multiphase fluid transport. The screw pumps were originally developed for high viscosity fluids from molasses to gasoline, but recently the technology has opened the doors for a wide range of applications within the petroleum industry.

Screw pumps, like other rotary positive displacement pumps, are self-priming and have a delivery flow characteristic that is independent of the differential pressure across the pump. The operation of the pump depends on the intermeshing of the two screws. As the screws rotate they create sets of moving sealed cavities in series between the pump inlet and outlet [7].

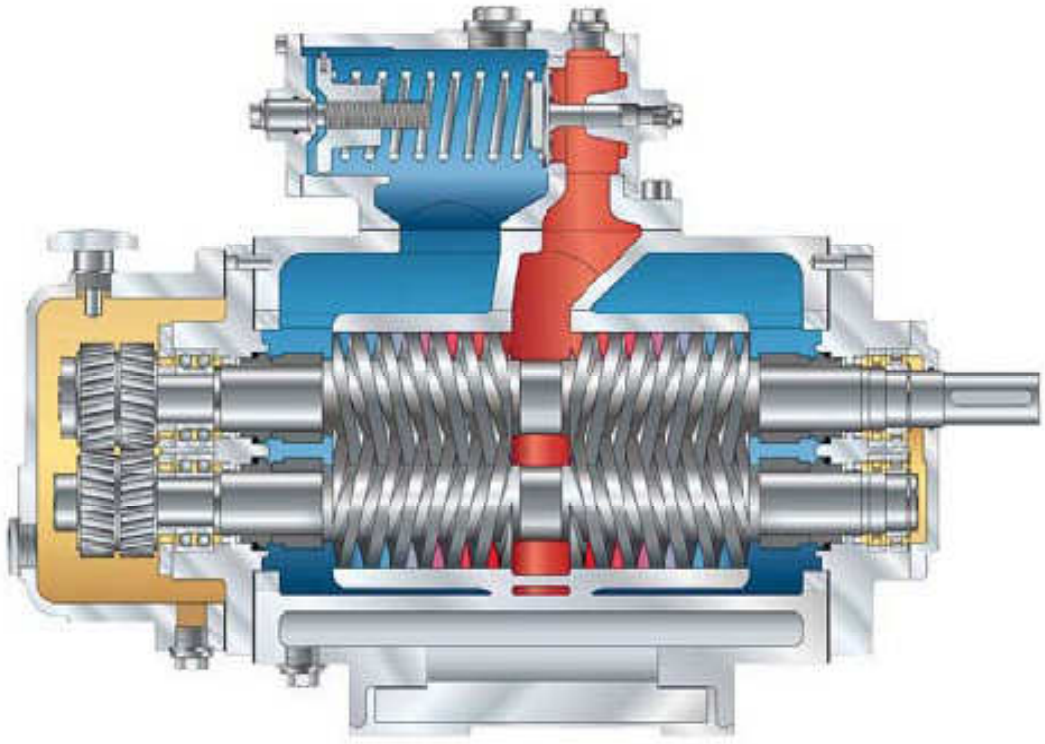

Figure 1.8 Sectional Drawing of a Twin Screw Pump (Leistritz Corp. 2010)

Figure 1.8 shows a cross-section of a typical twin-screw pump courtesy of Leistritz Corp. [8]. The pump suction where the fluid is introduced to the screws is in blue. The pump exit where the fluid is moved is in red. The exit of the pump is normally at a higher pressure relative to the inlet. Because of the unique operation of the pump, the fluid is moved from the low pressure inlet to the high pressure exit. The blue/red area between the inlet/exit shows where the fluid is undergoes a pressure increase. The area in yellow shows the gears and gear lubrication. The first screw is connected to the motor while the second is connected by the gears on the opposite side of the pump [7].

Figures 1.9, 1.10, and 1.11 show the basic geometries for the twin-screw pump that allows the positive displacement action to take place.

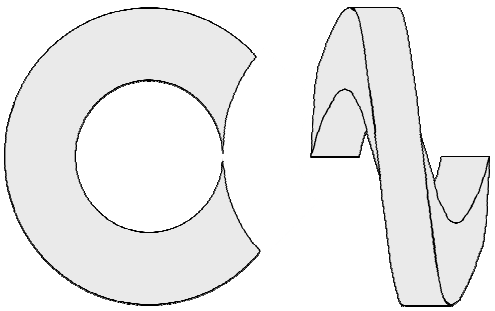

Figure 1.9 Fluid Volume Created by Screws

The sealed cavities created by the water sealing the clearances between the screws take the shape depicted in Figure 1.9. These cavities move axially as the screws turn, creating a low velocity, low shearing fluid movement compared to a centrifugal pump.

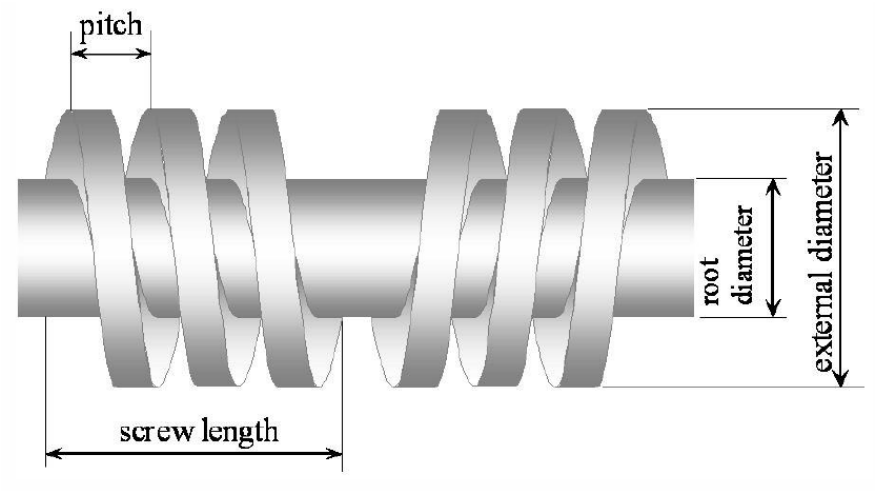

Figure 1.10 Important Screw Dimensions

Figure 1.10 shows the most important dimensions for the screw profile. These dimensions make up the necessary information to calculate the theoretical pump displacement. Knowing these dimensions, the following equations can be simply derived to describe the basic function of any positive displacement pump where V_g is the displacement of the pump for one single revolution of the screw. V_g is dependent solely on the geometry of the pump where *s* is the screw lead and *A* is the cross-sectional area of volume created by the screw, which varies with the screw diameters and length. The volume per revolution is

$$\mathrm{V_g} = \mathrm{A} * \mathrm{s}$$

Once the displacement is found multiplying by the rotational speed *n* gives the theoretical flow rate

$$\mathrm{Q_{th}} = \mathrm{V_g} * \mathrm{n}$$

The actual flow rate, *Q*, differs from the theoretical by the amount of "slip" the pump has. The screws are machined so that there is no contact between the screws and the housing. Therefore, a leak path between the series of cavities exists. This leakage

through the cavities is defined as the slip. The slip is dependent on the pressure differential across the pump that works against the fluid movement. The total flow through the pump is

$$Q = Q_{th} - Q_{slip}$$

Putting the actual flow over the theoretical flow will then give the volumetric efficiency

$$\eta_{Vol} = \frac{Q}{Q_{th}} = \frac{Q_{th} - Q_{slip}}{Q_{th}}$$

While there are more advanced models that will be described in the following sections, these basic equations provide a baseline understanding of pump performance from a volumetric standpoint.

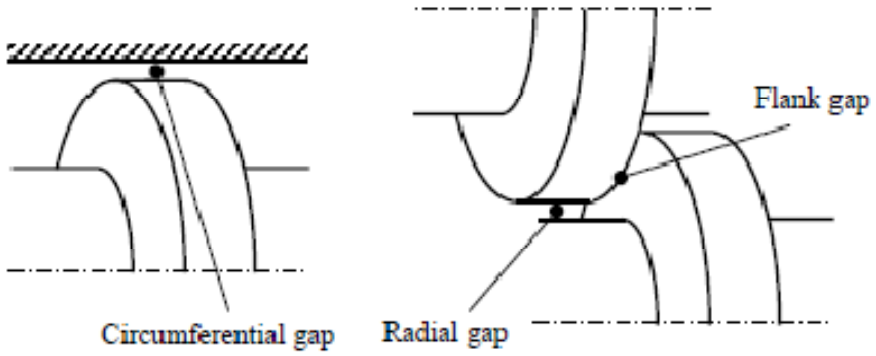

Figure 1.11 Twin Screw Internal Clearances

The different gaps between the screws and the chambers that transport the fluid can be seen in Figure 1.11. These clearances contribute to the slip rate. The slip as previously mentioned reduces the actual flow of the pump. The slip flow moves in the opposite direction of the fluid moved by the screws as seen in Figure 1.12.

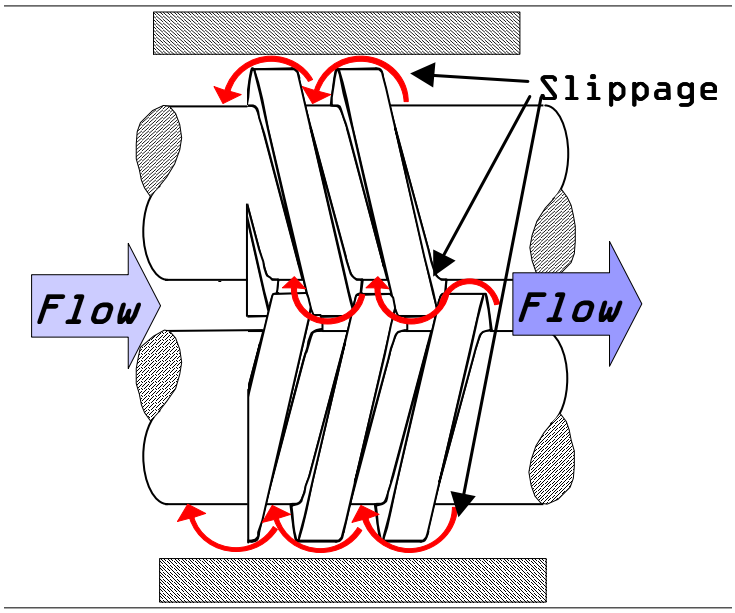

Figure 1.12 Visualization of Different Leak Paths

Fluid is driven by the pressure gradient between the circumferential, radial, and flank gaps. The slip flow is unavoidable because the pump design must maintain enough clearance between the screws to avoid metal-to-metal contact if the temperature of the pump were to rise. Close tolerances here allow the pump to run more efficiently because the slip is reduced but risks metal-to-metal contact with the screw-screw or screw-stator contact where either could cause a catastrophic failure.

The following Section 2 presents a survey of literature in the MPP field as well as the relevant theory of fluid mechanics applied to twin screw pumps. Section 3 will provide the current industrial solutions for twin-screw pumps operating under high GVF conditions. Section 4 will present the experimental facility and data analysis tools. Section 5 will show the results of the experiment and the relative discussion of the findings. Section 6 concludes the thesis with a final review of the results and a list of recommendations for future research.

2. LITERATURE REVIEW – ADVANCES IN MULTIPHASE PUMPING

This section focuses on the advances in modeling and validation of models for the twin-screw pump. It is important to know the history behind the models and experiments performed in the past to understand the phenomenon observed in the current research. The application of multiphase fluids in a twin-screw pump has created numerous complications that must be investigated for the progression of this technology to occur. The need for more information of these pumps running at high GVF has been limited in the past. Pump designers and companies are developing technologies specifically designed for that application and must evaluate these technologies. The current models developed for standard twin-screw pumps do not accurately predict the current assortment of issues found in pumping high GVF fluids. The historic information will allow a complete study of the currently installed Leistritz pump and allow a proper comparison to historic models to see how close those models are at reflecting the actual performance. The following section shows how the models and experimental research in the MPP field have advanced over nearly two decades.

2.1 Vetter and Wincek (1993-2000)

A short time after Bornemann started experimenting with MPP, Vetter and Wincek began modeling how twin-screw pumps work under multiphase conditions. Until this point the screw pumps' performance had been well documented for single phase flow but the complicated nature of multiphase flow required some simplifications. An important assumption made by Vetter and Wincek was that the pump could be modeled as a series of fluid-filled cylinders moving towards the center of the pump. Figure 2.1 shows the series of chambers and the direction of fluid flow. The most important assumption was that the fluid flow was separated into single phases due to the centrifugal forces acting on the fluid from the spinning screws.

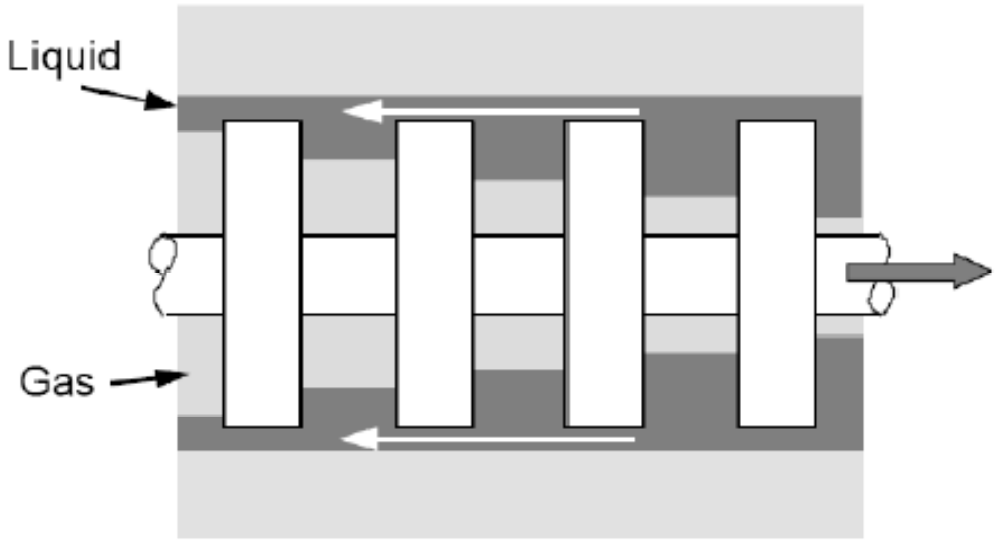

Figure 2.1 Simplified Model (Vetter and Wincek 1993)

The assumption of phase separation allowed the analysis of multiphase fluid to be broken down into single phase flow. This assumption was later tested by Vetter in a laboratory and was shown to be valid for GVF up to 85% [9][10].

The model was composed of a set of discs making up the chambers where the volumes of discs imitated the sealed chambers. The slip itself could then be modeled like a piston, compressing the gas as the chamber moved along while the liquid in the mixture acted like the chamber sealant. For GVF of up to 96%, the compression can be assumed isothermal.

In order for this model to predict the performance accurately very detailed measurements of the rotor were required. The slip model is completely dependent on the geometry of the screws. According to his analysis the circumferential gap between the screw and the stator was responsible for approximately 80% of the total leakage flow.

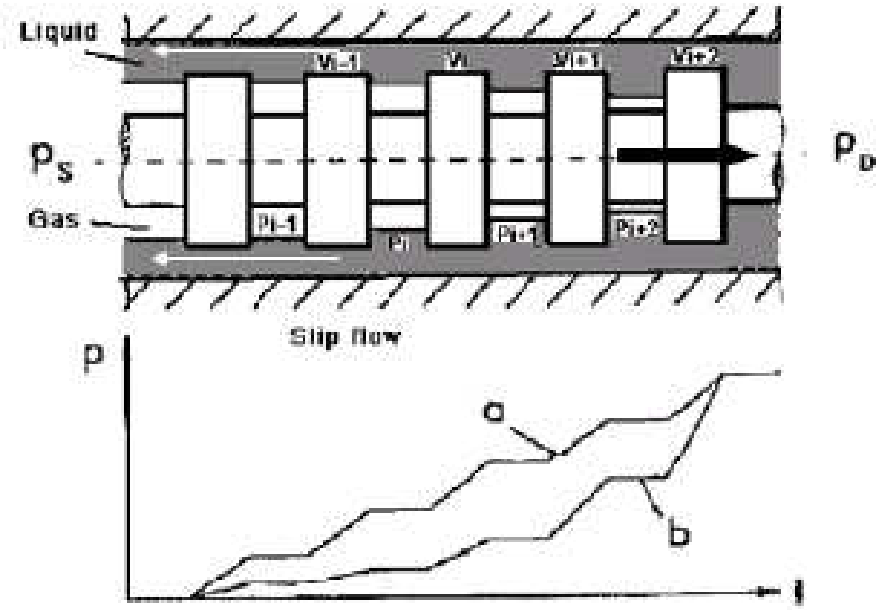

Figure 2.2 Pressure Profiles Along Screw Chambers (Vetter et al. 2000)

The experiments conducted to validate the model showed some interesting results. For the first time the pressure distribution across the screws was investigated. Figure 2.2 shows the pressure profiles for single and multiphase fluids transversing across the screw profiles. For single phase flow (profile a in Figure 2.2) the pressure profile linearly increases as the fluid travels from the suction to the pump exit. For GVF > 0 (profile b in Figure 2.2) the pressure profile is no longer linear. This means that unlike single phase flow, where each of the cavities equally contributes to the pressure increase, multiphase flow at high GVF has a non-linear pressure rise. The pressure increase is localized in the screw chamber closest to the pump exit.

2.2 Martin (2003)

Mercedes Martin from Texas A&M University developed a model to predict the performance of a twin-screw pump using single-phase water performance data. This approach does not depend on knowing the dimensions of the pump's internal clearances. The simplest situation using single-phase water is able to predict the "effective clearances" of the pump and estimate the performance characteristics. The model allows production engineers to evaluate the performance over a long period of operation, to diagnose loss of performance characterized by worn out clearances, and to give a practical way to analyze a pump in the field to evaluate its service viability.

The model was shown to provide a good correlation between the predicted and measured performance of a Bornemann twin-screw pump tested at the Texas A&M Riverside Campus. Other forms of modeling the performance of a twin-screw pump focus on meticulous calculations that require knowing detailed information about the complicated geometry of the screws. The model described by Vetter previously and the model developed by Klaus Räbiger found in a following section both require detailed knowledge of the pump geometry. These models would be better suited for the pump designer who develops and optimizes the pump performance. The requirements of Martin's proposed model involved only simple measurements typically provided by the pump manufacturer. Using the characteristic curve of the pump supplied by the manufacturer, an "effective clearance" can be calculated and used to estimate the pump's performance during multiphase operation without actually knowing the pump geometry.

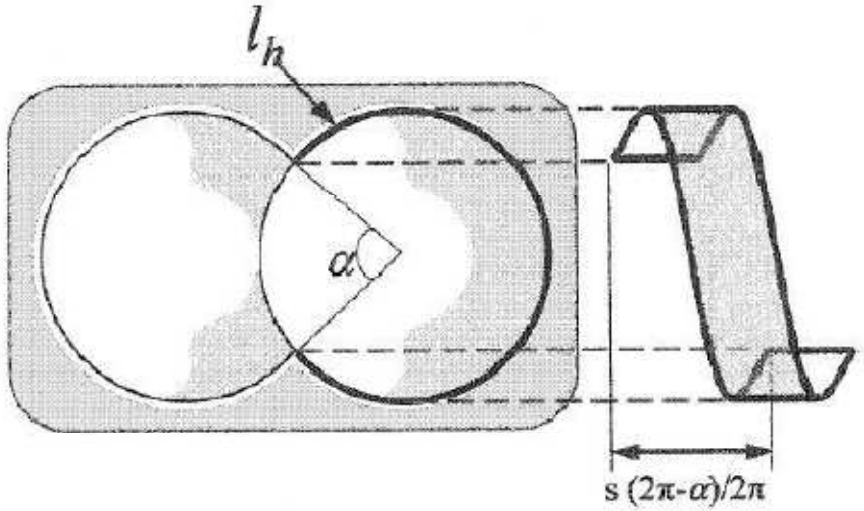

Figure 2.3 Effective Clearance from the Circumferential Flow Path (Martin 2003)

Figure 2.3 shows the circumferential gap between the rotors and the stator. It is assumed that most of the slip through the pump is going through this clearance. The helical arc, l_h, can be described by

$$l_h = (2\pi - \alpha) * \sqrt{\left(\frac{s}{2\pi}\right)^2 + {R_c}^2}$$

$L = s/2$ for most screws and α is the small channel where the two screws mesh. The complicated screw geometries can be simplified using a flat plat analysis for the circumferential clearance and the flank slip flow paths. The simplifications appear in Figure 2.4 and Figure 2.5.

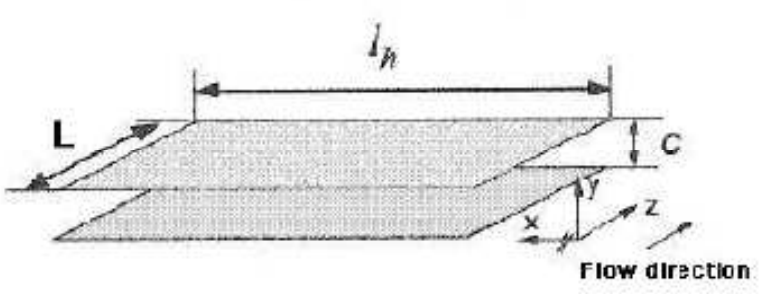

Figure 2.4 Flat Plate Assumption for Circumferential Slip Flow (Martin 2003)

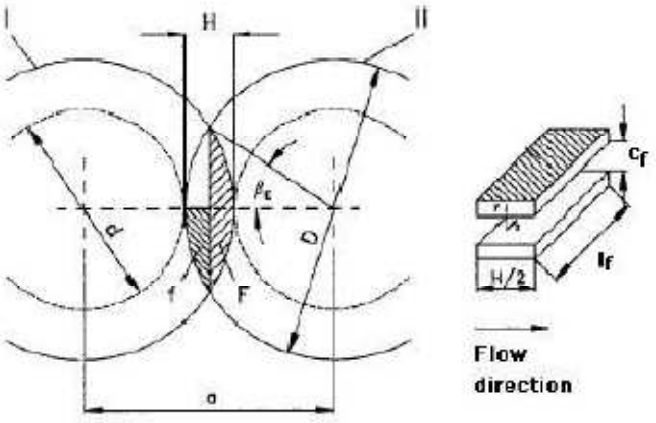

Figure 2.5 Flat Plate Assumption for Flank Slip Flow (Vetter 2000)

The slip through the simplified clearances was derived to be

$$Q_{slip,cir} = l_h \left(\frac{c_c^3}{0.033 * \rho^{0.75} * \mu^{0.25} * s} \right)^{0.57} \Delta P^{0.57}$$

for the circumferential and

$$Q_{slip,flank} = l_f \left(\frac{c_f^3}{0.033 * \rho^{0.75} * \mu^{0.25} * H} \right)^{0.57} \Delta P^{0.57}$$

for the flank slip.

The total slip is then

$$Q_{slip} = Q_{slip,circ} + Q_{slip,flank} + Q_{slip,root}$$

As previously mentioned by Vetter and Wincek, for the twin-screw pump 80% of the slip was due to the circumferential clearance while the flank clearance contributed 5% and the other 15% was due to the intermeshing root clearance between the screws. For the purpose of simplification it is easy to account for 85% of the slip through simple geometric relations as follows

$$Q_{slip} = 4\left[l_h\left(\frac{c_c^3}{0.033 * \rho^{0.75} * \mu^{0.25} * s}\right)^{0.57} + l_f\left(\frac{c_f^3}{0.033 * \rho^{0.75} * \mu^{0.25} * H}\right)^{0.57}\right]\Delta P^{0.57}$$

The assumption can then be made that 80% of the leakage can be accounted for by

$$Q_{slip} = 4l_h\left(\frac{c^3}{0.033 * \rho^{0.75} * \mu^{0.25} * s}\right)^{0.57}\Delta P^{0.57}$$

where actual flow is

$$Q = Q_{th} - Q_{sl}$$

The solution is

$$Q = Q_{th} - C_{eff} * \Delta P^{0.57}$$

where

$$C_{eff} = 4l_h\left(\frac{c^3}{0.033 * \rho^{0.75} * \mu^{0.25} * s}\right)^{0.57}$$

The C_{eff} is calculated by a linear regression obtained from the single-phase performance curve provided by the pump manufacturer. The effective clearance can be used to calculate the slip in the pump [11].

Using the effective clearance the slip becomes

$$Q_{slip} = f_c l_h \frac{C_{eff}^{\ 3}}{6\mu * s} \Delta P$$

The correction factor f_c was introduced to account for laminar and turbulent flow. The effective clearance is found by using a low viscosity fluid, normally water, where the pump operates in the turbulent region. After comparing all the data between three different pump manufacturers it was then suggested using f_c = 5 for laminar flow and f_c = 1 for turbulent flow.

The results obtained for the Bornemann pump in particular show a very close correlation between the performance estimation found from the effective clearance method compared with the actual pump performance. The model predicted the behavior of the pump within a 10% range of the actual performance. These results are for intermediate GVFs between 50 and 90%. At higher than 90% GVF the model slightly over predicted the flow rate. The results for the higher RPM were similar.

A series of sensitivity studies were also performed by varying specific variables of interest such as liquid phase viscosity, pump speed, inlet pressure, and the GVF while holding all other parameters constant. From Chan's analysis it was concluded that:

- At a given pressure increasing the gas content will decrease the slip and increase the pump rate
- As the pump speed is increased for a given GVF, the slip decreases
- As the inlet pressure is decreased, the pump flow rate is decreased due to the reduction in gas compressibility with pressure
- Increasing the liquid viscosity along with the gas compressibility greatly reduces the slip at increasing gas fractions
- The liquid in the pump is greater at higher ΔP's due to the liquid recirculation

2.3 Chan (2006)

Evan Chan from Texas A&M University proposed that by increasing the viscosity of the liquid phase the volumetric efficiency could be improved. It has been known that twin-screw pumps lose their volumetric efficiency during high GVF operation. The fundamental idea is that the viscosity of the liquid phase is the dominant variable in the leakage flow that causes slip. Therefore it has been predicted that increasing the liquid viscosity will increase volumetric efficiency. The increase of viscosity in the liquid fluid was obtained using guar gel.

Evan Chan's experimental results showed that at high GVFs the viscosity of the fluid was not an important parameter for pump performance. The increase in viscosity did not increase the total flow rate of the pump. This finding was not shown by the previous models of twin-screw pumps operating at high GVFs. Chan's conclusion was that the non-Newtonian nature of the guar gel lost its viscosity during the temperature increase while operating at a high GVF. The previous models used up to this point, mainly Martin's model, were not capable of compensating for the temperature and shear effects of the fluid. Future models would need to include this factor along with multiphase flow effects in the clearances. A call for more tests at higher differential pressures was also proposed but not studied at this time.

Secondary to the experimental research, an analytical model was developed for through-casing injection of a fluid directly into the screw chambers. This proposed solution was meant to increase volumetric efficiency and reduce vibrations found during field tests of the pump operation. By choosing the chamber to inject fluid into the pressure rise shown by Vetter in Figure 2.2 for multiphase flow, could be made more linear. The hypothesized pressure profile appears in Figure 2.6.

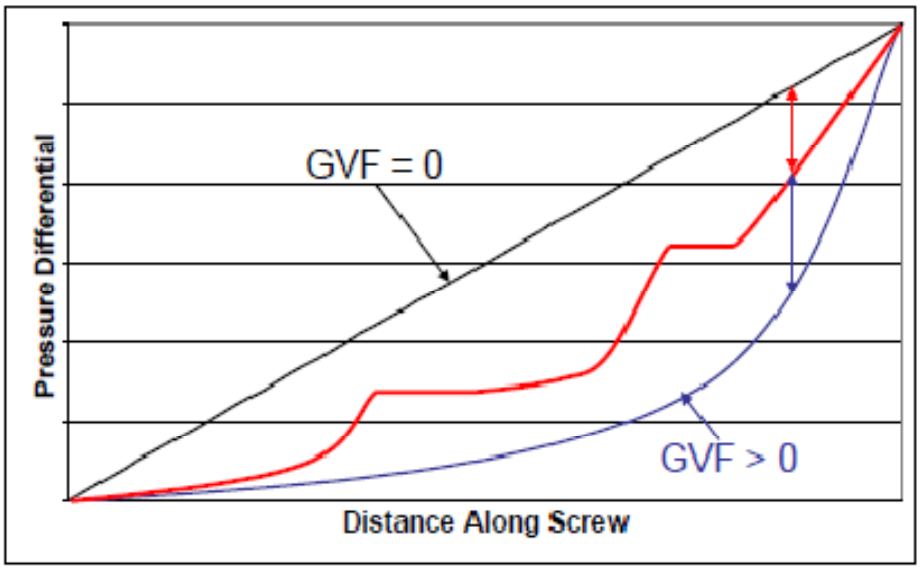

Figure 2.6 Theoretical Pressure Profile for Through Casing Injection (Chan 2006)

The method hypothesized by Chan was only done analytically due to the extensive modification to the pump casing that would need to be completed to conduct the investigation. The calculations showed that the through-casing liquid phase injection is feasible and that more ideal pressure profiles and increased well boosting could be obtained.

Each chamber of the pump was modeled as a piston with the liquid phase compressing the gas phase. Injecting fluid into the piston increased the liquid volume, therefore increasing the overall pressure. Conclusions regarding the through casing injection show that depending on where the pump needed the most compression assistance, the additional required horsepower to pressurize the fluid could be kept minimal. Chan showed that the pressure increases in at specific screw locations could be a feasible way to linearize the pressure profile in the pump [12].

Alternatively, when using the seal flush as a means to create the seal under high GVF conditions, the water stored in the recirculation tank is at the same pressure as the outlet of the pump. When the water is introduced to the seal, it is fed through the inlet where it returns to the inlet pressure. This means that the pump has to re-pressurize the liquid along with the gas. The additional horsepower needed to re-pressurize the fluid decreases the mechanical efficiency. As shown by Vetter and Wincek the majority of the pressurization occurs in screw stages closest to the pump outlet. If the through-casing injection was administered in these screw stages the horsepower required to re-pressurize the liquid would be kept to a minimum.

2.4 Xu (2008)

The work Xu presented is a continuation of Chan's work on the same test facility at Texas A&M. The proposed through casing injection method hypothesized by Chan is investigated experimentally per the recommendations of Evan Chan.

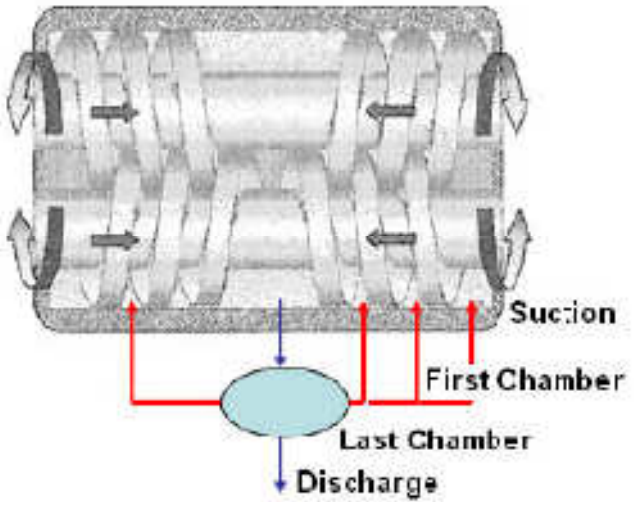

Figure 2.7 Diagram of Proposed Injection (Xu 2008)

Figure 2.7 shows the injection locations along the screw profile. This was the same Bornemann pump that was used for Chan's viscosity study as well. In comparison, the increase of liquid viscosity for this experiment is done by injecting the high viscosity fluid directly into the screw chambers compared to allowing the high velocity mixture to mix fully with the working fluid upstream of the pump suction.

It was found that different performance in terms of total flow rate and volumetric efficiency could be realized by injecting the viscous fluid at different locations along the screw profile. The experimental results show that there is a decrease in total flow when the differential pressure is increased. A baseline comparison with water, followed by injecting higher viscosity fluid at the indicated injection points resulted in an increase in total flow. The best position to inject the viscous fluid was at the suction. The best volumetric efficiency was also achieved by injecting the high viscosity fluid closest to the pump suction. The results of this investigation show that the injecting of viscous fluid directly into the chambers is an efficient way to increase the volumetric efficiency but it also shows that injecting the fluid at the pump suction is the best option [13].

Xu's extensive testing with the full-scale pump performed showed a good match between the predicted MPP performance and the experimental research. Along with improved performance, both volumetric efficiency and total flow rate, the pressure profile along the screw is becoming more linear and is dependent on the injection location of the viscous fluid. Contrary to Chan's conclusions, Xu concludes that the viscosity is still the determining factor in pump performance even at high GVFs. By injecting the fluid directly into the chamber, the viscous fluid is able to create the seal that compresses the gas. The best solution presented by Xu to increase the pump performance is to inject a high viscosity fluid directly into the suction of the pump.

2.5 Räbiger (2009)

The main topic of Klaus Räbiger was to develop a fluid dynamic and thermodynamic model to simulate the operation of twin-screw pumps operating at high GVFs. The fluid dynamic model was done using CFD software and the end result was aimed primarily at the pump designer. Very intricate solid design models done in a CAD program set the geometry of the screws and gave very close results to the actual pump performance. While the model and prediction of performance will not be applicable to the current investigation, it is worth mentioning that the results given by the model showed that it is possible to simulate the pump performance with multiphase fluid. Along with the CFD model, a heat transfer and thermodynamic pump model was developed as well.

A complete description of the power going into the pump was used to explain the temperature rise associated with pumping the fluid. The initial drive power, HP_{drive}, from the electric motor is split between three different groups: HP_{net}, $HP_{leakage}$, and $HP_{friction}$. HP_{net} is the power required to move the fluid through the pump, whether it be single or multiphase. The $HP_{leakage}$ is the amount of power lost in "re-pumping" the slip. This also includes the liquid recirculation loop. The final division of power, $HP_{friction}$, is introduced to the fluid as heat. While HP_{net} and $HP_{leakage}$ make up a portion of the power that is doing work on the fluid, nearly all of the $HP_{friction}$'s contribution is lost in heat generation that is transferred to the working fluid. A diagram of the power distribution can be seen in Figure 2.8.

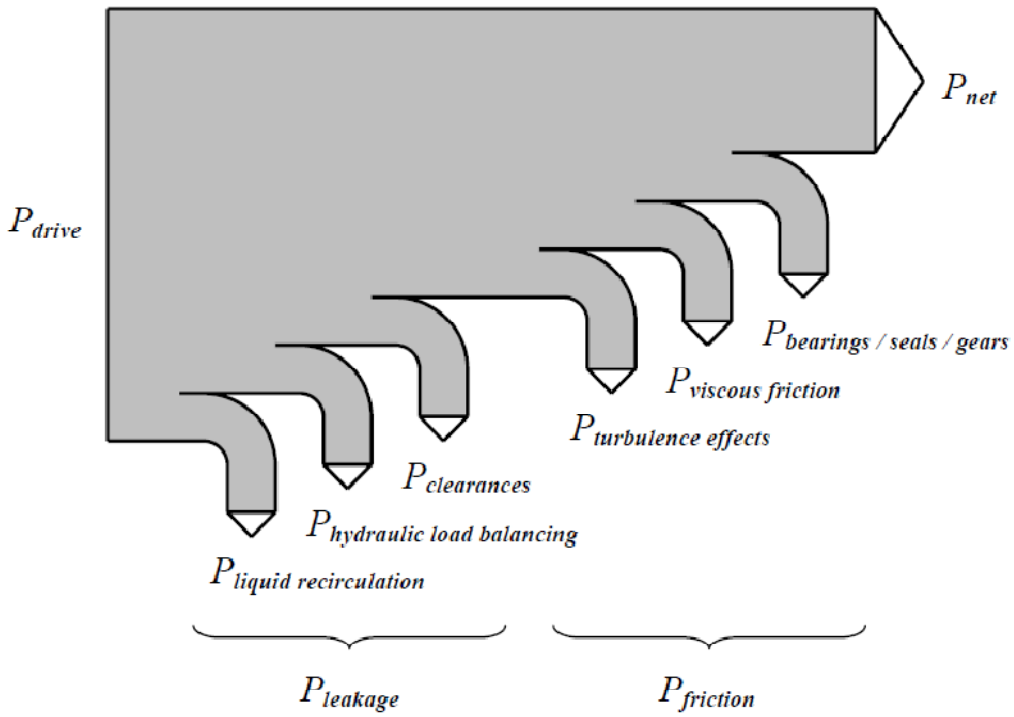

Figure 2.8 Power Distribution During Pumping Operation (Räbiger 2009)

As the GVF increases, the temperature difference between the inlet and the outlet becomes larger. To see why the temperature rises it is necessary to look at the power distribution entering and exiting the pump. HP_{net}, the power used to move the working fluid is a summation of HP_{liq} and HP_{gas}. The following equations

$$\mathrm{HP_{liq}} = \frac{\mathrm{Q_{liq}} * \Delta \mathrm{P}}{1714}$$

$$\mathrm{HP_{gas}} = \mathrm{P_{in}} * \mathrm{Q_{gas}} \frac{\ln\left(1 + \frac{\Delta \mathrm{P}}{\mathrm{P_{in}}}\right)}{229.7}$$

$$\mathrm{HP_{net}} = \mathrm{HP_{liq}} + \mathrm{HP_{gas}}$$

are used to calculate the various horsepower requirements of the pump. Where Q_{liq} is in GPM, Q_{air} is in ACFM, all pressures in psi, and after the conversion factors, HP_{liq} and HP_{gas} are in horse power. An equivalent equation to HP_{liq} must also be used to calculate the power lost to the liquid recirculation system. The heat generation from the liquid recirculation system term can sometimes be overlooked at low GVFs while sufficiently cool water enters the pump inlet to conduct the generated heat away from the pump. As the GVF goes up, the amount of liquid that is able to remove heat from the system is reduced. At a critical GVF there is not enough liquid to dissipate the generated heat from $HP_{friction}$ and the operating temperature of the pump will continue to rise. The power dissipated into the fluid is shown by

$$\mathrm{HP_{heat-up}} = \mathrm{HP_{drive}} - \mathrm{HP_{net}} - \mathrm{HP_{friction}} = (\mathrm{c_l}\dot{\mathrm{m}}_\mathrm{l} + \mathrm{c_G}\dot{\mathrm{m}}_\mathrm{G})\Delta\mathrm{T}$$

The theoretical model predicted heat rise along the screw from the pump inlet to the pump exhaust. This heat rise is related to the pressure increase of the fluid as it is raised from the inlet pressure level to the exhaust.

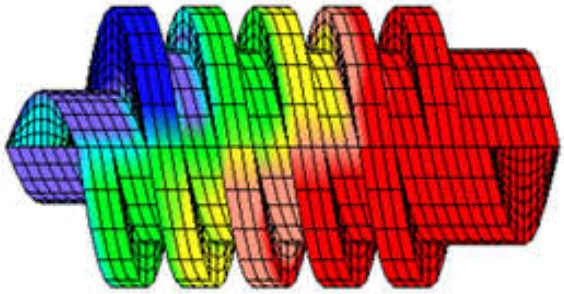

Figure 2.9 Temperature Distribution Along Screw (Räbiger 2009)

The heat distribution is most important when operating at high GVF and high differential pressures. There is a loss of volumetric efficiency due to the metal expanding and the heat transferring to the gas phase. As the screw expands due to thermal expansion, the cavities between the screws shrink and volume transferred per revolution decreases as well. The raise in temperature for the gas phase raises the density and expands the gas so it takes up more volume. This means for a set inlet volumetric flow rate there could be different mass flow rates depending on the gas expansion. Figure 2.9 shows the temperature distribution along the screw in Räbiger's model.

Räbiger's model was able to predict the volumetric flow rate and can be a utilized as a valuable tool for a pump designer. The noticeable trends show that the volumetric flow rates decrease with an increase in the GVF and differential pressure. His investigation of the friction power that causes the temperature rise within the pump showed that as the GVF and differential pressure goes up the differential temperature across the pump increases as well. The volumetric efficiency was also shown to follow the same trend as the volumetric flow rate through the pump, decreasing with an increase of GVF and differential pressure.

The investigation done by Räbiger shows that the major pump performance characteristics can be modeled quite thoroughly using commercially available CFD software. It also investigates the temperature characteristics of the pump during operation. While the performance modeling is beyond the scope of the current investigation, the temperature rise is of considerable interest. The current investigagion will look at the temperature difference between the pump inlet and outlet and examine the effect on the friction power entering the fluid [14].

3. METHODS FOR MULTIPHASE PUMPING

This section will present two of the current solutions that screw pumps use in MPP as well as the objectives for the proposed investigation. The current solutions, such as liquid recirculation and digressive screw geometry, have been proven to enhance the performance of twin-screw pumps and allow multiphase pumps to meet the design goals presented by rigorous standards. As the multiphase technology matures, it is necessary that the performance as well as the efficiency increase.

Although twin-screw pumps have successfully operated in oilfields around the world, the worldwide demand for energy requires more efficient, cost effective measures to meet these demands. More detailed information about the performance of twin-screw pumps is required to promote informed decisions about the utilization of this technology. A particular interest in this study will investigate gas volume fractions above 90% at running speeds between 1800 and 3600 RPM. These running speeds are higher than past research has considered. Past research has shown that increasing the pump speed can increase the volumetric efficiency of twin-screw pumps. It is also of interest to investigate the performance advantage of utilizing a liquid recirculation system to help increase volumetric efficiency at high GVFs.

3.1 Liquid Recirculation

The current design compromise is a balancing act between performance and reliability. The principles of positive displacement pumping show that the gas is compressed by the liquid phase of the mixture and moves axially from the suction to the discharge of the pump. At high GVF operation, the amount of liquid accompanying the gas is very small and above a certain GVF the pump loses its ability to compress the gas to the exit pressure and the gas recalculates, slips, back to the pump inlet. This loss of pressure

event causes all the power used to compress the gas to turn into internal energy and it causes a rapid increase of temperature within the pump. Although tighter screw tolerances can increase the volumetric efficiency, under the high GVF operation the thermal expansion of the rotors under high GVF operation may cause them to rub, damaging the machine.

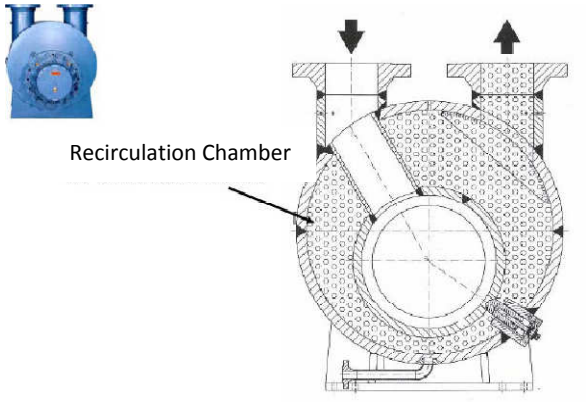

Figure 3.1 Internal Recirculation of Bornemann Twin-Screw Pump (Bornemann 2006)

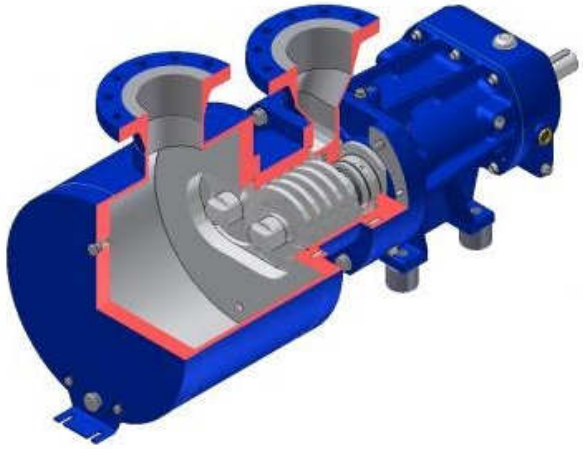

Figure 3.2 Bornemann Internal Recirculation Cut Away (Bornemann 2006)

Figure 3.1 and Figure 3.2 show the solution by Bornemann Pumps. To ensure that adequate liquid is delivered to the pump suction there is an enlarged housing intended to store liquid as it passes through the pump. At high GVF this stored liquid is re-circulated to the suction. The re-circulated fluid has the capacity to dissipate the heat generated in the gas compression and distribute it evenly along the screws to avoid warping issues [15].

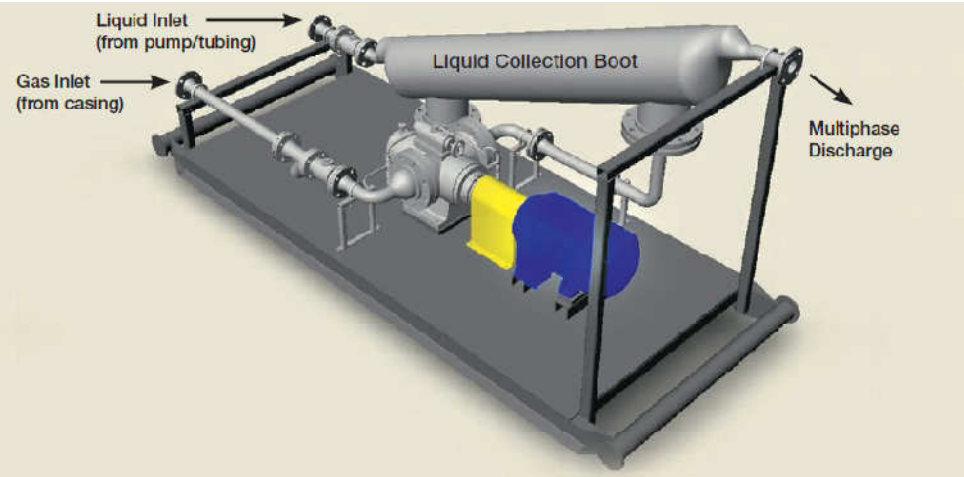

Figure 3.3 Leistritz Multiphase Pump Assembly (Leistritz Corp. 2010)

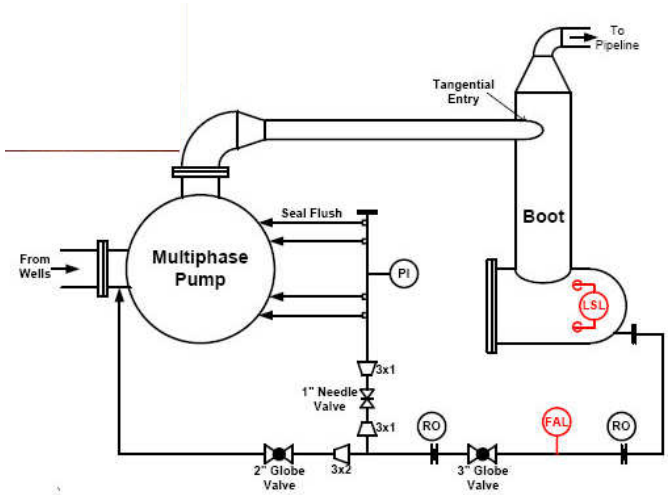

Figure 3.4 External Recirculation "Seal Flush" Diagram (Leistritz Corp. 2010)

A similar solution made by Leistritz Corporation involves a special seal flush system. Liquid from the pump exhaust is passed through a liquid collection boot. This is similar to the reservoir in the Bornemann pump housing. Figure 3.3 shows a digital rendering of a typical MPP package from Leistritz and Figure 3.4 shows a basic schematic for the principle operation. The basic principle of the liquid collection boot is to act as a reservoir for fluid in high GVF running conditions. The large volume of fluid in the tank allows the pump to operate at 100% GVF for extended amount of time. The operation of the system is simple. The fluid inside of the tank is stored at the exhaust pressure and the tank is connected to the pump housing via stainless steel tubes. As the liquid flows through the seal, it is emptied into the pump suction and the differential pressure across the pump inlet to exhaust drives the fluid from the boot.

The temperature limit that governs the time spent at 100% GVF depends upon the seals that separate the screw chamber from the bearings and gear housing. If the pump runs at a temperature higher than the designed temperature of the seals, there is risk of seal failure. The circulated liquid then becomes the main factor in the increasing temperature of the seals. As the liquid re-circulates, it absorbs the heat created by the compression of the multiphase fluid and returns to the knockout boot. Once there, it is reintroduced to the pump suction and the temperature rises again. This continuous cycle will repeat until the maximum pump temperature is reached or a suitable way of removing the heat in the knock out boot is implemented. The effective GVF at the suction because of the liquid recirculation is

$$\mathrm{GVF_{eff}} = \frac{\mathrm{Q_{gas}}}{\mathrm{Q_{gas}} + \mathrm{Q_{liq}} + \mathrm{Q_{flush}}}$$

3.2 Digressive Screw Geometry

Figure 3.5 Diagram of Digressive Screws (Rohlfing 2006)

Bornemann developed the digressive screw geometry for twin-screw pumps, seen in Figure 3.5, to help increase the gas compression in high GVF situations. The principle is similar to the design of screw compressors that varies the chamber volumes along the screw to compress the gas. As the gas is compressed, the volume required to move the fluid to the next chamber decreases. By varying the pitch along the screw, the chamber volumes are decreased along the length of the screw and this decreases the chamber volume that leads to the build of compression [16].

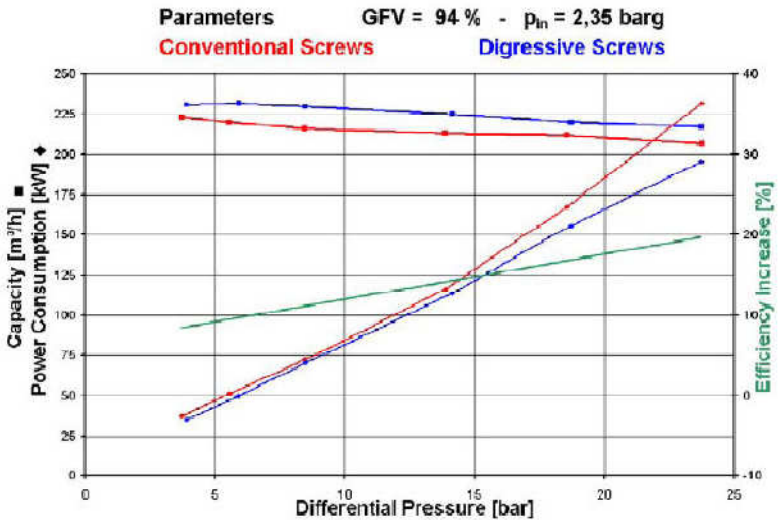

Figure 3.6 Results from Digressive Screw Geometry (Rohlfing 2006)

The experimental results for digressive pitch screws performed by Bornamann are shown in Figure 3.6. The results show a gain in total flow rate at every differential pressure, a slight decrease in power consumption, and a gain in efficiency, corresponding to the improved capacity. It was shown that as the fluid moved towards the pump exhaust, the reduced chamber volume required less liquid to seal the chamber clearances and compress the gas. While the digressive screw profile improved the performance of the pump, the temperature issue still existed. Also, because the geometry has been modified especially to operate under high GVF conditions, the pump loses some of its capacity for liquid slugs or pure liquid flow. Geometrically, this makes sense because liquid is considered incompressible under most circumstances so the decreasing chamber volumes would leave the liquid no place to go as the fluid moves from the inlet to the exhaust.

3.3 Current Investigation

The main goal of the proposed research is to characterize the performance of a multiphase twin screw-pump operating at extreme gas volume fractions at high RPM. The major focus presented in this thesis will consist of:

- Steady state performance of the Leistritz system under high GVF (>90%)
- The effect of inlet pressure on performance
- The effect of different operating speeds
- Temperature rise associated with temperature of the seal recirculation
- Thermal effect on pump performance

The pump will be supplied by Leistritz Corp. and will be installed in the Turbomachinery Laboratory where the facilities for multiphase flow already exist. The experiments on the twin-screw pump will aim to simulate the environment that the pump operates under in the field. Air and water flow rates will be individually controlled and metered

via control valves operated with a LabView based data acquisition system. The current investigation will vary inlet pressure between 10 and 50 psi; gas volume fractions between 0 and 100%; and the pump differential pressure will be varied from 0 to 250 psi by throttling an exit control valve. All of the proposed experiments will fall within the pump's operational range.

The analysis will also take an in depth look at how a the liquid recirculation described in the following section affects the pump performance characteristics as well as the thermal considerations involved when implementing a liquid recirculation system. Twin-screw pumps utilize two intermeshing steel screws that are located within a steel housing typically lined with a rubber insert. At high gas volume fractions there is a minimal amount of liquid present and there is a rise in heat generation associated with operation at high gas volume fractions. By analyzing the thermal characteristics of the liquid recirculation system the safe operating limits for the pump can be identified.

4. EXPERIMENTAL FACILITY

This section focuses on the multiphase experimental facility set up at the Turbomachinery Laboratory at Texas A&M University. The facility was used for all of the research described in this thesis. The resources at the Turbo Lab make an ideal location to conduct the investigations of MPP pumps operating at high GVF. The experimental facility was used to test the Leistritz twin-screw pump under a laboratory controlled environment that fully simulated operation under real life circumstances. Although the testing was done under ideal test conditions, the information received from this facility will be able to give engineers performance maps of the MPP operating within the desired operating conditions. The facilities allow the easy installation and testing of MPPs that allow the rapid testing and development of this technology. Section 4.1 will concentrate on the overall system infrastructure installed in the laboratory that allows a modular approach to investigating MPP technology; section 4.2 will focus on the Leistritz pump assembly; and section 0 will focus on the data acquisition, and instrumentation.

4.1 Experimental Hardware

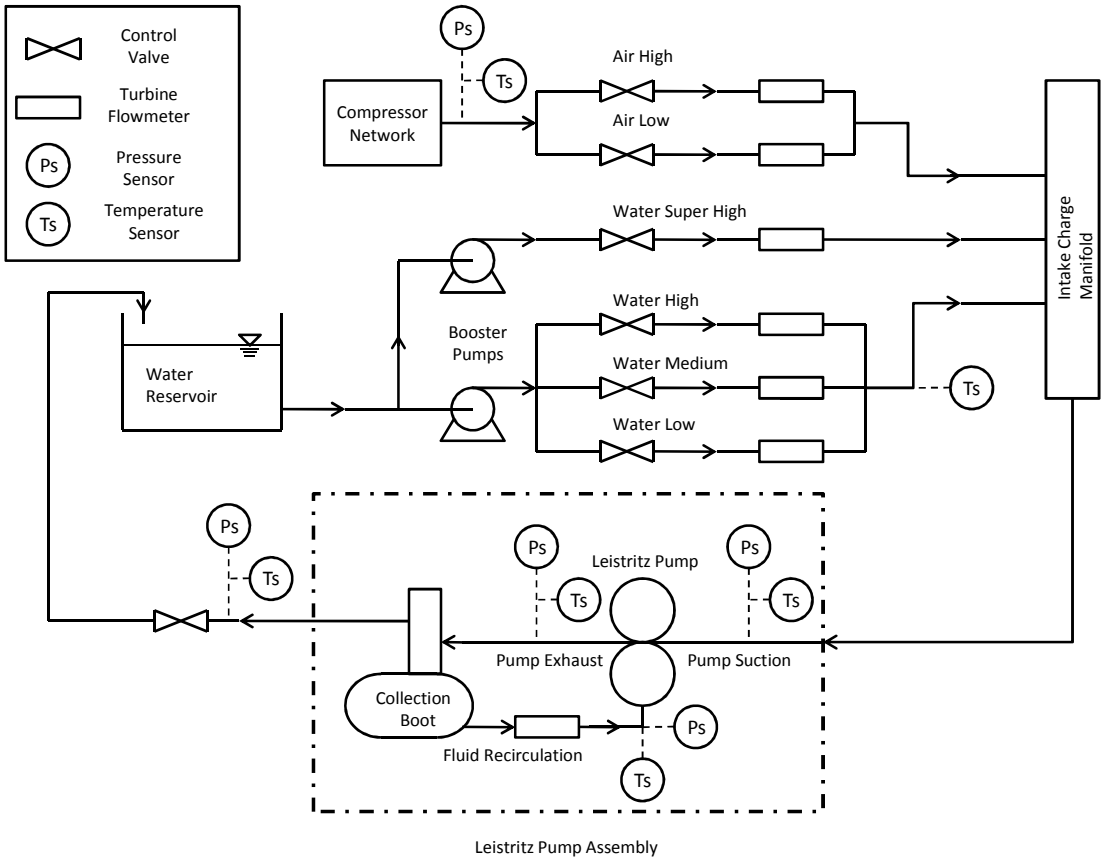

Figure 4.1 Flow Loop Diagram

Figure 4.1 shows the circuit diagram for the system flow loop. All of the components will be described in detail in the following section. The general layout appears above. The water is sent through the twin booster pumps regulated by the control valves while the compressed air comes from the air compressor network and combines with the water in the intake charge manifold. After the intake charge manifold, the multiphase fluid mixes through the piping network until it is picked up through the Leistritz pump assembly where the fluid is forced to move though a differential pressure change. The

water is then separated by the collection boot and finally the remainder of the fluid flows out of the assembly and through the outlet valve and back into the water reservoir where the gas disperses into the atmosphere. The LabView based data acquisition system simultaneously monitors an array of pressure and temperature sensors along with a series of turbine meters.

Figure 4.2 Water Supply Reservoir

Figure 4.3 Booster Pump #1 (Up to 130 GPM)

Figure 4.4 Booster Pump #2 (Up to 500 GPM)

Figures 4.2, 4.3, and 4.4 show the water supply system located outside of the laboratory. The water reservoir has a capacity of 5000 gallons. The water from the reservoir is then fed to the dual centrifugal pump system where the capacities for the

pumps are 130 and 500 GPM respectively for pumps 1 and 2. The reservoir volume is sufficient to ensure that any entrained air in the water is dissipated before it enters the booster pumps. The water pressure is controlled via back pressure regulators set to 120 psi. After exiting the booster pumps, the water flows through separate pipelines and enters the laboratory where the flow control system is located.

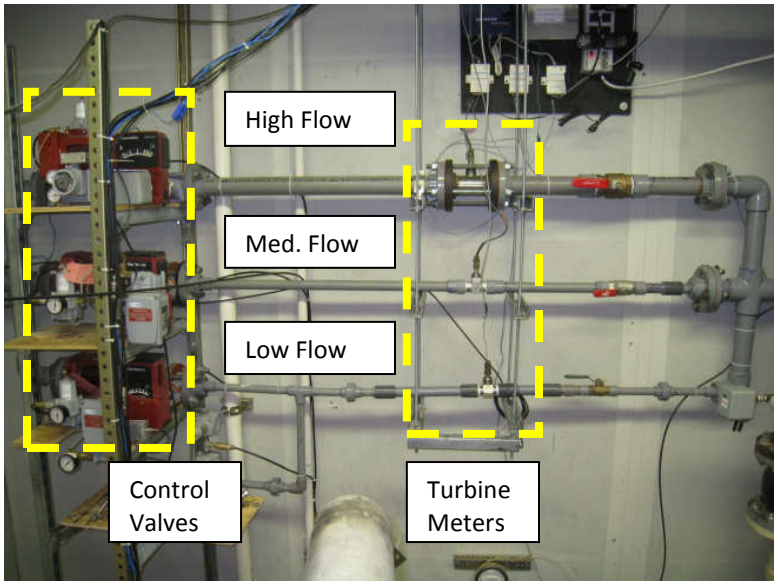

Figure 4.5 Low, Medium, and High Water Control and Measurement System

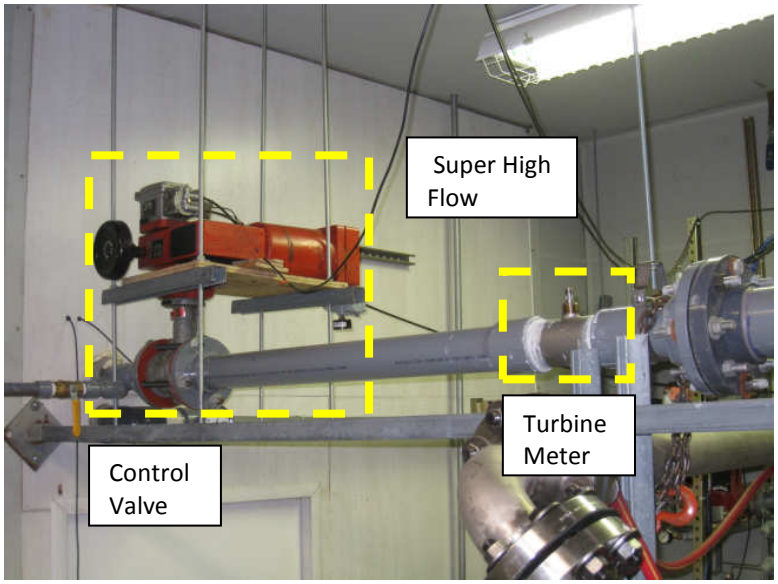

Figure 4.6 Super High Water Control and Measurement

Figure 4.5 and Figure 4.6 show the water control system once the booster pumps feed water into the laboratory. Both figures show electro-pneumatic valves that are controlled by a 4-20mA input supplied by the LabView program developed specifically for this application. The control valves regulate the flow rate of water entering the positive displacement pump system. A total capacity of 630 GPM is available from the parallel water systems. After a specified flow is regulated through the control valves, a set of parallel turbine meters monitors the volume of water being displaced. All of the water going through the system is closely monitored.

Figure 4.7 Air Compressor Network

The air compressor network shown in Figure 4.7 is made up of three 100 psi oil free screw compressors that are used for this study. They are capable of supplying above and beyond the volume and pressure required for studying the effects of running MPPs at high (>95%) GVF applications. Once the air is compressed, it is stored in a sealed tank and a pipeline is plumbed directly into the laboratory area where it is met with an air control system.

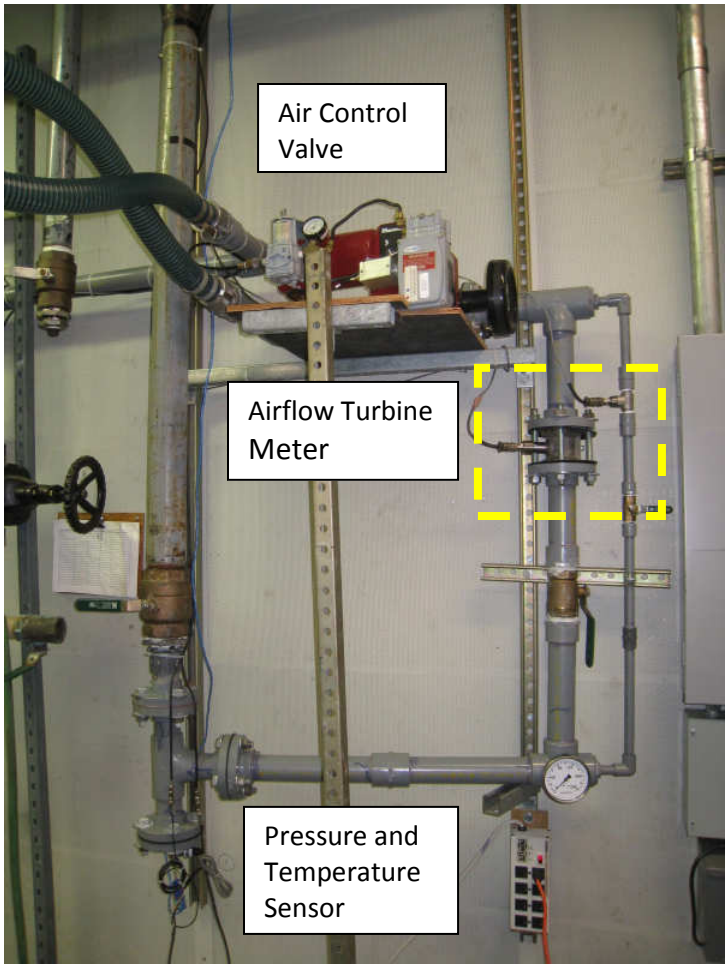

Figure 4.8 Low and High Air Control Valves and Measurement

Figure 4.8 shows the airflow control system. It is comprised of an electro-pneumatic valve operated from 4-20mA, temperature thermocouple, pressure transducer, and set of parallel turbine meters that monitor overlapping ranges of airflow. The LabView data acquisition system monitors the sensor data and the control valve. The main difference between the water and the air control systems is that the water system controls the liquid flow rate (GPM) while the air system controls the pressure (psi) at the pump inlet. The total flow rate moving through the pump's control volume can be recorded through a series of calculations that will also be presented in Section 4.4.

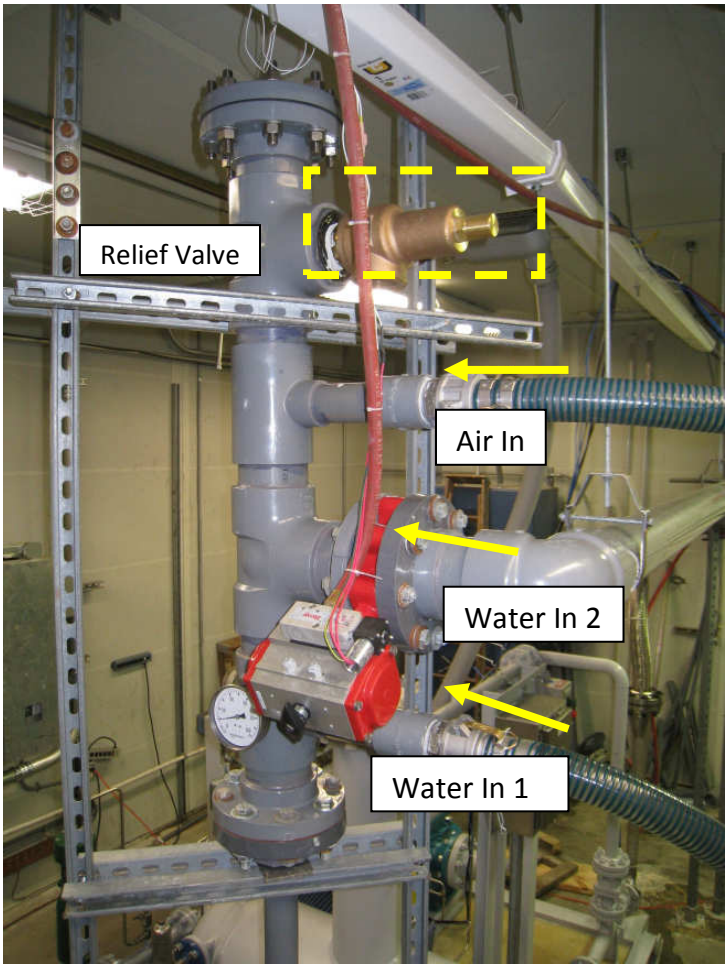

Figure 4.9 Intake Charge Manifold

After the air and water pass through the control systems, the two fluids are injected into the intake charge manifold shown in Figure 4.9. This manifold is a common chamber that is fed to the inlet of the pump assembly. There are two water inlets: one for up to 130 GPM and the second for water flow up to 500 GPM. The 500 GPM inlet is separated by a butterfly valve to seal the intake charge manifold from the long pipe that feeds the water inlet 2. A relief valve is also installed on the manifold to provide a measure of safety for the equipment.

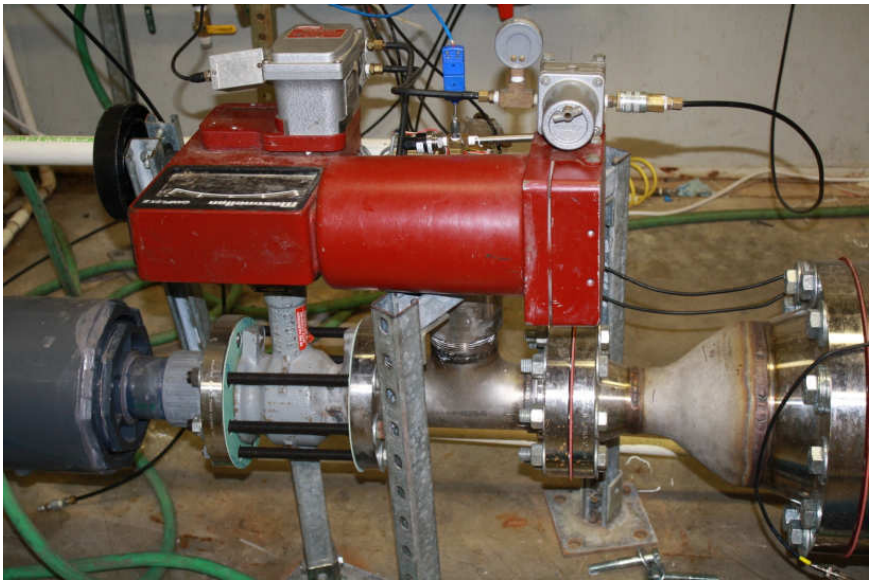

Figure 4.10 Exit Control Valve

The exit control valve shown in Figure 4.10 is also an electronic-pneumatic control valve operated from 4-20mA. This control valve regulates the exit pressure of the pump via a manual control in the LabView program. The restriction caused by the control valve simulates the pressure head caused by the pipeline in a real world application.

Figure 4.11 Variable Frequency Drive

The final component that makes up the testing infrastructure at the MPP laboratory is the VFD, shown in Figure 4.11, that supplies the driven pumps with electricity. The VFD can support up to a 200HP motor and has a variable frequency between 5 and 60 Hz. It also has an analog output that is connected to the data acquisition system that gives a 0-10V reading that gives a percentage of full output. This is then used to calculate the electrical horsepower being consumed by the pump motor. The accuracy of the analog output is 1%.

4.2 Leistritz Twin Screw Pump Assembly

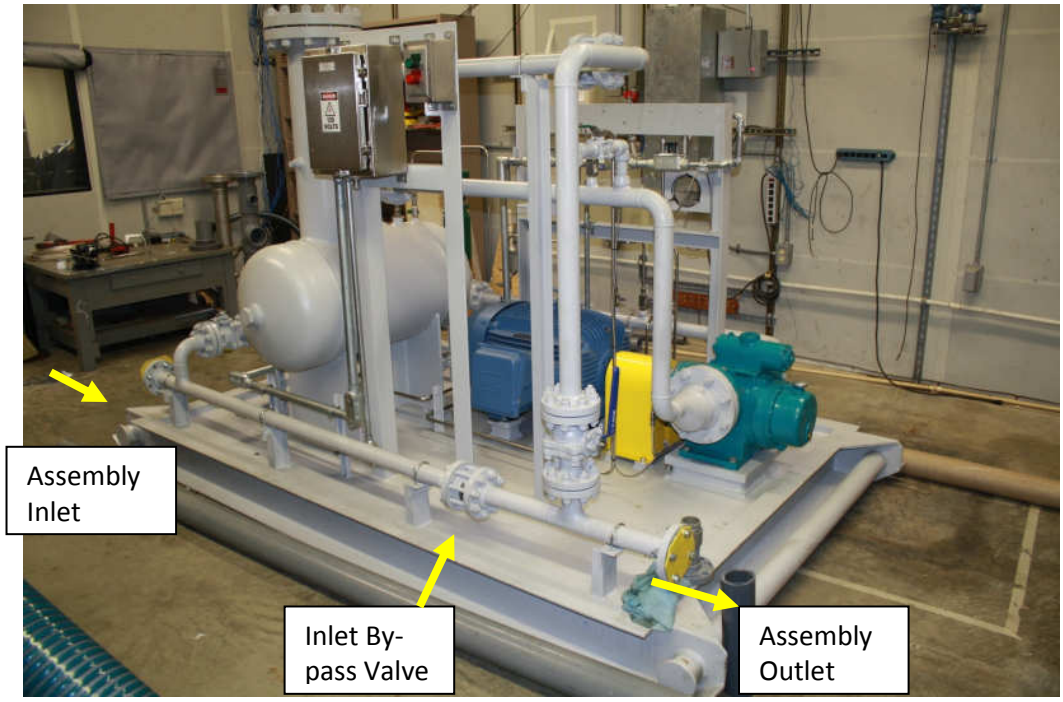

Figure 4.12 Leistritz Pump Assembly 1

The Leistritz Pump Assembly was received as shown in Figure 4.12. The unit is marketed as a MPP total solution and is designed especially for high GVF operation. The system includes a liquid recirculation system where the liquid is stored in a liquid knockout tank and is re-circulated to the pump suction through the seal flush system. The GVF is calculated at the Assembly Inlet but an Effective GVF is calculated using the seal flush liquid as well. All of the fluid exits the assembly outlet and then travels outside the laboratory and back into the water reservoir. There is also an Inlet by-pass valve located between the assembly inlet/outlet that opens when the pump assembly is subjected to a negative differential pressure. During the zero differential pressure data points, the by-pass valve was replaced by solid flange blanks so the skid did not operate under the by-pass condition.

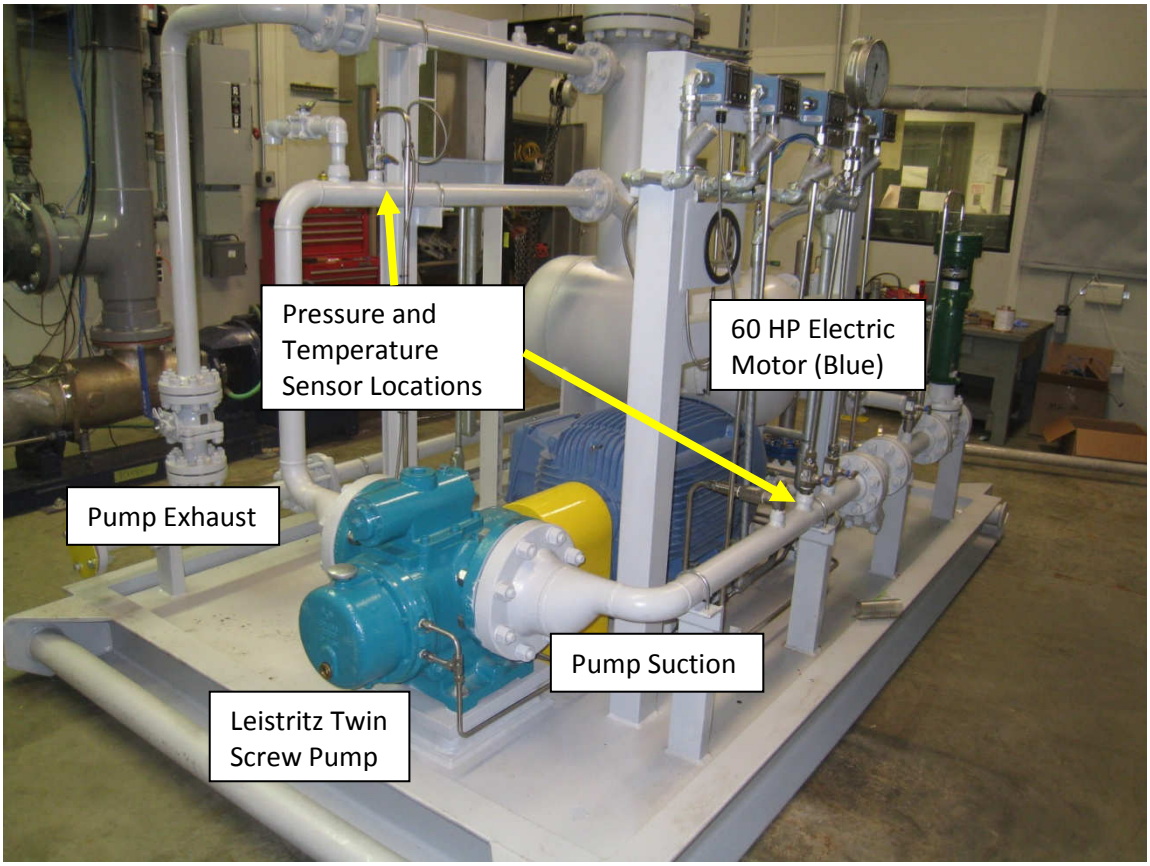

Figure 4.13 Leistritz Pump Assembly 2

Figure 4.13 shows an alternative view of the pump assembly. This view shows the positions of the temperature and pressure sensors located near the pump inlet and exhaust. The Leistritz pump is shown in aqua and the driving motor is pictured in blue.

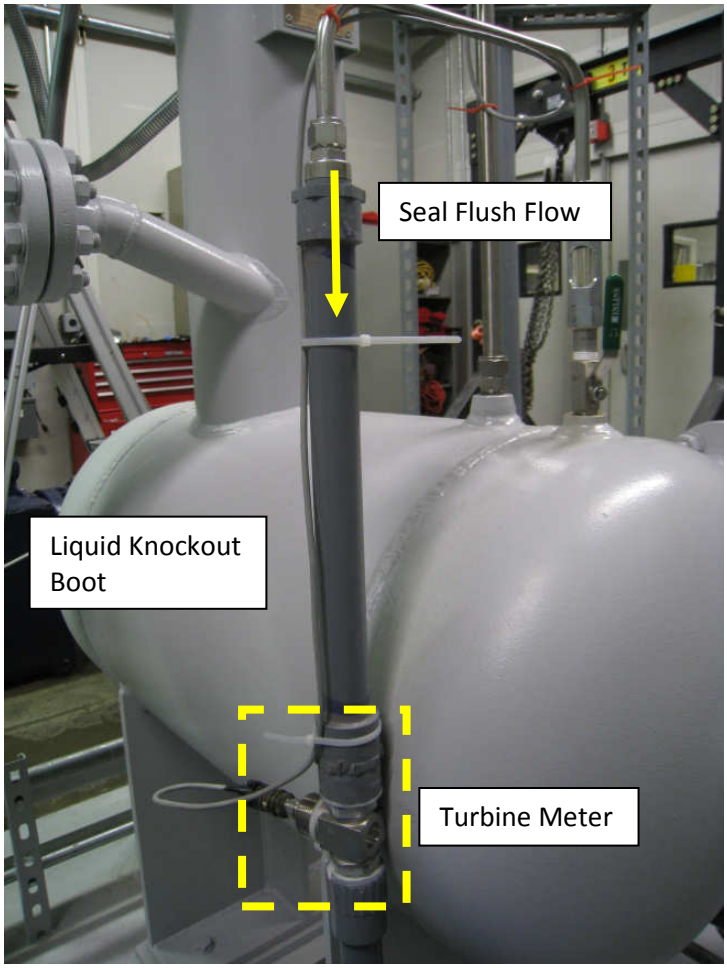

Figure 4.14 Liquid Knockout Boot with Flow Recirculation Monitoring

The liquid knockout boot and seal re-circulation system are shown in Figure 4.14. The seal flush flow is forced out of the knockout boot and flows through a turbine meter to record the volumetric flow rate entering the seals. This flow rate and fluid temperature are measured and used to conduct a study on how the temperature of the liquid seal flush affects the exhaust temperature of the fluid exiting the pump. A cutaway view is shown in Figure 4.15. It is assumed that the de-mister located in the knockout boot captures nearly 100% of the liquid that is exhausted by the pump.

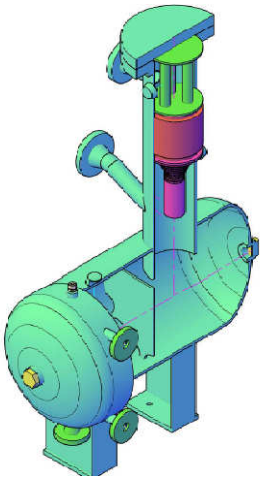

Figure 4.15 Knockout Boot Cutaway

Similar to the “Through-casing” injection method proposed by Chan, the Leistritz pump achieves something similar by injecting fluid through the seals. By using the recalculated fluid collected in the water collection boot pressurized by the exhaust pressure of the pipeline or in the case of the experimental facility the output control valve, a differential pressure is developed across the seal from the seal flush lines to the intake of the pump. This allows the fluid flush to flow through the seals and into the multiphase fluid flow adding a liquid phase to the suction of the pump.

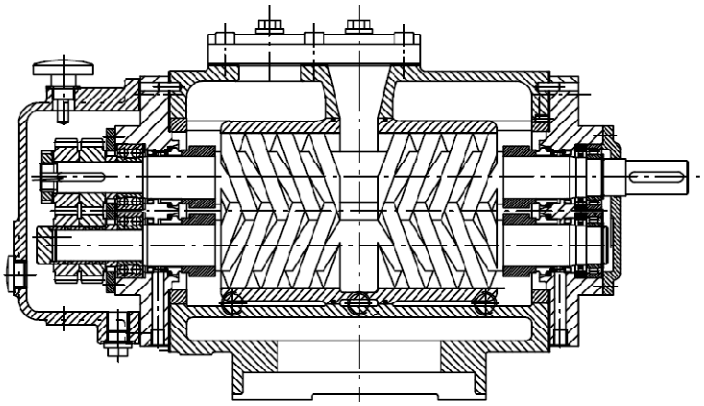

Figure 4.16 Cross Section View of the Particular Twin Screw Pump (Leistritz Corp. 2010)

Figure 4.16 is a cutaway of the received twin-screw pump. The following geometries were given by Leistritz and make up the volume the pump displaces for every shaft revolution

$$V_g = \frac{B^2 * s * X}{4x10^8}$$

where the pump pitch *s* is 40 mm, the outer diameter of the screw *B* is 82mm, and the *X* factor is an empirical value based on the rotor design. The *X* value for the L4MG 82/40 is 3.6. The final displacement is equal to 0.242 l/revolution. Converting the volume to gallons gives 0.0639 gallons/revolution. Multiplying the volume/revolution by the rotational speed will give a theoretical flow rate for each of the running speeds in this investigation. This information will be used to calculate the volumetric efficiency.

4.3 Data Acquisition and Sensors

To track the operating conditions of the pump, a wide variety of sensors were implemented to monitor the performance of the pump. LabView 2009 was used to write the data acquisition program based on National Instruments data acquisition cards.

Figure 4.17 and Figure 4.18 show the user interface for the data acquisition system. The LabView front panel is the way the user interacts with the pumping system. From this view all of the vital pressure, temperature, and flow readings from the sensors can be seen and recorded. This is also where the outputs to the control valves are entered.

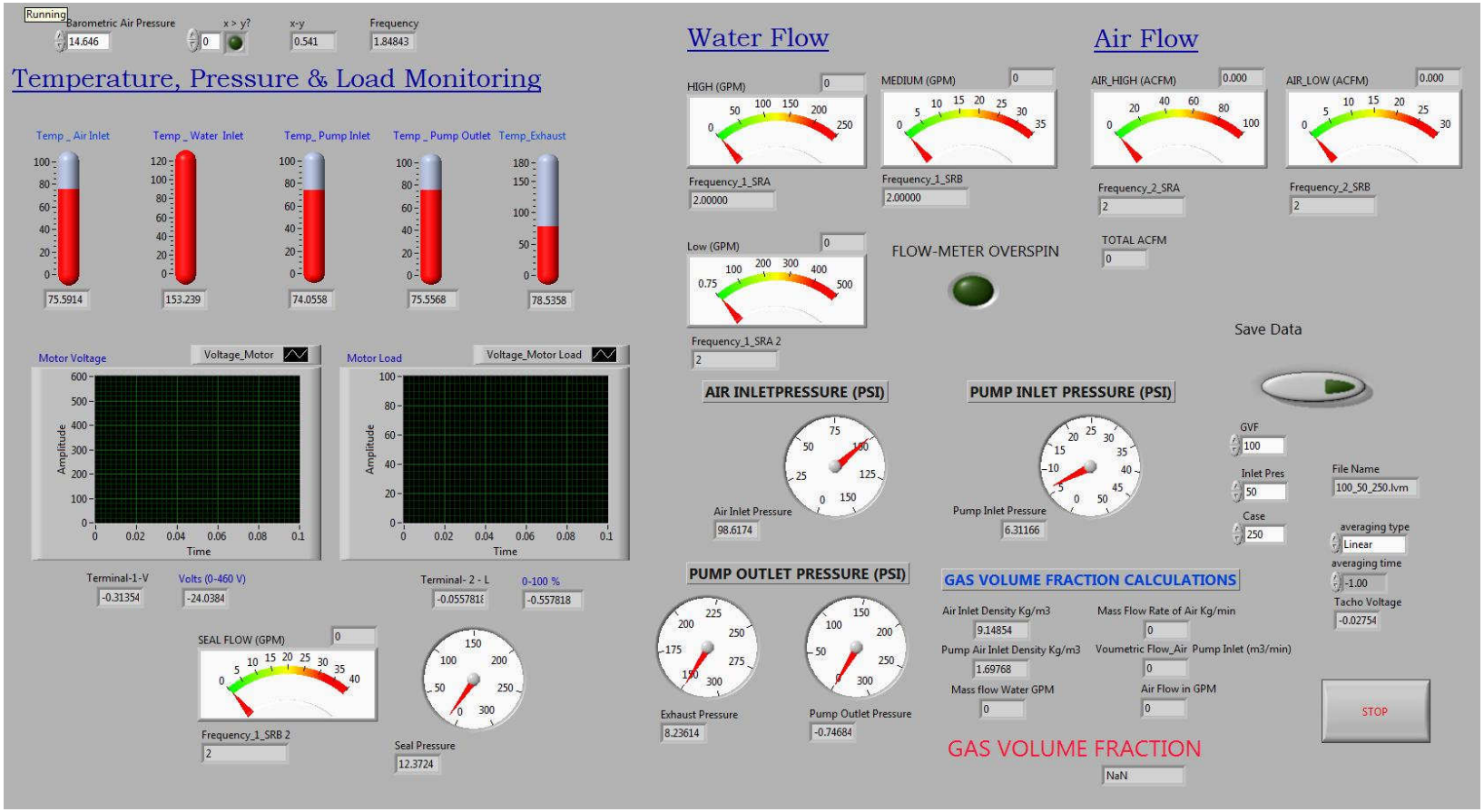

Figure 4.17 LabView Front Panel 1

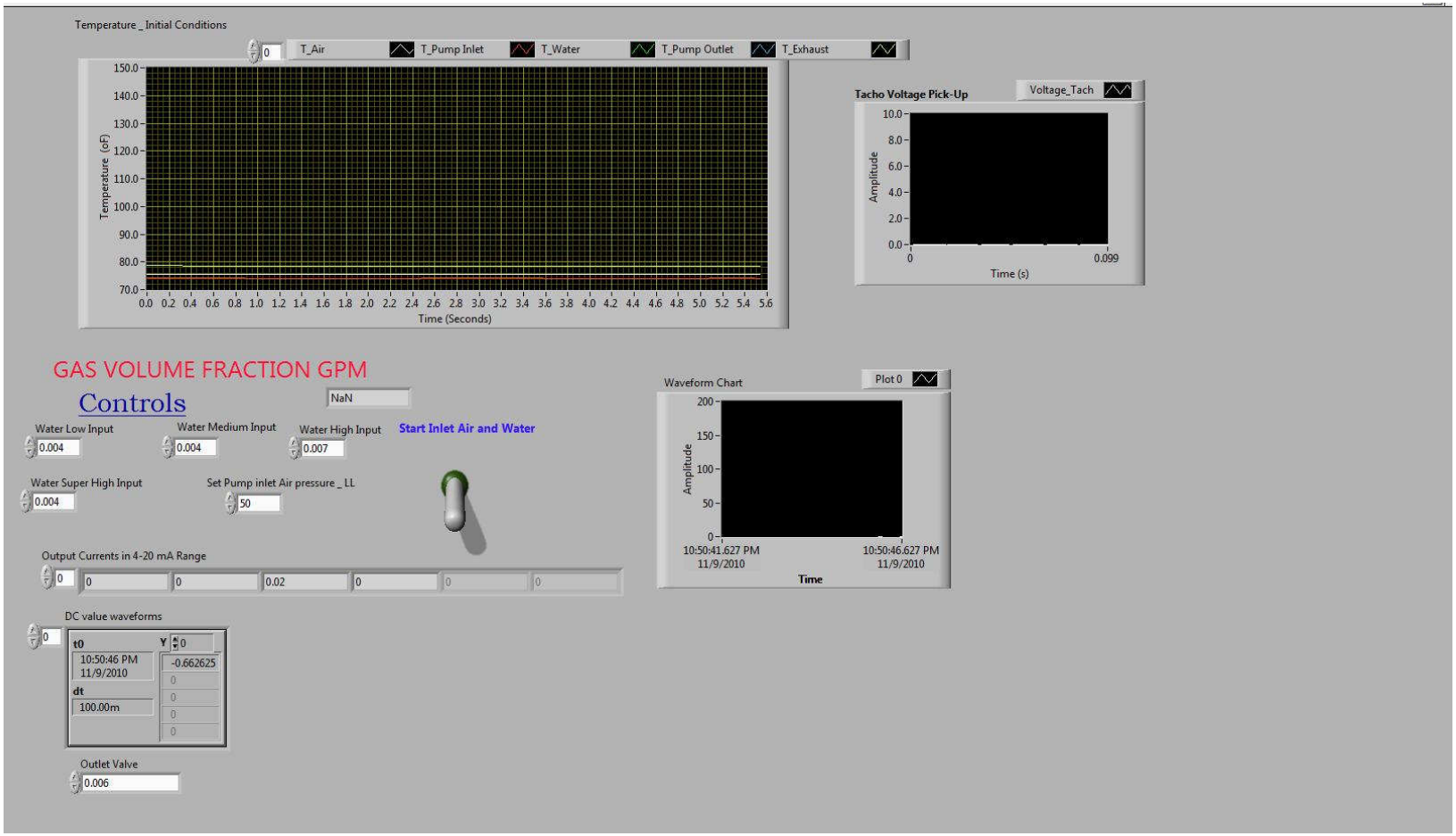

Figure 4.18 LabView Front Panel 2

The pressure sensors used were PX481 A series from Omega Engineering. The design specifications are as follows:

- Excitation: 9 to 30 Vdc
- Output: 1 to 5 Vdc (3 wire)
- Load Resistance: 50,000 Ω minimum
- Accuracy: 0.3% BFSL maximum (Includes linearity, hysteresis and repeatability)
- Range: Varies based on location in the system
    - Water Inlet: 0-150 psi
    - Air Inlet: 0-150 psi
    - Pump Inlet: 0-200 psi
    - Pump Exhaust: 0-300 psi
    - Seal Pressure: 0-500 psi
    - Outlet Valve: 0-300 psi

The temperature sensors used were thermocouples sourced from Omega Engineering. They were constructed according to the following specifications:

- T-Type thermocouples
- 304 Stainless steel sheath
- Accuracy: ±0.22°F
- Ungrounded $1/16^{th}$ inch and $1/8^{th}$ inch probe diameters

The thermocouples were integrated with a National Instruments NI9213 with a built-in CJC that converts the voltage potential of the thermocouple and translates it into a reading for the LabView program.

Two types of flow meters were used: one for air and the other for water. All of the fluid flow meters were turbine meters and the working principle was identical between the two. A standard practice of making sure there was a length of smooth straight pipe

of 10*Diameter leading up to the meter and a 5*Diameter length of pipe exiting the meter. This ensures that there is no unnecessary turbulence entering the turbine meter. As the fluid enters the turbine meter, it passes through a set of vanes that further stabilize the flow. It then moves past a turbine and this fluid motion causes the turbine to rotate with a speed proportional to the fluid velocity. As the turbine rotates, the blades pass through a magnetic field generated by the sensors' magnetic pickup and generate an AC voltage pulse. The pulses send an output whose frequency is proportional to the volumetric flow rate.

The turbine meters specifications are as follows

Air:

- High Flow : 10-100 ACFM
- Low Flow: 2-32 ACFM

Water:

- Super High: 40-650 GPM
- High: 25-250 GPM
- Medium and Seal: 5-35 GPM
- Low: 0.75-7.5 GPM

The turbine meters produced an output of 30 mV p-p sine waves and Omega IFPX-W signal conditioners were used to convert output from the turbine meter to a digital signal. The accuracy for both the liquid and gas turbine meters is ±1% of the flow reading. The data is then transferred via a network connection directly to the Ethernet port on the PC and read directly by the LabView software.

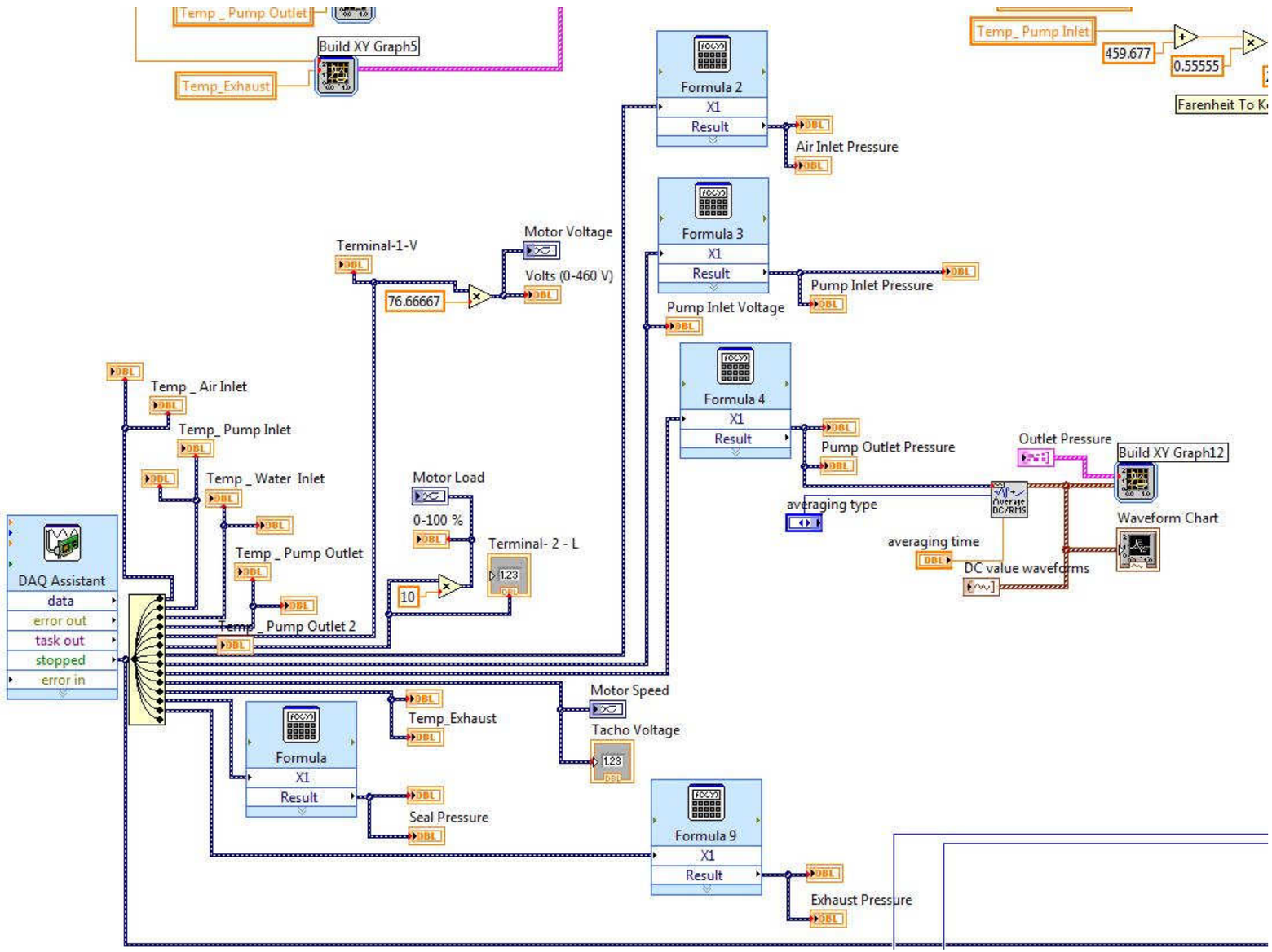

Figure 4.19 Analog In Block Diagram

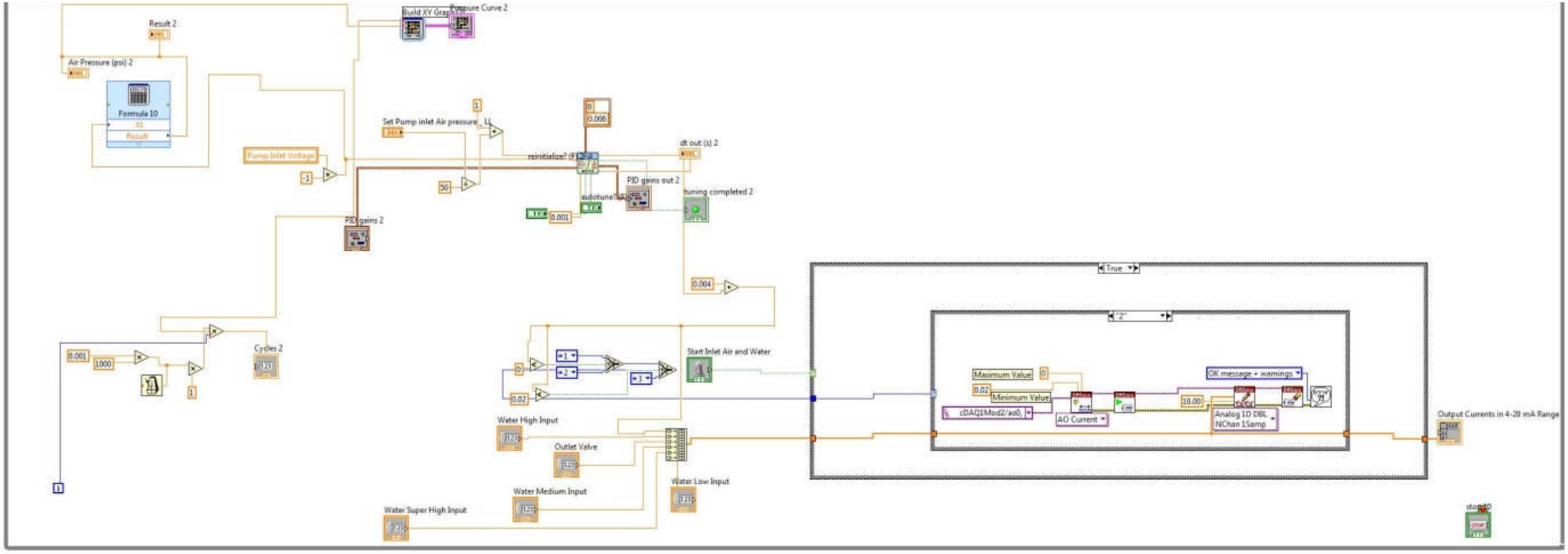

Figure 4.20 PID Block Diagram

Figure 4.19 shows a block diagram of the sensor inputs. The DAQ assistant was used as the main means for interpreting the sensor data from the USB to the analog data recorded by the program. A typical uncertainty analysis is shown in APPENDIX C TYPICAL UNCERTAINTY ANALYSIS for typical calculations performed throughout this thesis. The Kline and McClintock technique for calculating uncertainty was used.

The control valves were all of a similar type and construction and consisted of Masonneilan : Camflex Series Rotary Control Valves. The valves operated by means of an electro-pneumatic actuator and were controlled by a 4-20 mA signal sent from a National Instruments NI-9265 unit. The controls were an analog output that was manually set in the LabView software. There was no PID control on the valves used to supply the water, and the operator has to adjust the current outputs.

The air is controlled by a PID loop within the LabView program and used the following:

- NI LabVIEW PID and Fuzzy Logic Toolkit
- Auto-tuning function to improve performance of PID loop
- Air pressure control : Closed loop using PID

Using the PID loop, it was possible to set the inlet pressure at a constant value and allow the computer to adjust the output to the control valves based on varying operating conditions and GVF. The process block diagram appears in Figure 4.20.

The following hardware was used to interpret the signals from the variety of sensors, to send, and to input to the PC via a USB connection.

NI9205- A2D Convertor for Analog Sensors:

- 32-Ch ±200 mV to ±10 V
- 16-Bit
- 250 kS/s (Analog Input Module)

NI9213- Temperature ATD Convertor:

- Built-in CJC (cold-junction compensation)
- High-speed mode for up to 1,200 S/s (aggregate)

NI9265 – Analog Outputs

- 4-Channel
- 100 kS/s
- 16-Bit
- 0 to 20 mA (Analog Output Module)

Table 4.1 shows a complete list of the sensors being used.

Table 4.1 List of Sensors

Sensor #	Symbol	Measured Quantity	Principle	Type/Manufacturer
1	P_a	Pressure – Air Inlet	Solid State	Omega- PX 481 series
2	P_p	Pressure– Pump Inlet		
3	P_e	Pressure – Pump Exhaust		
4	P_o	Pressure – Outlet		
5	P_s	Pressure - Seal		
6	T_a	Temperature – Air Inlet	Peltier Effect	Omega- T type Ungrounded
7	T_w	Temperature -Water		
8	T_p	Temperature – Pump Inlet		
9	T_e	Temperature – Pump Exhaust		
10	T_o	Temperature – Outlet		
11	T_e	Temperature – Air Inlet		
12	T_s	Temperature – Seal		
13	Q_{w1}	Flow-Water-Super High	Turbine Meter	Omega FTB-111 Range- 40-650 GPM
14	Q_{w2}	Flow-Water- High		Daniel Range- 25-250 GPM
15	Q_{w3}& Q_s	Flow-Water-Medium and Seal		Omega FTB-1425 Range – 5-50 GPM
16	Q_{w4}	Flow-Water-low		Omega – FTB 1422 Range – 0.75-7.5
17	Q_{a1}	Flow- Air High	Turbine Meter	Daniel- 10-100 ACFM
18	Q_{a2}	Flow- Air Medium		Omega – FTB- 935 2-28 ACFM

To start recording, the user selects a “Start Recording” button on the front panel and the data is stored in a .lvm (LabView Measurement) file. The files were indexed based on the specific test required. The data acquisition was capable of recording at 1000 samples/s and fulfilled the needs of the current investigation.

4.4 Gas Volume Fraction

Figure 4.21 shows the calculation done in LabView to display the real time GVF. The GVF is dynamic and can change with a change in inlet pressure, water flow rate, and any number of outside variables. To ensure that the correct GVF is achieved, it is necessary for LabView to display the actual GVF at all times during pump operation; and to ensure that the GVF is calculated at the pump inlet, a mass flow rate is calculated as the air enters the test cell. After the multiphase fluid is mixed in the inlet manifold and travels down the piping network to the pump, a temperature and pressure reading is taken at the pump inlet. Using the ideal gas law, a volumetric flow rate is calculated in real time. The inlet volumetric flow rates determines the GVF. A sample calculation that shows the entire process appears in APPENDIX A SAMPLE GVF CALCULATION.

.

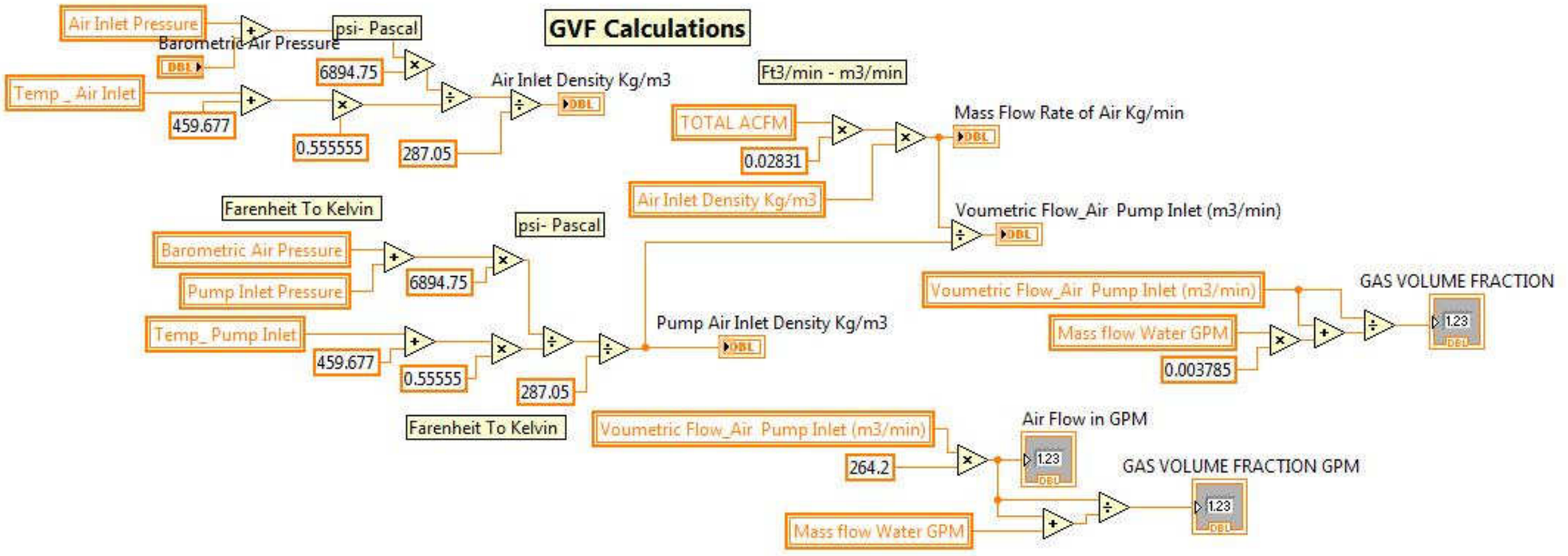

Figure 4.21 LabView GVF Calculation

5. RESULTS AND DISCUSSION

This section presents the results and discussion of the work presented in the current investigation. Section 5.1 will present the results from the steady state pump performance and section 5.2 will present the results from the temperature rise study. The first section will focus on the steady state performance of the Leistritz system under high GVF (>90%) conditions, the effect of inlet pressure on performance, and the effect of different operating speeds. Table 5.1 shows the matrix used to determine the parameters specified for the investigation.

Table 5.1 Parameter Matrix

GVF	ΔP (psi)	Inlet P (psi)
0	50	10
50	100	50
90	150	
95	200	
98	250	
99		
100		

The second section takes a more in depth look at the effect of temperature on the pump system including the temperature rise associated with temperature of the seal recirculation and the thermal effect on pump performance. The results obtained from this study were found operating the pump at 100% GVF under a variety of pressure differentials between the pump suction and exhaust. One hundred percent GVF is the most interesting data point regarding field operation as it is the most extreme condition the pump will be subjected to in the field.

In the following section, the data presented will be associated with one of two control volumes: a pump assembly control volume and a pump only control volume. The difference is the inclusion of the seal flush rate. For the information such as the total flow rate and global GVF, the control volume is assumed to be the entire Leistritz assembly. This assumption is possible because of the high efficiency knockout boot. The knockout boot is assumed to be nearly 100% efficient at separating all water from the exhaust flow. Therefore, the total flow and GVF entering and exiting the pump assembly is assumed to remain constant.

The second control volume is used for calculating the pump efficiencies. The pump is designed to work with a liquid recirculation system that injects a specified amount of water into the inlet of the pump because all of the fluid going through the pump must be accounted for. This applies to the volumetric and mechanical efficiencies. While the inlet and the outlet of the pump assembly are considered to have constant flow and GVF properties this assumption cannot be used for the pump control volume due to the amount of liquid recirculation. It is very important that the total volume, GVF, and mechanical power are calculated with the seal flush liquid incorporated. The fluid stored in the liquid recirculation system can also be referred to as the seal flush liquid.

The following results' sections show the trends discovered in the current investigation using typical figures that summarize the results found for a range of operating conditions. A complete collection of figures and plots appear in APPENDIX D SUPPLEMANTARY PLOTS.

.

5.1 Steady State Performance

5.1.1 Volumetric Efficiency

Figure 5.1 to Figure 5.9 characterize the volumetric efficiency measured under the prescribed matrix of parameters. Figure 5.1 and Figure 5.2 show how the volumetric efficiency changes as a function ΔP, GVF, and speed. Remember that the volumetric efficiency is given by

$$\eta_{\mathrm{Vol}} = \frac{\mathrm{Q}}{\mathrm{Q_{th}}}$$

where *Q* is the actual fluid flow through the pump assembly, not including the seal flush flow, measured by the LabView data acquisition system and Q_{th} is given by

$$\mathrm{Q_{th}} = \mathrm{V_g} * \mathrm{n}$$

and V_g was given by the physical dimensions of the pump

$$\mathrm{V_g} = \frac{\mathrm{B}^2 * \mathrm{s} * \mathrm{X}}{4\mathrm{x}10^8}$$

The two inlet cases are presented by the two figures. The contours at each speed stay consistent between the two inlet pressure cases. The results remain consistent with previously published information on the performance of twin-screw pumps.

As the pump speed is increased the volumetric efficiency increases from about 50% to a mid 80%. It is interesting that the difference between 1800 and 2700 RPM is drastic while the difference between 2700 and 3600 RPM is nearly indistinguishable. This would indicate that to retain a sufficient volumetric efficiency that the pump speed should be kept above 2700 RPM.

It is important to understand why the contour shown at 1800 RPM appears incomplete. The rotational speed of the pump is unable to overcome the amount of slip found while operating above 150 psi of differential pressure. If the differential pressure is too great, the pump is rendered inoperable at the half speed conditions. The consequences of this condition result in zero flow entering or exiting the pump assembly control volume.

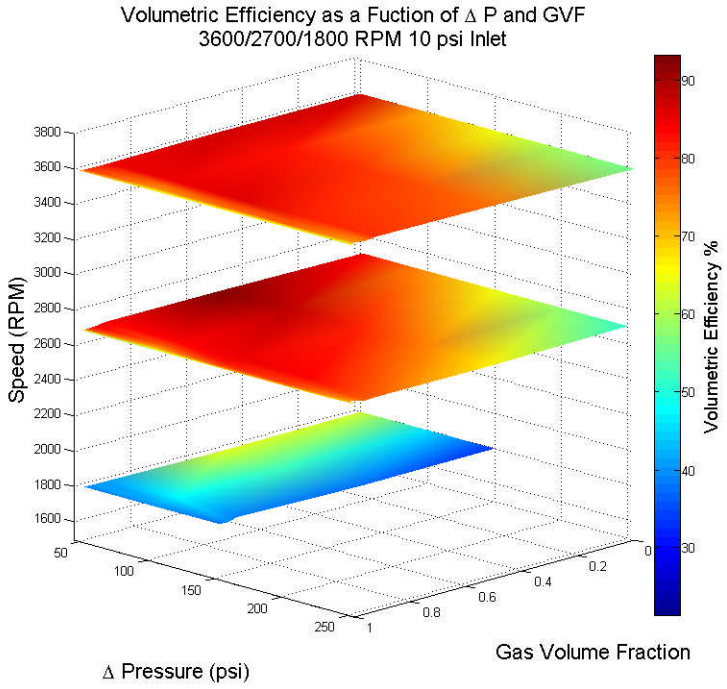

Figure 5.1 Volumetric Efficiency Summary (All Speeds, 10 psi Inlet)

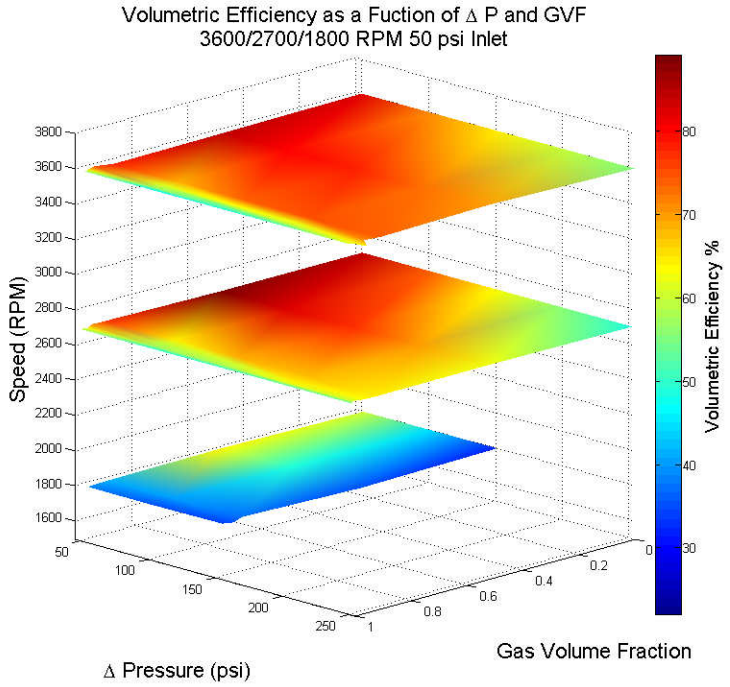

Figure 5.2 Volumetric Efficiency Summary (All Speeds, 50 psi Inlet)

Slight differences between Figure 5.1 and Figure 5.2 are shown by Figures 5.3, 5.4, and 5.5. The last three figures represent the differences between the inlet pressure conditions. Looking at the same pump speed and distinguishing between the inlet pressures shows much more defined differences in the pump performance. The 10 psi inlet condition shows increased volumetric efficiency for all three speed conditions. A less abrupt loss of efficiency at the high GVF occurs at the lower inlet pressure.

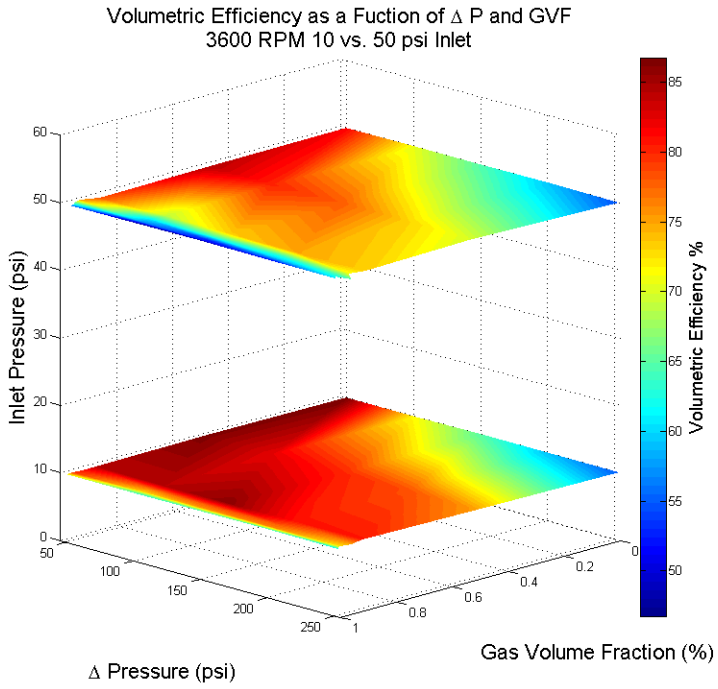

Figure 5.3 Volumetric Efficiency Summary (3600 RPM, Both Inlet Pressures)

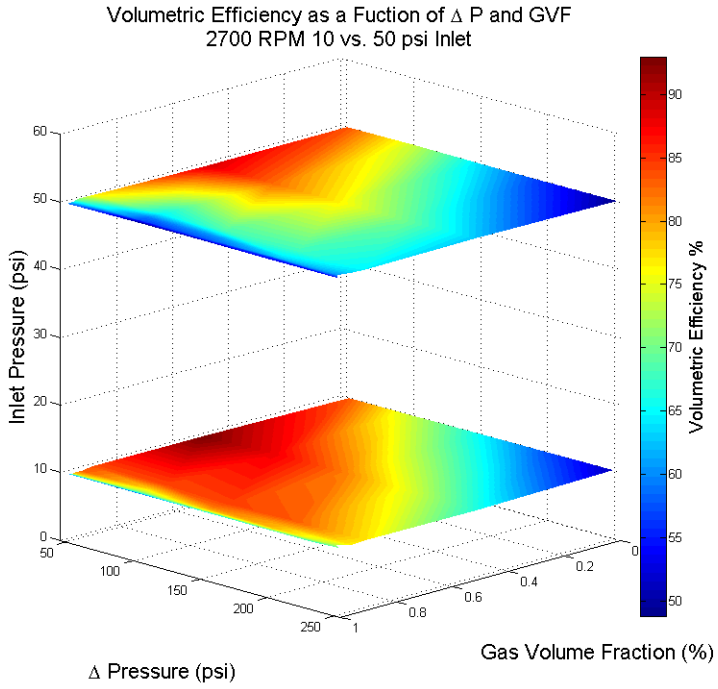

Figure 5.4 Volumetric Efficiency Summary (2700 RPM, Both Inlet Pressures)

Figure 5.5 again shows how the performance of the pump running at half speed severely suffers. The pump cannot overcome the amount of internal slip that occurs along the screws and cannot pass any liquid through the pump assembly control volume.

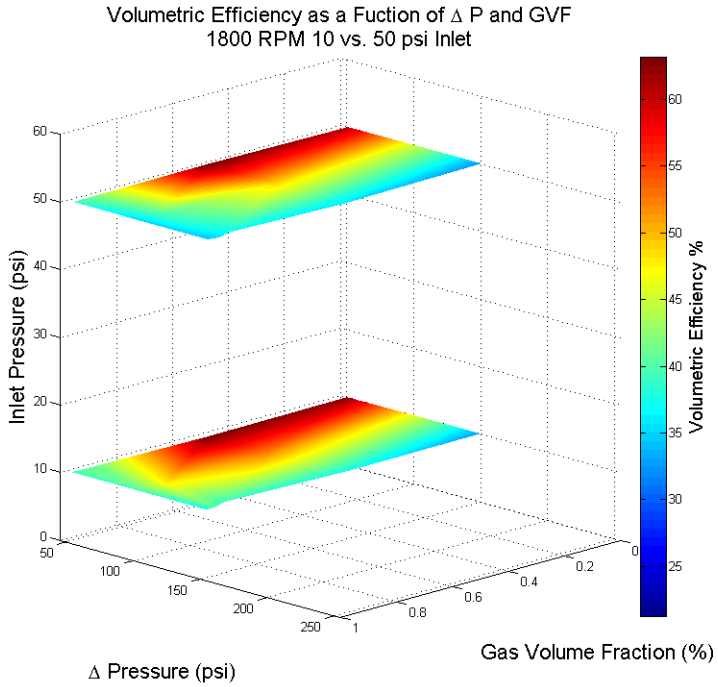

Figure 5.5 Volumetric Efficiency Summary (1800 RPM, Both Inlet Pressures)

An alternate interpretation of the volumetric efficiency appears in Figure 5.6 and Figure 5.7. The line plots show the exact shape of the previously presented contours. The typical shape of the contour is shown by the 3600 RPM operating speed for both 10 and 50 psi inlet conditions. These plots represent the 2700 and 1800 RPM line plots found in the Appendix.

The basic shape of Figure 5.6 and Figure 5.7 remains the same between the two inlet conditions. The trends for 0 and 50% GVF are completely different than the 90%+ GVF. This agrees with previously published material where the volumetric efficiency increases up to a certain GVF and then starts to decline. The decline of volumetric efficiency occurs at 90% GVF and decreases for each increase of GVF up to 100% gas. It is interesting that the volumetric efficiency is constant and even increases with an increase in differential pressure. This can be attributed to the increase of seal flush fluid being introduced to the pump inlet due to the increased pump exhaust pressure.

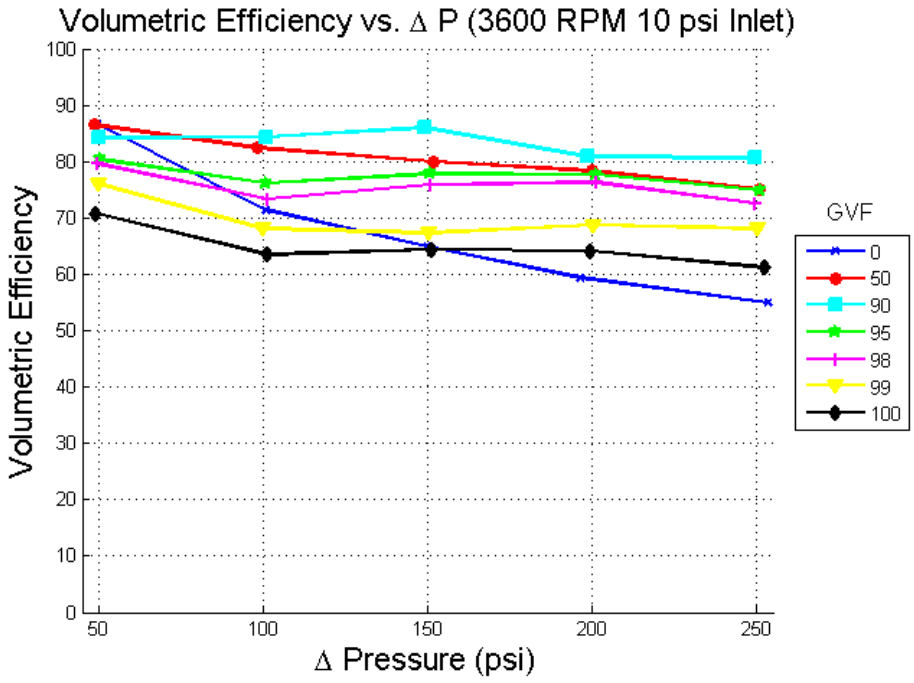

Figure 5.6 Volumetric Efficiency vs. ΔP (3600 RPM, 10 psi Inlet)

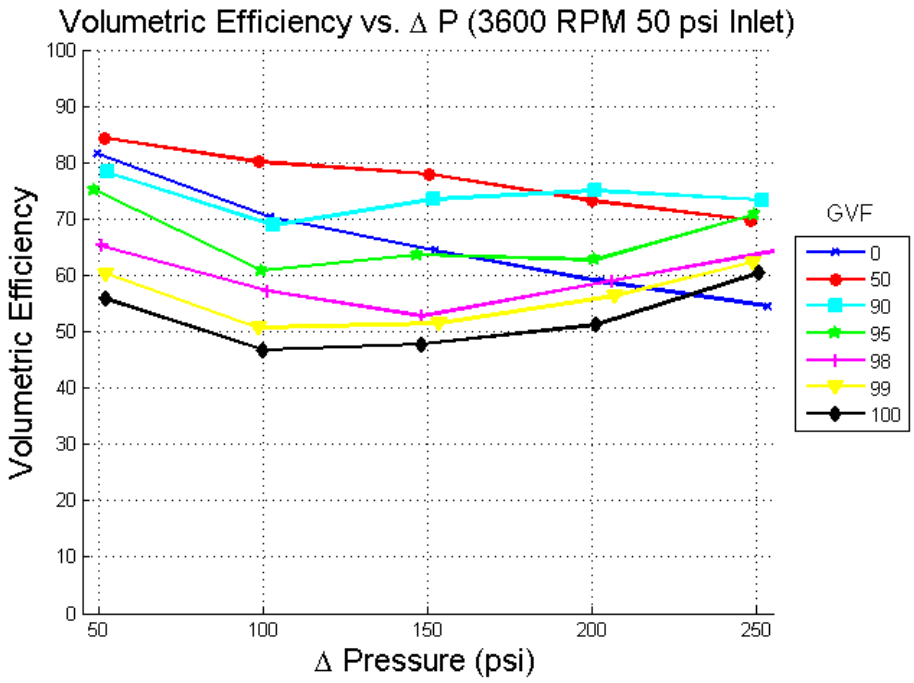

Figure 5.7 Volumetric Efficiency vs. ΔP (3600 RPM, 50 psi Inlet)

Figure 5.8 and Figure 5.9 compare the volumetric efficiencies between 1800 and 3600 RPM for the 10 and 50 psi inlet condition. It is unnecessary to show the volumetric efficiency for 2700 RPM because it lays directly on top of the volumetric efficiency found for 3600 RPM. Increasing the pump speed from 1800 to 3600 RPM drastically increases the volumetric efficiency. Note that the volumetric efficiencies for the 10 psi inlet are higher than the 50 psi inlet condition. The lower inlet pressure also reduces the spread of efficiencies. At a 50 psi inlet the average difference between 90 and 100% GVF is 23% compared to 18% for the 10 psi inlet.

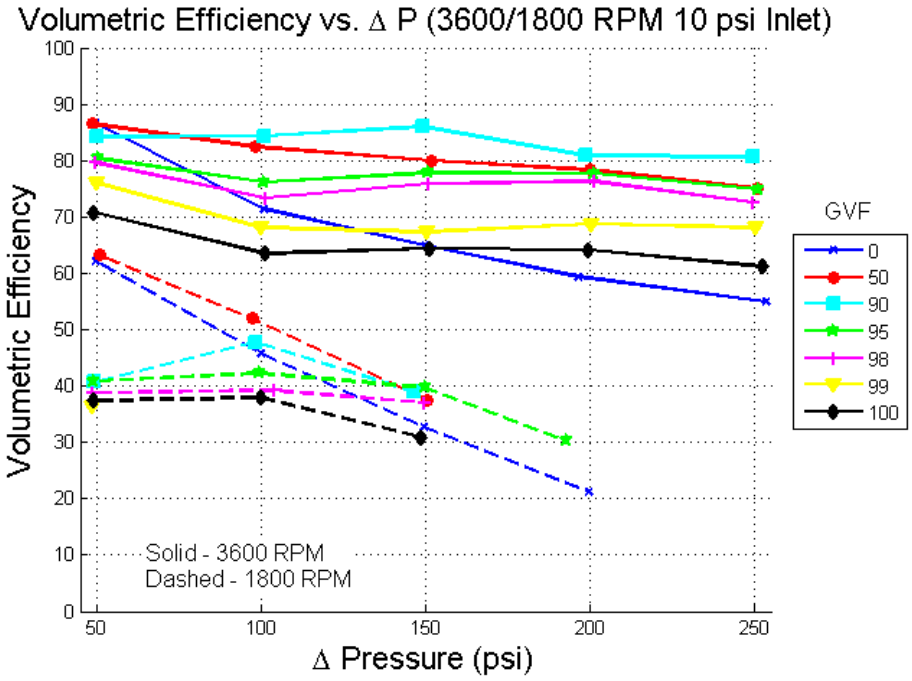

Figure 5.8 Volumetric Efficiency vs. ΔP (3600 and 1800 RPM at 10 psi Inlet)

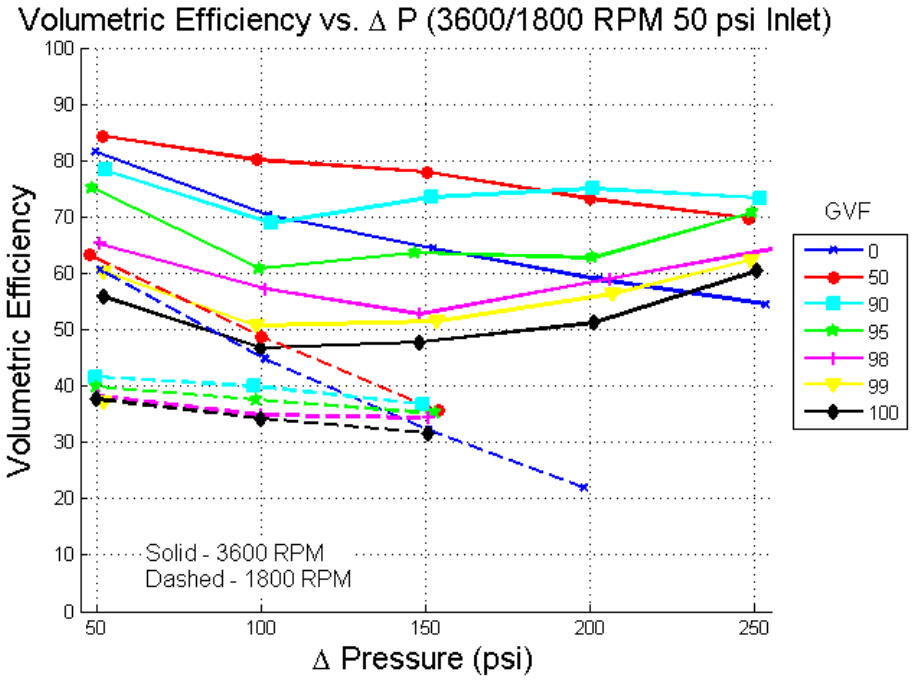

Figure 5.9 Volumetric Efficiency vs. ΔP (3600 and 1800 RPM at 50 psi Inlet)

The previous figures describing the volumetric efficiency were calculated using the total flow through the pump including the seal flush. This information is indicative of how the pump is performing but an overall look at the system performance is necessary. Figure 5.10 and Figure 5.11 show the volumetric efficiency calculated using the assembly as the control volume. The assembly volumetric efficiency only calculates the fluid entering and exiting the assembly and does not include the seal flush fluid. The following figures show a lower volumetric efficiency using assembly control volume as opposed to the pump control volume.

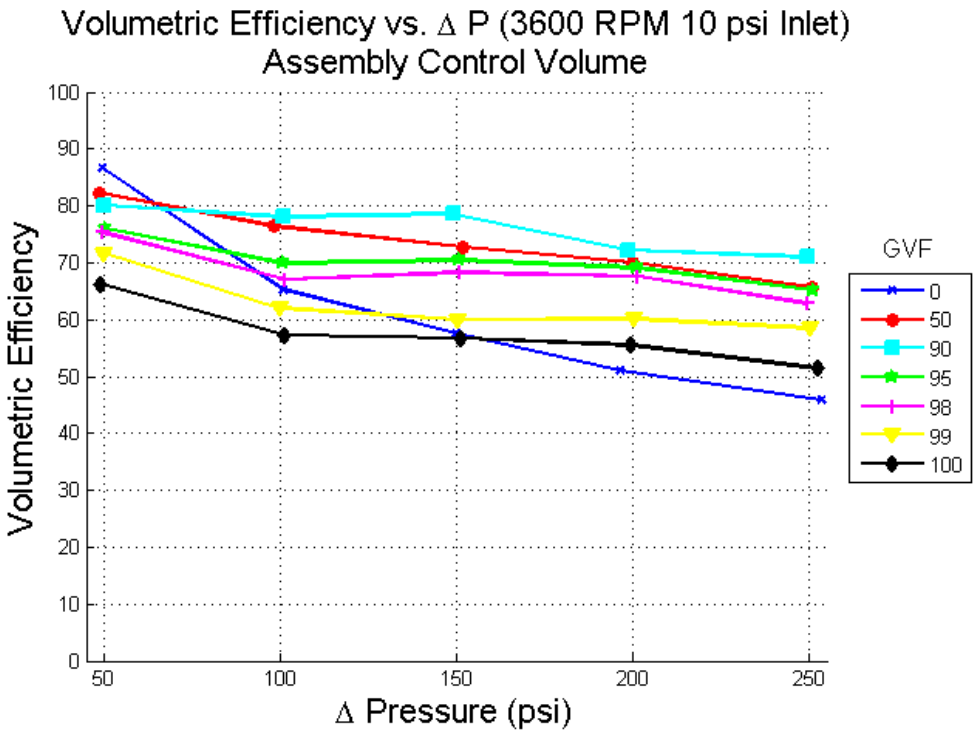

Figure 5.10 Volumetric Efficiency vs. ΔP (3600 RPM, 10 psi Inlet, No Flush)

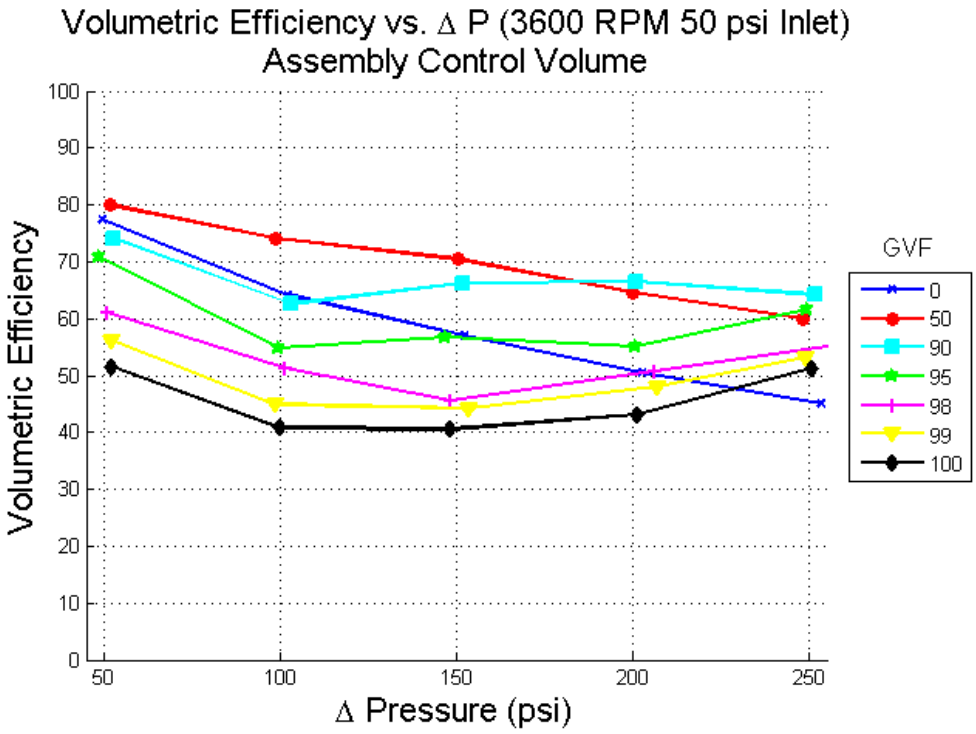

Figure 5.11 Volumetric Efficiency vs. ΔP (3600 RPM, 50 psi Inlet, No Flush)

5.1.2 Total Flow

Compared to the volumetric efficiency, the total flow presented in Figure 5.12 to Figure 5.18 represents the total flow entering and exiting the pump assembly and does not include the seal flush fluid. The total flow is simply the volumetric flow rate of air added to the flow rate of water. Figure 5.12 and Figure 5.13 show the comparison of flow for each pump speed at the 10 and 50 psi inlet conditions. For each increase in pump speed the total flow is increased. This is largely intuitive and follows the theory behind positive displacement pumps. As the speed increases the total volume moved is increases.

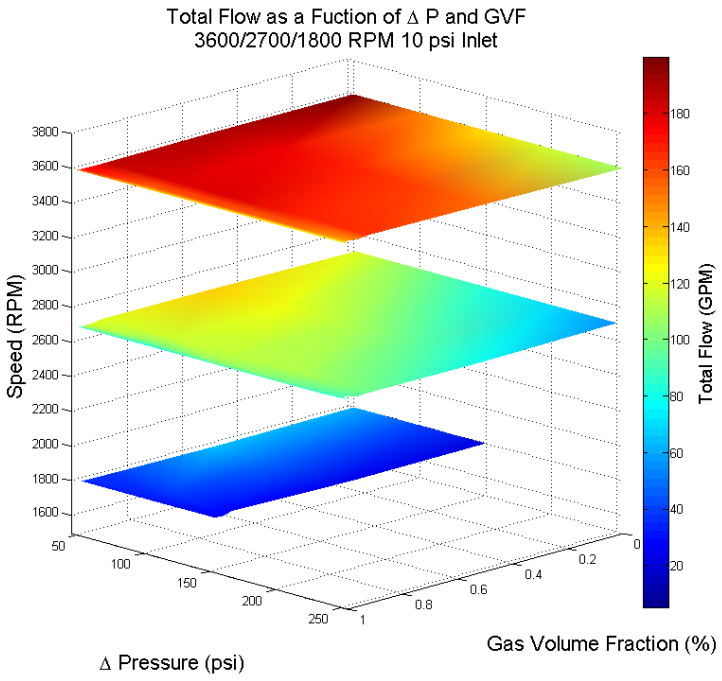

Figure 5.12 Total Flow Summary (All Speeds, 10 psi Inlet)

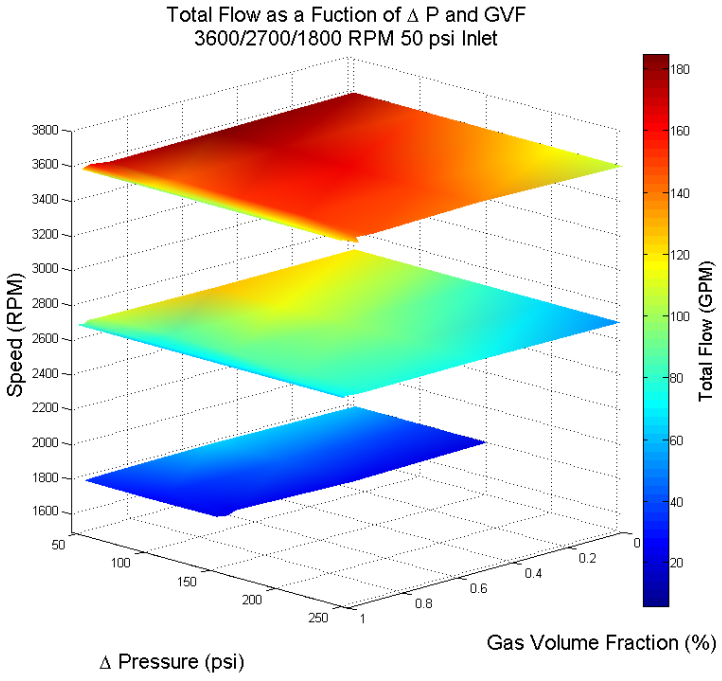

Figure 5.13 Total Flow Summary (All Speeds, 50 psi Inlet)

Comparing the performance between the different inlet pressure conditions shows that the 10 psi inlet has a higher total flow than the 50 psi inlet condition for each of the three pump speeds. The results agree with the volumetric efficiencies and have the same trend/basic contour as well.

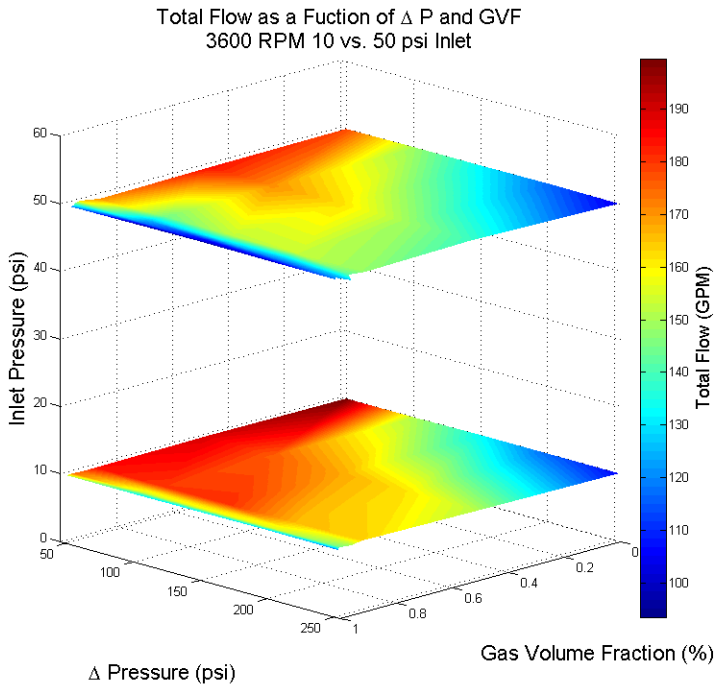

Figure 5.14 Total Flow Summary (3600 RPM, Both Inlet Pressures)

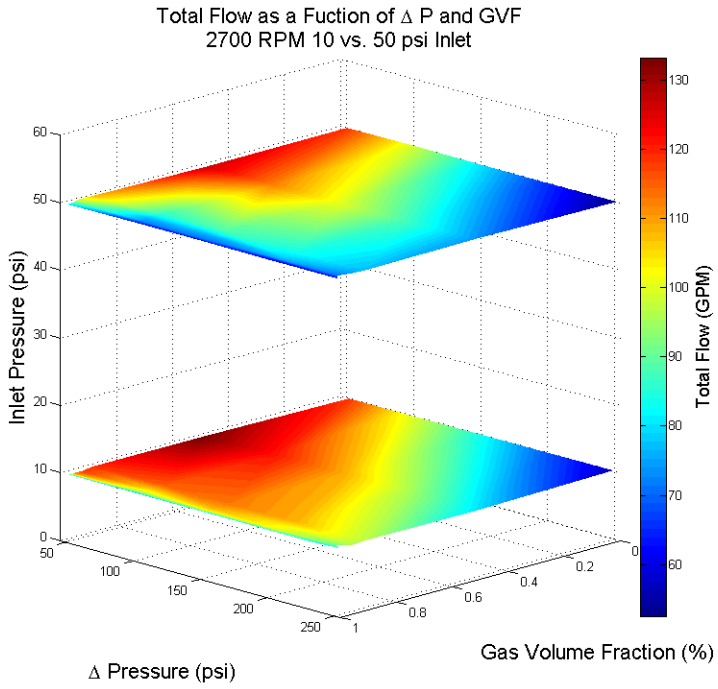

Figure 5.15 Total Flow Summary (2700 RPM, Both Inlet Pressures)

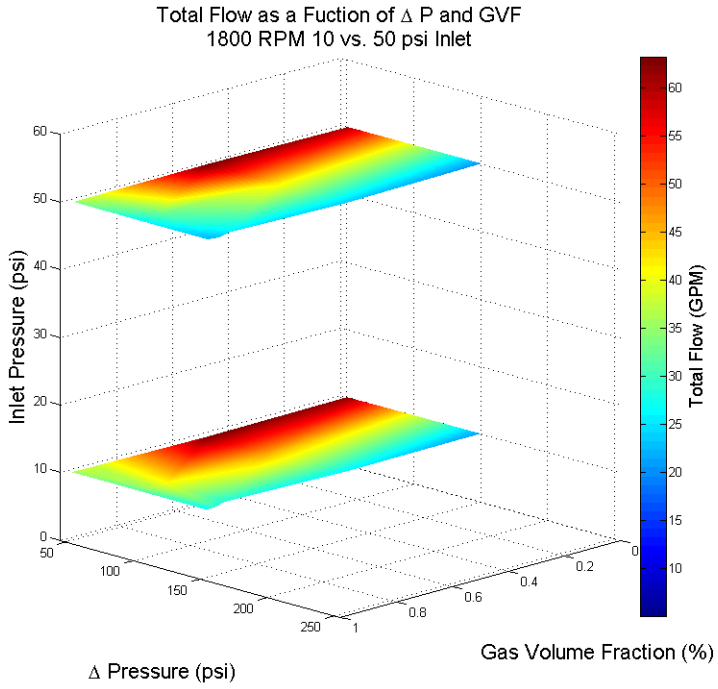

Figure 5.16 Total Flow Summary (1800 RPM, Both Inlet Pressures)

While the contour plots follow similar trends as the volumetric efficiency, the line plots show some important differences. Figure 5.17 and Figure 5.18 show how the total flow changes with differential pressure and GVF. At the 10 psi inlet condition the total flow entering the pump assembly continuously decreases indicating the increased slip that occurs due to the higher exhaust pressure relative to the constant inlet pressure.

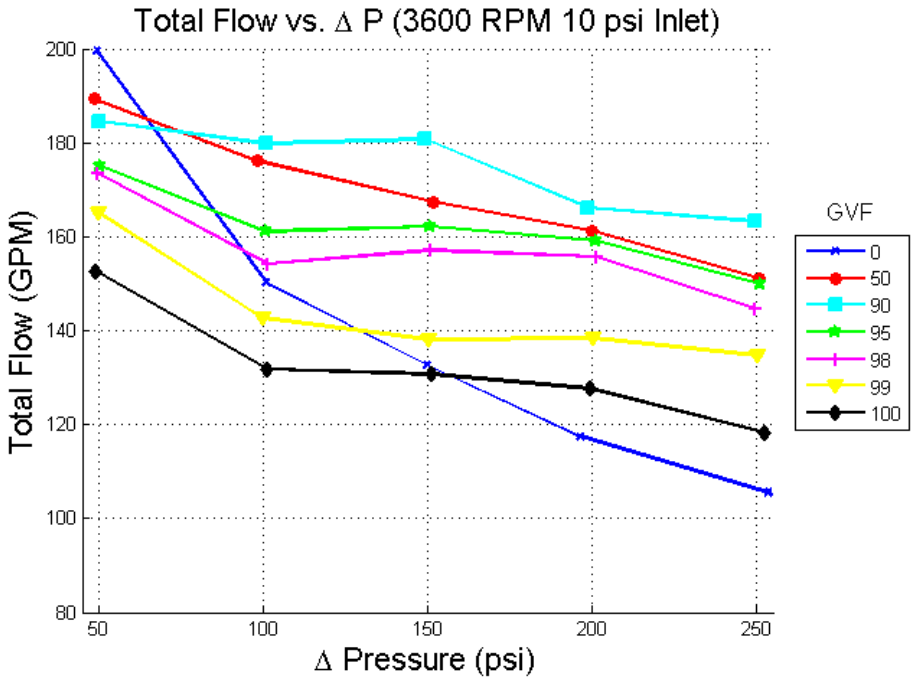

Figure 5.17 Total Flow vs. ΔP (3600 RPM, 10 psi Inlet)

Figure 5.18 shows a strange phenomenon that follows very similarly to the volumetric efficiency trend where the total flow increases as the differential pressure increases. Similarly to the volumetric efficiency, the total flow at the 50 psi inlet is marginally less than the 10 psi inlet and the span of values is greater as well.

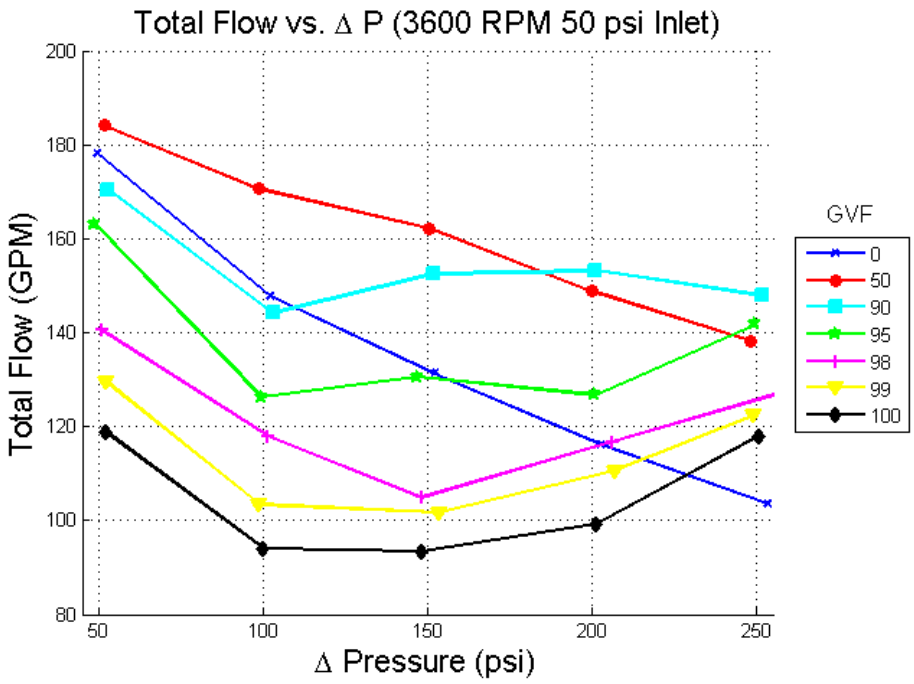

Figure 5.18 Total Flow vs. ΔP (3600 RPM, 50 psi Inlet)

5.1.3 Mechanical Efficiency

The mechanical efficiency shown from Figure 5.19 to Figure 5.25 is calculated directly from the VFD. The load on the VFD directly relates to the amount of horsepower being used to move the working fluid. The load is also referred to as the electrical power used by the motor to maintain the set pump speed. The percentage is calculated from knowing HP_{liq} and HP_{gas}. The horsepower to move the multiphase fluid from low to high pressure is divided by the output of the VFD. A more in depth look between the

calculated and measured power will be addressed in Figure 5.26 and Figure 5.27. Note that the mechanical efficiency is found by the following equations

$$HP_{liq} = \frac{Q_{liq} * \Delta P}{1714}$$

$$HP_{gas} = P_{in} * Q_{gas} \frac{\ln\left(1 + \frac{\Delta P}{P_{in}}\right)}{229.7}$$

$$HP_{net} = HP_{liq} + HP_{gas}$$

And the mechanical efficiency is then

$$\eta_{mech,VFD} = \frac{HP_{net}}{HP_{VFD}}$$

Figure 5.19 and Figure 5.20 compare the mechanical efficiency between the two inlet conditions at each specified pump speed. The two plots show a trend different from the volumetric efficiency where the 50 psi inlet has a higher efficiency than the 10 psi inlet at 3600 RPM. For the 10 psi inlet pressure the mechanical efficiency is fairly constant between 2700 and 3600 RPM while the 50 psi inlet shows an upward trend that continues up to 3600 RPM.

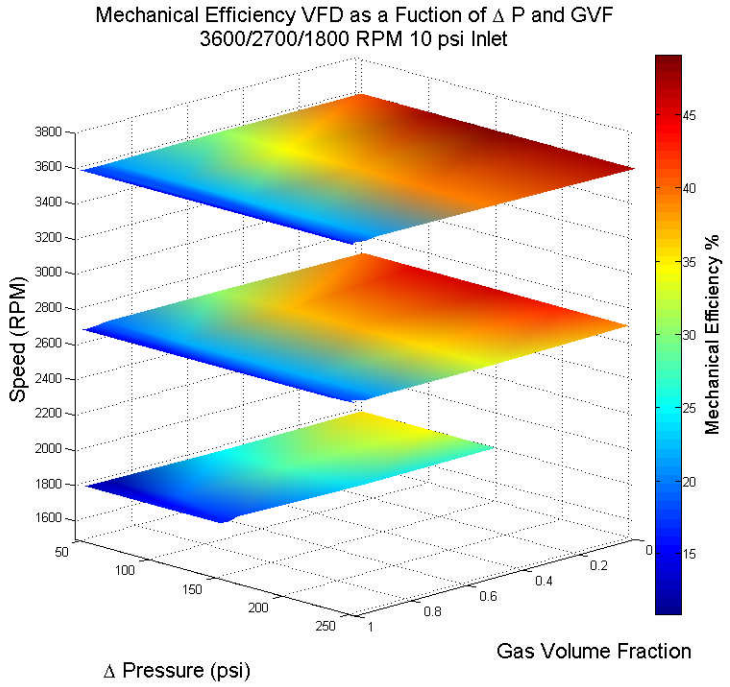

Figure 5.19 Mechanical Efficiency Summary (All Speeds, 10 psi Inlet)

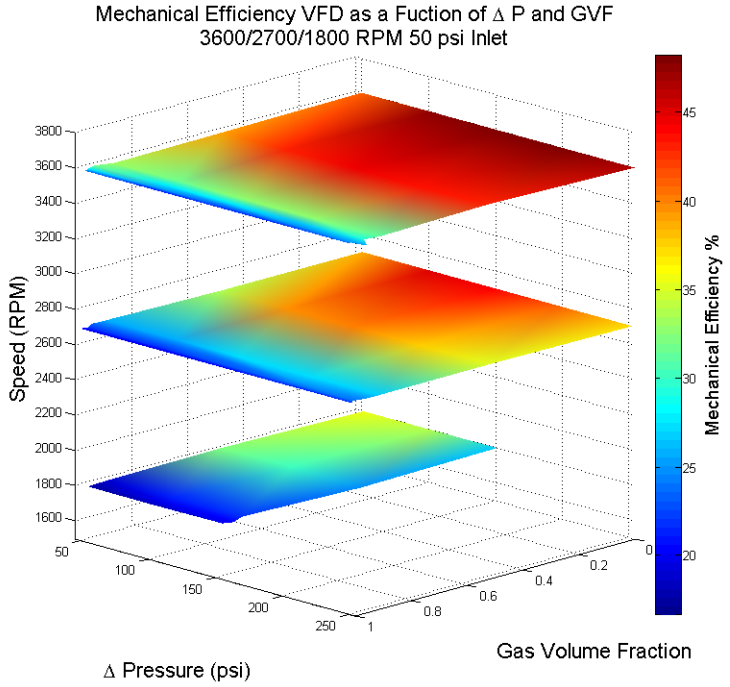

Figure 5.20 Mechanical Efficiency Summary (All Speeds, 50 psi Inlet)

The higher mechanical efficiency at 50 psi compared to 10 psi at the inlet can be seen more clearly in Figures 5.21, 5.22, and 5.23. The higher efficiency tends to stay in a more optimal zone as the GVF increases. The mechanical efficiency also shows less of a dependence on the differential pressure across the pump. The total pump slip drastically impairs the performance for the total flow and volumetric efficiency while the mechanical efficiency seems to depend more on the GVF.

Table 5.2 Horsepower Required to Compress Gas at 250 ΔP and 100% GVF

P_{in} (psi)	Q_{gas} (ACFM)	ΔP (psi)	HP_{gas} (HP)
10	15.34	250	2.18
50	15.34	250	5.98

The reason the mechanical efficiency is higher at 50 psi than 10 psi is because the power put into the fluid as calculated in Table 5.2. The increased power needed to compress the gas at 50 psi also increases the total HP_{net} being put into the system while the electrical power from the VFD stays constant. The electrical power from the VFD depends only on the differential pressure from the pump inlet to the pump outlet. Therefore, if the HP_{VFD} is held constant and HP_{net} increases the mechanical efficiency will also increase. This physical interpretation relates the increase of the mechanical efficiency to the increase of pump inlet pressure.

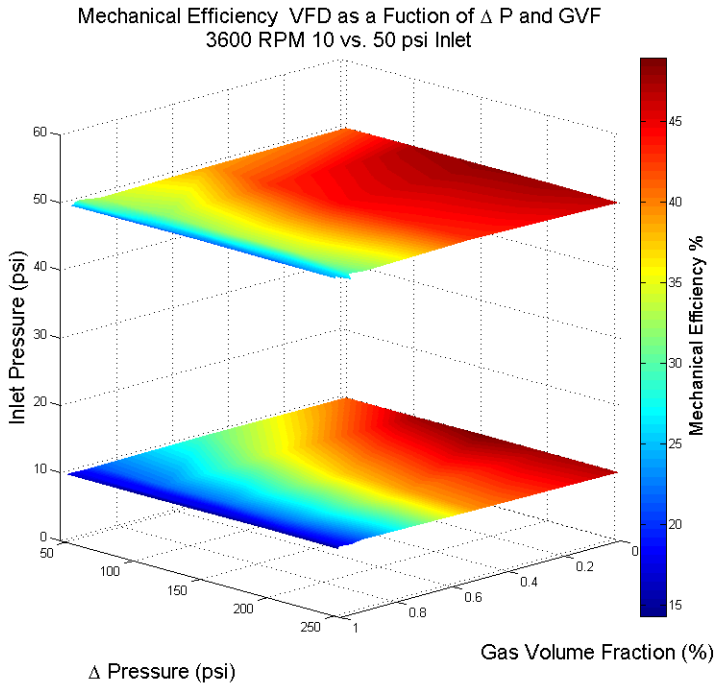

Figure 5.21 Mechanical Efficiency Summary (3600 RPM, Both Inlet Pressures)

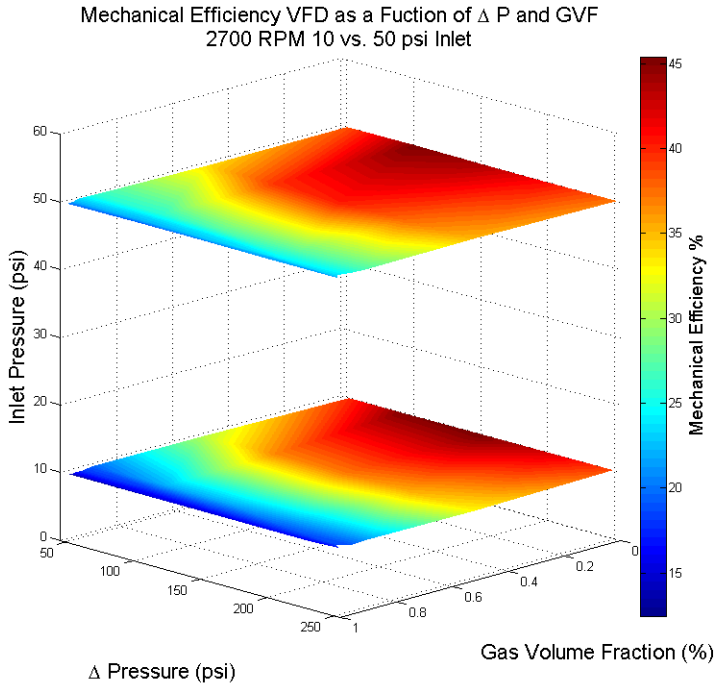

Figure 5.22 Mechanical Efficiency Summary (2700 RPM, Both Inlet Pressures)

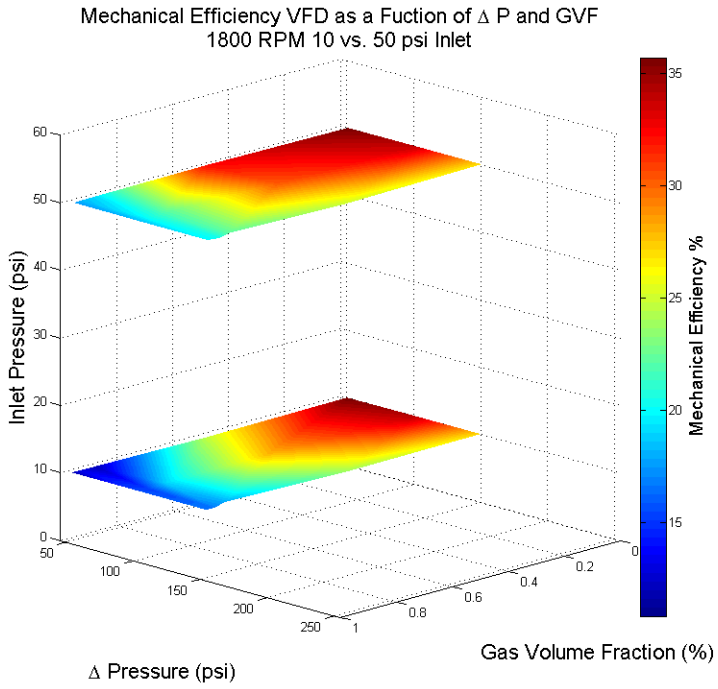

Figure 5.23 Mechanical Efficiency Summary (1800 RPM, Both Inlet Pressures)

The typical line plots at 3600 RPM show the common trend that occurs at 2700 and 1800 RPM. Unlike the volumetric efficiency the highest mechanical efficiency is at 0% GVF and trends downward to 100% GVF. No appreciable gains in efficiency occur as the differential pressure increases showing a higher dependence on GVF than differential pressure. While the spread between the volumetric efficiencies increased for the 50 psi inlet pressure, the opposite occurs in the mechanical efficiency. There is a 5% tighter grouping between the highest and lowest efficiency between the 50 and 10 psi inlet conditions.

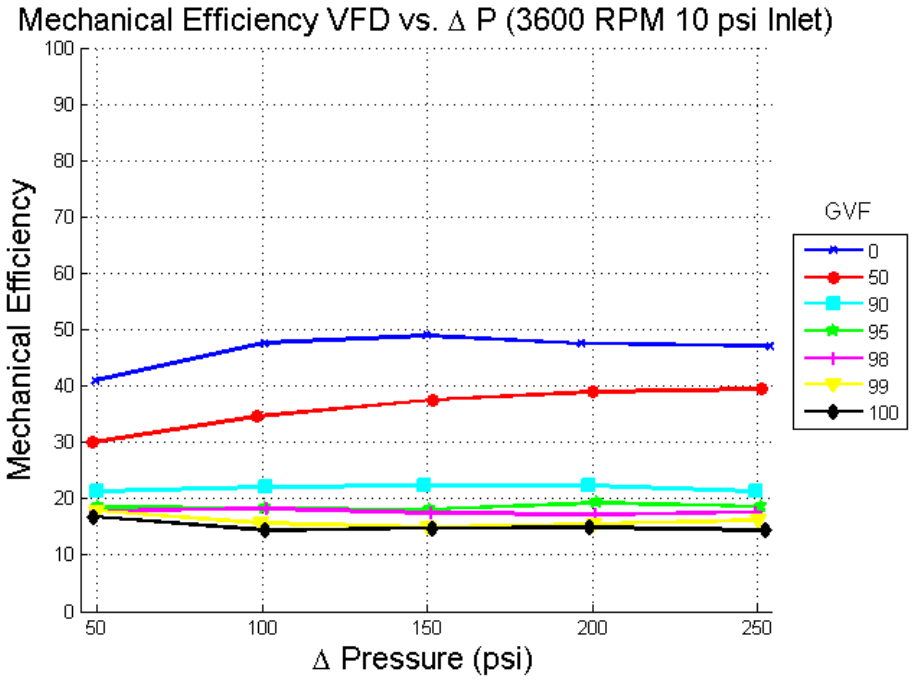

Figure 5.24 Mechanical Efficiency VFD vs. ΔP (3600 RPM, 10 psi Inlet)

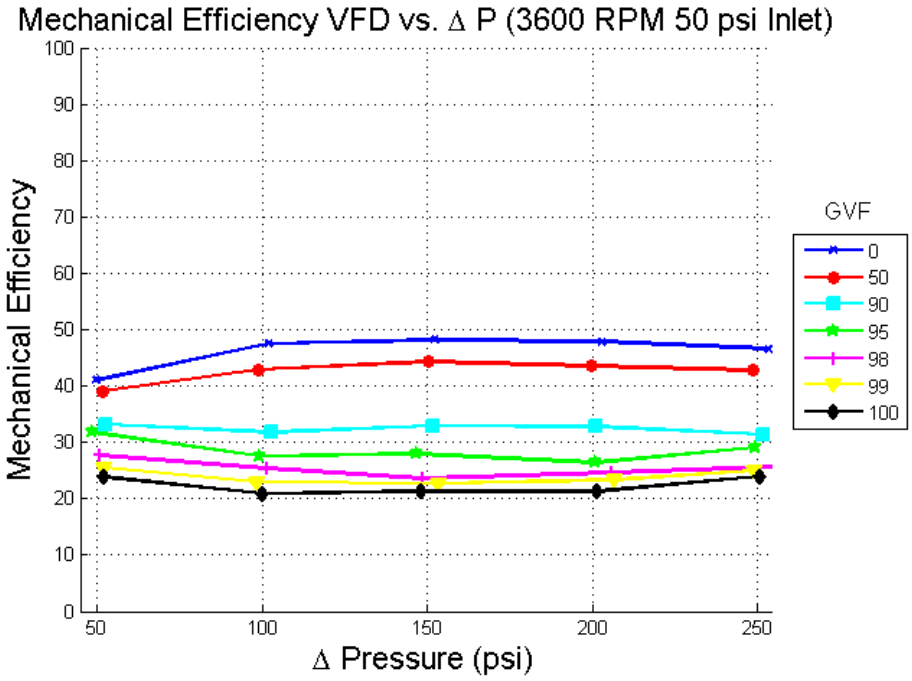

Figure 5.25 Mechanical Efficiency VFD vs. ΔP (3600 RPM, 50 psi Inlet)

It is important to understand the fundamental problem in calculating the mechanical efficiencies shown in Figure 5.26 and Figure 5.27. Using the formulas provided by Räbiger there is a situation that occurs when the GVF is 0% where the formula for mechanical efficiency reaches unity. This poses a problem because for a real process it is impossible to have a 100% efficiency. Comparing the actual efficiency with the calculated efficiency shows a similar trend and the same trend is preserved at both 10 and 50 psi inlet conditions. Note, that calculating the mechanical efficiency from the typical power equations will over predict the mechanical efficiency. There are losses not taken into account by the equations presented by Räbiger that become important once the heat rise between the pump inlet and exhaust become more drastic.

$$\eta_{\mathrm{mech,calc}} = \frac{\mathrm{HP_{net}}}{\mathrm{HP_{calc}}}$$

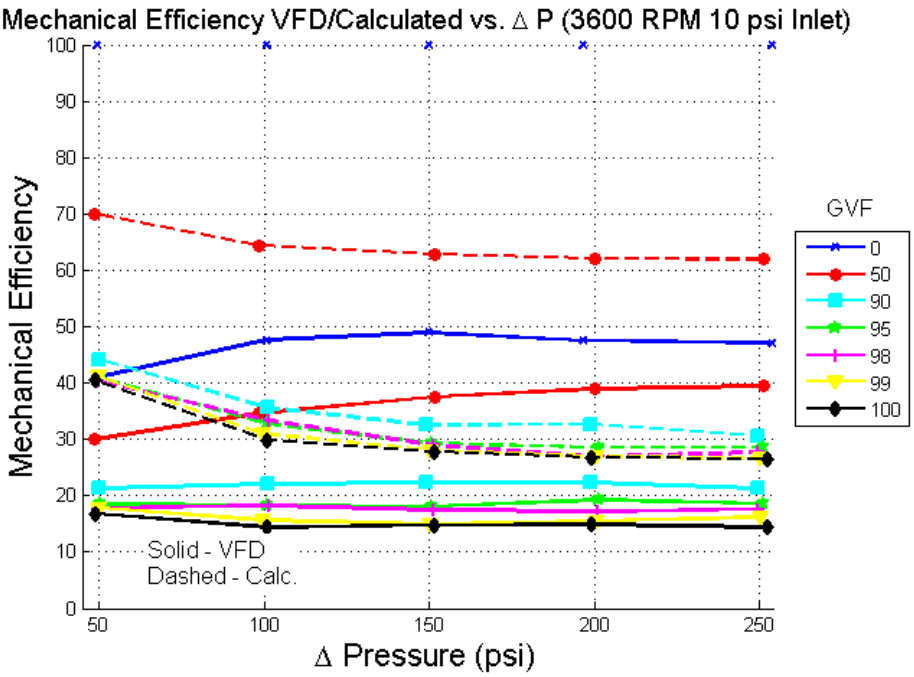

Figure 5.26 VFD Compared with Calculated Power (3600 RPM, 10 psi Inlet)

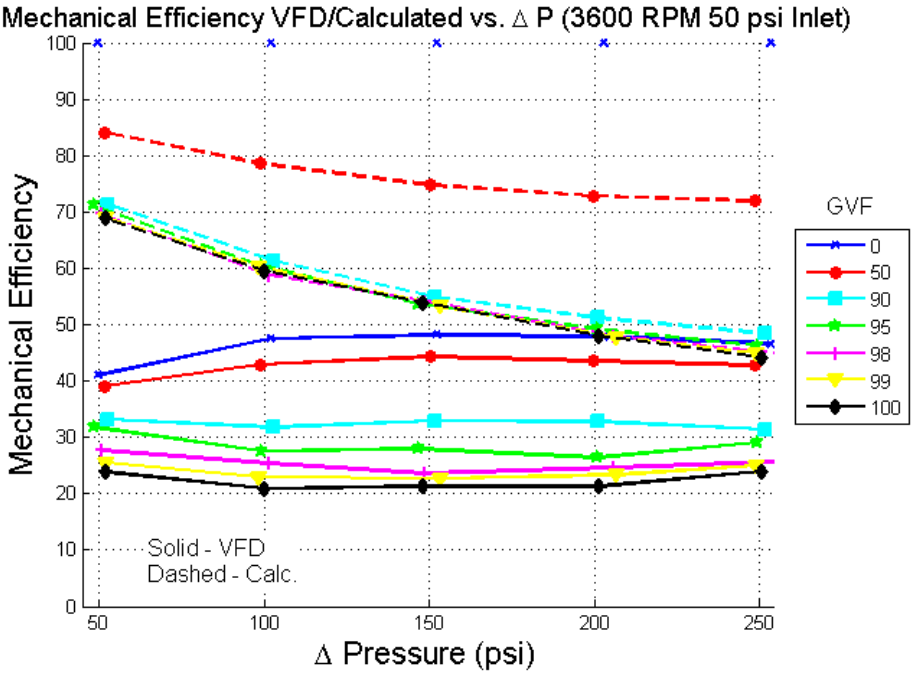

Figure 5.27 VFD Compared with Calculated Power (3600 RPM, 50 psi Inlet)

The previous figures describing the mechanical efficiency were calculated using the total flow through the pump including the seal flush. This information is indicative of how the pump is performing but an overall look at the system performance is necessary. Figure 5.28 and Figure 5.29 show the mechanical efficiency calculated using the assembly as the control volume. The assembly mechanical efficiency only calculates the fluid entering and exiting the system and does not include the seal flush fluid. The following figures show an even further decrease in mechanical efficiency when the seal flush fluid is not included in the calculation. The particular area of interest at 250 psi differential pressure and 100% GVF shows a total mechanical efficiency of about 5% and 15% for the 10 and 50 psi respective inlet pressure. This is a 33% and 40% lower mechanical efficiency for the 10 and 50 psi respective inlet pressure compared to using the pump as the control volume.

Section 5.1.4 will present an analysis done on the electrical power consumed by the motor at each data point. This comparison will show that the electrical power is purely dependant on the differential pressure across the pump. This means that the electrical power will stay constant at the same differential pressure but the power required to compress the gas increased from 2.18 to 5.98 Hp as the inlet pressure increased from 10 to 50 psi. That is a ratio of 2.74 for the gas compression power, shown in Table 5.2, while the ratio of mechanical efficiencies is 3.0.

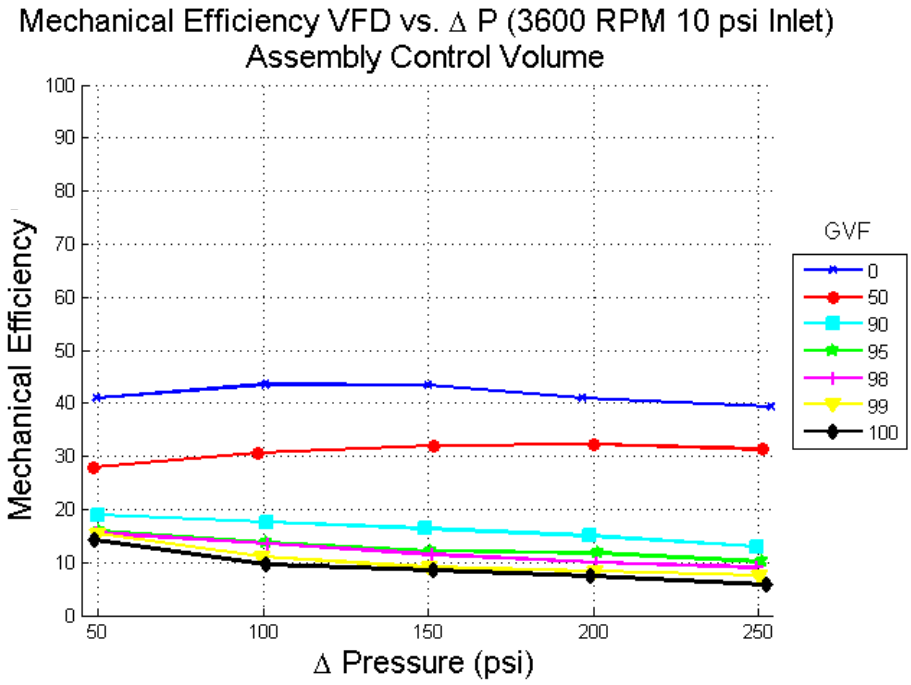

Figure 5.28 Mechanical Efficiency VFD vs. ΔP (3600 RPM, 10 psi Inlet, No Flush)

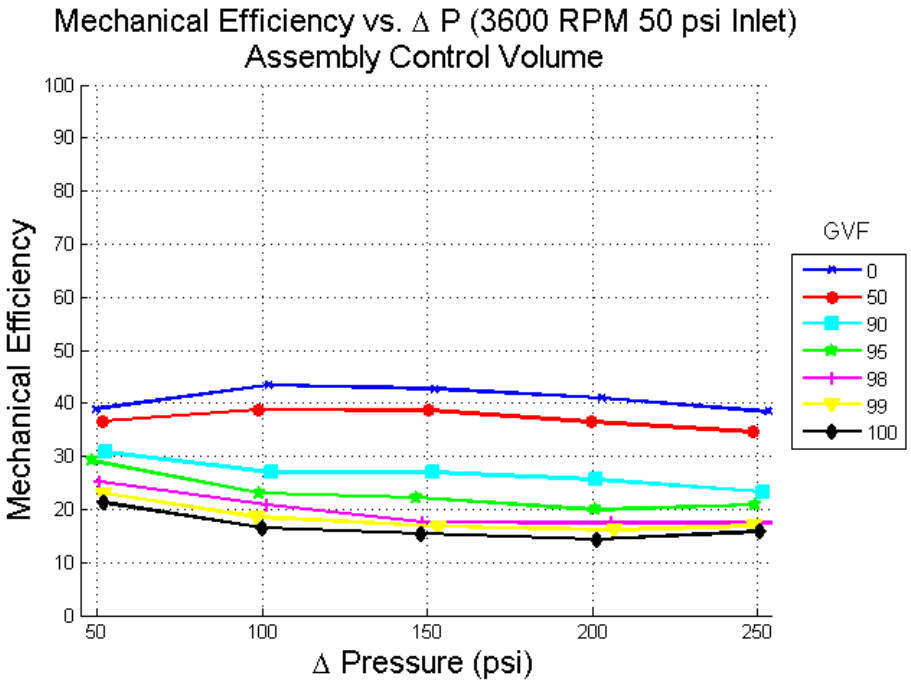

Figure 5.29 Mechanical Efficiency VFD vs. ΔP (3600 RPM, 50 psi Inlet, No Flush)

5.1.4 Load vs. Differential Pressure

A common analysis performed on positive displacement pumps is a load vs. differential pressure comparison. The load here is defined as the electrical horsepower required by the motor from the VFD to maintain the set rotational speed of the motor. A more detailed analysis of the energy distribution is done in the following Section 5.2. The term load and electrical power can be used interchangeably. This investigation, as previous investigations show, the load completely depends on the differential pressure across the pump. A unique difference seen in the current investigation is that the power required to pump 0 and 50% GVF is marginally higher than the power required for the 90%+ GVF cases. However, this only occurs at the highest running speed of 3600 RPM and is consistent between the 10 and 50 psi inlet cases.

Figure 5.30 shows the load vs. differential pressure for 3600 RPM, Figure 5.31 for 2700 RPM, and Figure 5.32 for 1800 RPM. The 10 psi inlet is also representative of the 50 psi inlet and a comparison between the three speeds appears in Figure 5.33.

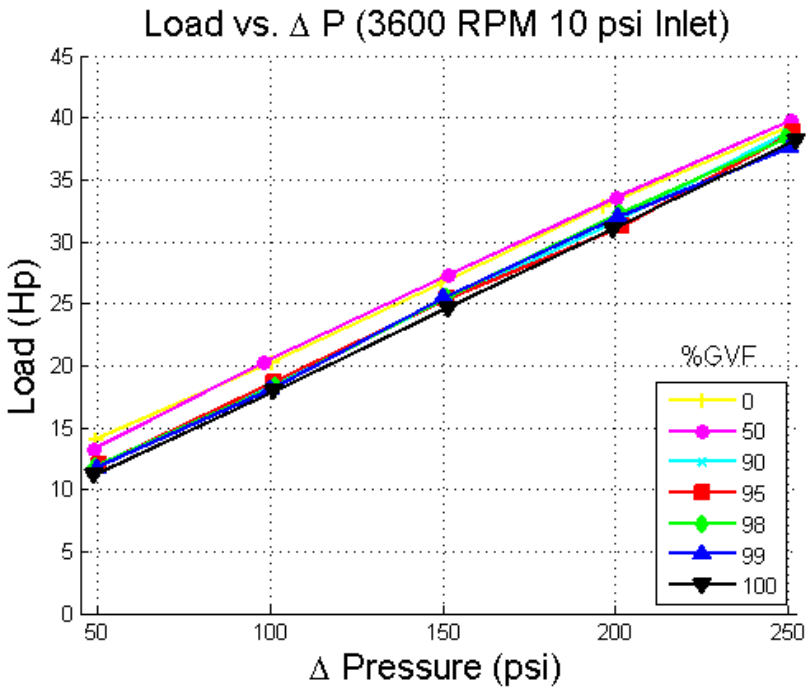

Figure 5.30 Load vs. ΔP (3600 RPM, 10 psi Inlet)

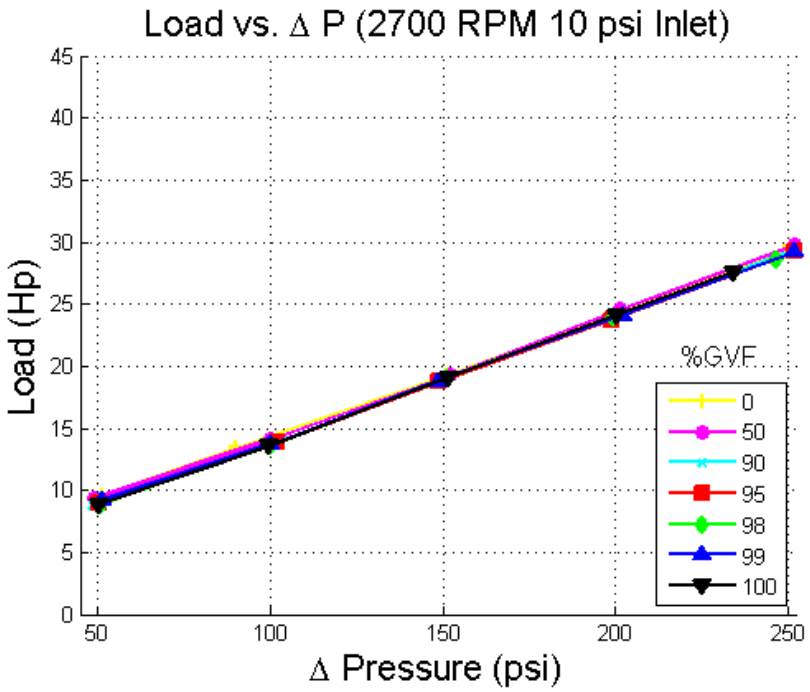

Figure 5.31 Load vs. ΔP (2700 RPM, 10 psi Inlet)

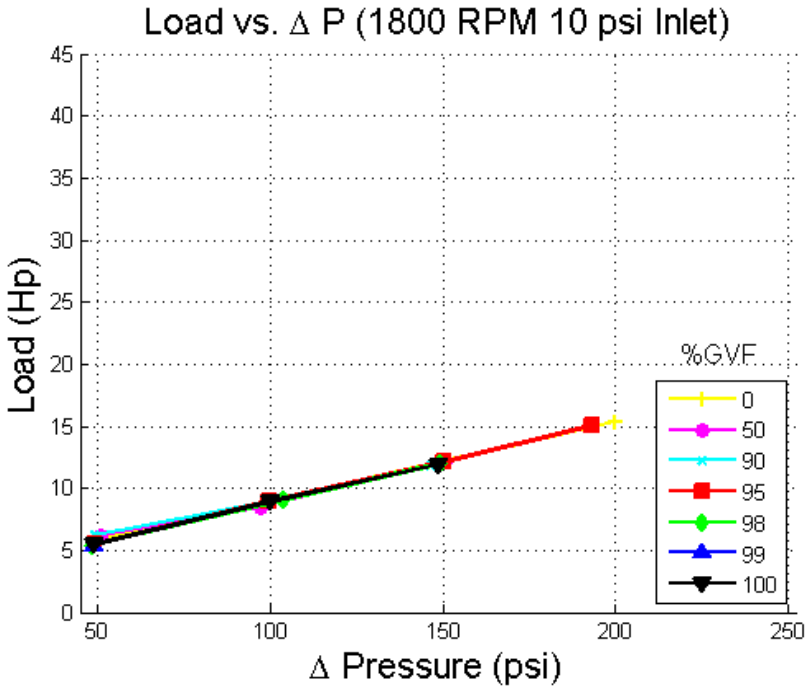

Figure 5.32 Load vs. ΔP (1800 RPM, 10 psi Inlet)

Figure 5.33 shows an average load for each of the speed and inlet conditions. The results are consistent with previously published research and show that the results agree with the theory of positive displacement pumps. The increase of load with the differential pressure is linear and can accurately provide the horsepower requirements for any combination of pump speed, inlet pressure, or GVF. The data at 1800 RPM does not include the highest pressure since the total pump through flow was zero at this differential pressure. The data in Figure 5.33 was curve fit with the following results for the equation

$$\mathrm{Load(Hp)} = (\mathrm{m} * \Delta\mathrm{P}) + \mathrm{b}$$

and is summed up in Table 5.3.

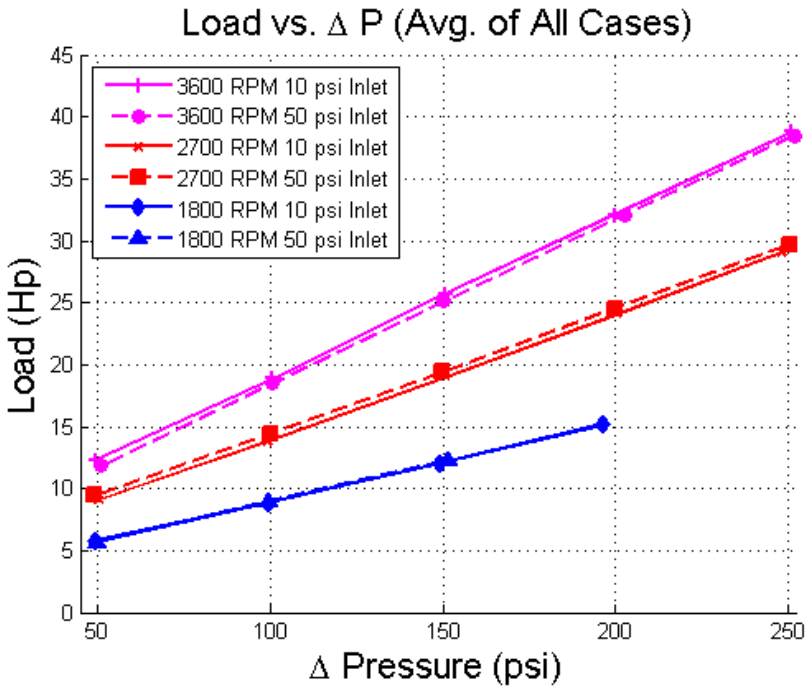

Figure 5.33 Load vs. ΔP (Average of All Cases)

Table 5.3 Power Consumption Line Regression from Figure 5.33

RPM	*b*, Hp	*M*, $\frac{\text{Hp}}{\text{psi}}$
3600	0.130	5.4
2700	0.100	4.2
1800	0.064	2.5

5.1.5 Exhaust Temperature

A correlation between the exhaust temperature and the volumetric performance was discovered and will be explained more in depth in the following section. However, comprehension of the steady state exhaust temperature is important to understanding the conclusions regarding the pumps operating temperature. The following figures, Figure 5.34 to Figure 5.37, describe the temperature distributions as a function of the pump parameters, similar to the previous descriptions.

The first two figures, Figure 5.34 and Figure 5.35, show the comparison for each of the three speeds at the different inlet conditions. While it seems that the figures do not follow a specific pattern, it was discovered that the fluid entering the pump has a dramatic effect on the exhaust temperature. Although this may not seem like a novel idea at first, the temperature of the stored fluid in the knockout boot contributes significantly to the temperature rise through the pump. As the fluid accumulated in the boot is trapped and re-circulated, it constantly goes through heating cycles from the low-pressure inlet to the high-pressure exhaust. The heat accumulated in the knockout boot can be significant and will be investigated further in the following Section 5.2. If not watched closely the heat stored in the knockout boot can skew performance results and contribute to dramatic pump operating temperatures.

The heat of the liquid in the knockout boot combined with the temperature of the ambient water stored in the supply tank can contribute to the result of the temperature for 2700 RPM as indicated in Figure 5.35. This event does not follow the intuitive trend. On the other hand, the results agree with previous publications that show the pump temperature rises with increasing differential pressure and GVF.

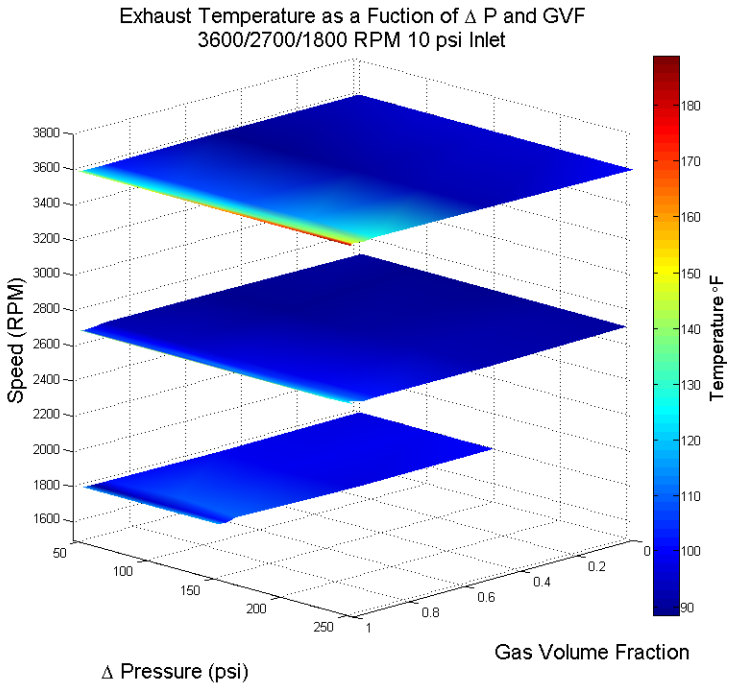

Figure 5.34 Exhaust Temperature Summary (All Speeds, 10 psi Inlet)

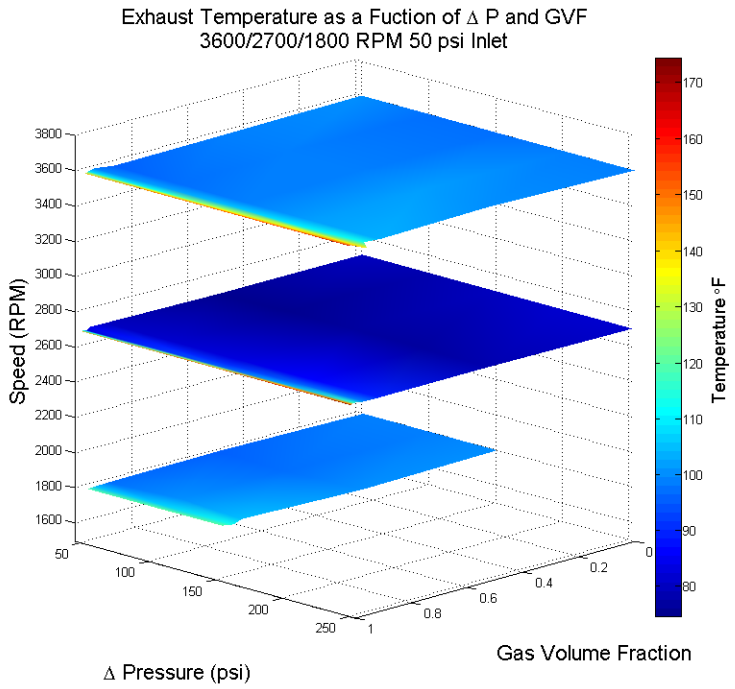

Figure 5.35 Exhaust Temperature Summary (All Speeds, 50 psi Inlet)

The increase of temperature as a function of GVF and differential pressure is clearly indicated in Figure 5.36 and Figure 5.37. All three pump speeds show similar trends. The inlet conditions of the pump contribute significantly to the exhaust temperature. While the seal flush temperature has a dramatic effect on the exhaust temperature, due to the constant heating of the knockout boot. The external water entering the assembly can also have an effect. While the inlet temperature remained constant for the majority of the investigation, after long periods of pump operation the water supply tank does rise marginally. This can cause a subtle effect on the exhaust temperature but because the water is mixing with air at a constant temperature the overall inlet temperature is affected much more by the seal flush fluid which was typically much higher than the inlet temperature of the pump.

These results are contrary to Räbiger. Räbiger was able to show a direct correlation between the friction power and the differential temperature across the pump. The

addition of the liquid recirculation system makes replicating the correlation shown by Räbiger impossible. This is because of a complex fluid interaction at the pump inlet where the seal flush liquid is introduced to the fluid entering the pump. More information about the thermodynamics and heat transfer of the seal flush fluid's interaction with the pump inlet fluid would need to be known to make a similar correlation between the friction power and the differential temperature across the pump.

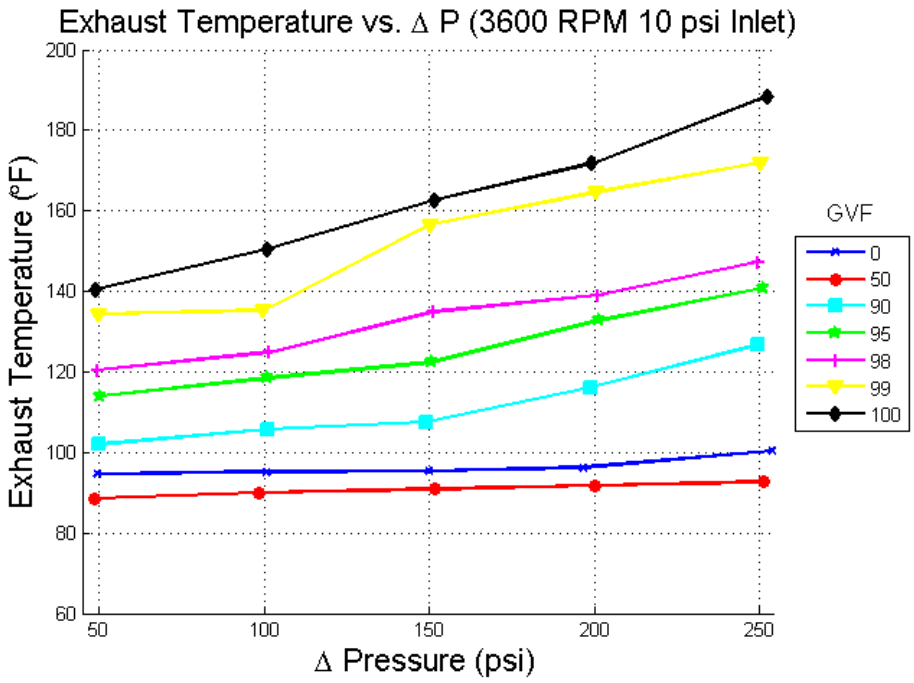

Figure 5.36 Exhaust Temperature vs. ΔP (3600 RPM, 10 psi Inlet)

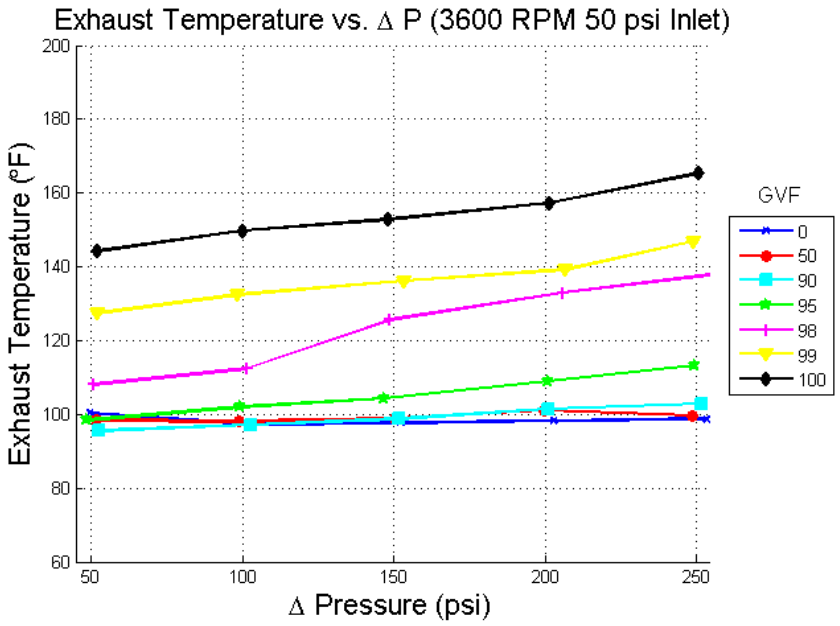

Figure 5.37 Exhaust Temperature vs. ΔP (3600 RPM, 50 psi Inlet)

While the pump is in operation, it is extremely important to keep a close watch on the temperature rise between the pump inlet and exhaust. There is a constant addition of heat to the seal flush fluid that continues to cause the exhaust temperature to rise. The inlet temperature remains constant because the temperature reading is taken before the fluid enters the screw cavity, which is where the seal flush fluid is injected.

For the higher pump inlet pressure comparing Figure 5.37 to Figure 5.36 the exhaust temperature is lower for the 50 psi inlet compared to the 10 psi inlet pressure. The rise in mechanical efficiency rises with the higher inlet pressure as well. These two important factors are related. The exhaust temperature goes down as the pump inlet increases and the pump is more efficient under that condition so less energy from the heat of compression is rejected into the liquid from the gas. The exhaust temperature increases with ΔP and GVF. This is due to the heat produced by the compression of the gas. The heat produced increases with gas flow rate and with increasing the pressure rise across the pump.

It is important to remember that while heat is constantly added to the liquid recirculation knockout boot, the assembly will not reach a steady state operating temperature unless there is an influx of water cool enough to remove the heat added during the compression process. The temperature of the pump will not reach a steady state condition unless there is external water entering the pump assembly. The external water entering the pump assembly adds cooling capacity and the slope of the temperature rise over time will be lower. The temperature rise slope will also be lower for lower differential pressure and lower GVFs. Figure 5.38 characterizes the typical surface plot of the temperature distribution during the steady state investigation.

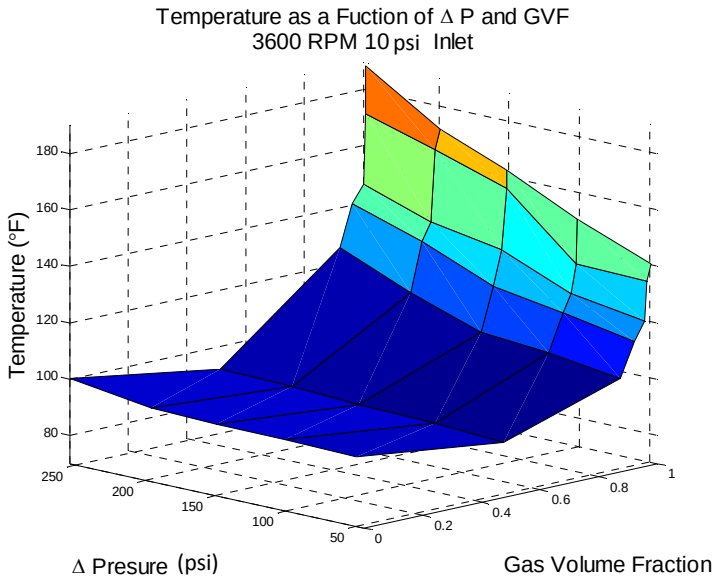

Figure 5.38 Typical Temperature Distribution for Pump Operation

This typical temperature can be modified if the pump operation is maintained for enough time so that added heat circulates through the liquid recirculation circuit. This is a particular problem for high differential pressure and high GVF. Sharp rises in temperature were noticed above 95% GVF where the amount of cool external water is not sufficient to remove the heat added by the rise in pressure through the pump.

5.2 100% GVF Temperature Study

The particular point of interest in the current investigation is the pump operation at 100% GVF. The 100% GVF is a worst case scenario for a pump designer. As seen from the previous publications, the twin-screw pump starts to lose volumetric efficiency as the GVF is increased. In particular, at 100% GVF the pump relies solely on the liquid recirculation loop to remain operable. When applying a liquid recirculation system, the desired result is twofold: first to increase the volumetric efficiency and second to dissipate the heat created by the fluid movement from a low to high pressure.

The following investigation takes an in depth look at the temperature rise associated with steady state pump operation at 100% GVF for an extended period of time. To characterize the heat rise while using the recirculation tank, three separate conditions were analyzed. The basic principle was to set the differential pressure, inlet pressure, and seal flow rate, and record the length of time required for the pump to reach the maximum operating temperature. The pump was run at 3600 RPM and the inlet pressure was held at 10 psi. The variables were the differential pressure at 250 and 150 psi. The third condition was held at 250 psi differential pressure and the seal flush rate was held at 6% of the total flow rate. In the following Figure 5.39 to Figure 5.46, the legend describing the line colors shows the differential pressure that was held for the condition. The third condition is labeled “250 Recommended.” It is labeled “Recommended” to show that the 250 differential test was re-administered with the lower seal flush rate recommended by Leistritz Corp. The level of fluid in the knockout tank was set at ~20 gallons for all three conditions ensuring that the temperature rise time did not depend on the thermal capacity stored in the tank.

Figure 5.39 shows the three conditions at a snapshot of the total run time. All three conditions showed the same result: the temperature continued to rise until the maximum operating temperature of 180 °F was reached. The red, blue, and green lines

represent the exhaust temperature, while the magenta, cyan, and yellow lines show the temperature of the seal flush liquid being injected into the pump inlet. Changing the differential pressure has a drastic affect on the slope of the curve. As the differential pressure increases, the rate of temperature increase rises as well. When the seal flush liquid flow rate was reduced there was no obvious change in slope indicating the heat generation rate remained constant. Since the seal flush flow rate was decreased, the temperature rise through the pump was increased.

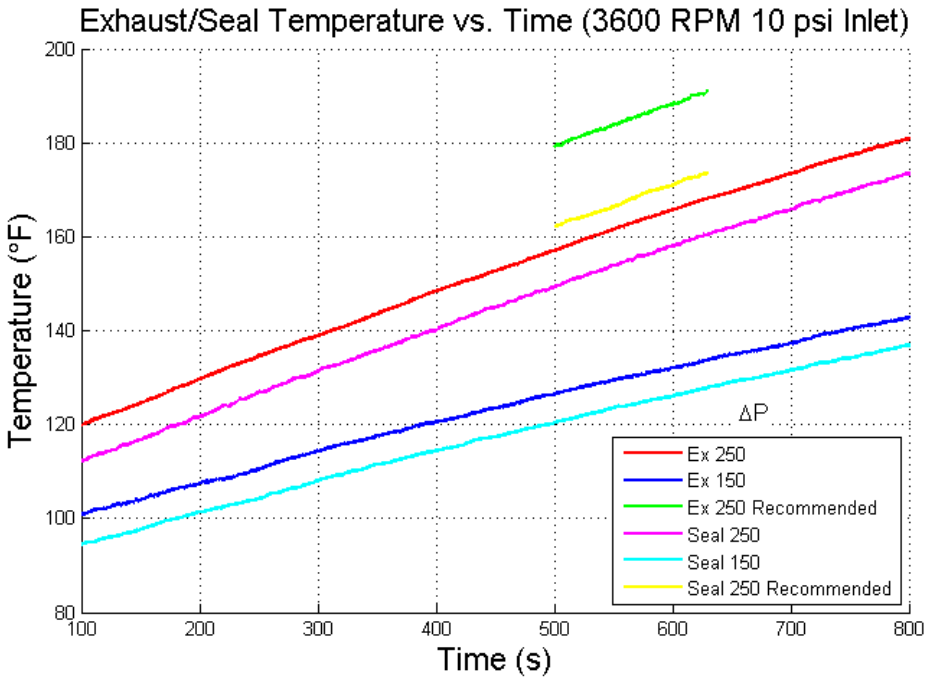

Figure 5.39 Exhaust Temperature Compared with Seal Flush Temperature

Figure 5.39 shows that the temperature rise over time is a linear function that does not appear to reach an asymptote before the maximum pump operation temperature. Figure 5.40 confirms the temperature rise through the pump is a linear function with time. The red, blue, and green lines represent the different conditions and show a strong linearity at this time range. The differential temperature has a slight downward slope that seems to indicate a slight skew between the seal flush temperature and the

exhaust temperature. Also, the differential temperature for the "250 Recommended" trial is approximately three times larger than the same condition with the high seal flush rate, "250." This indicates that the same amount of heat is being added to the fluid passing through the pump.

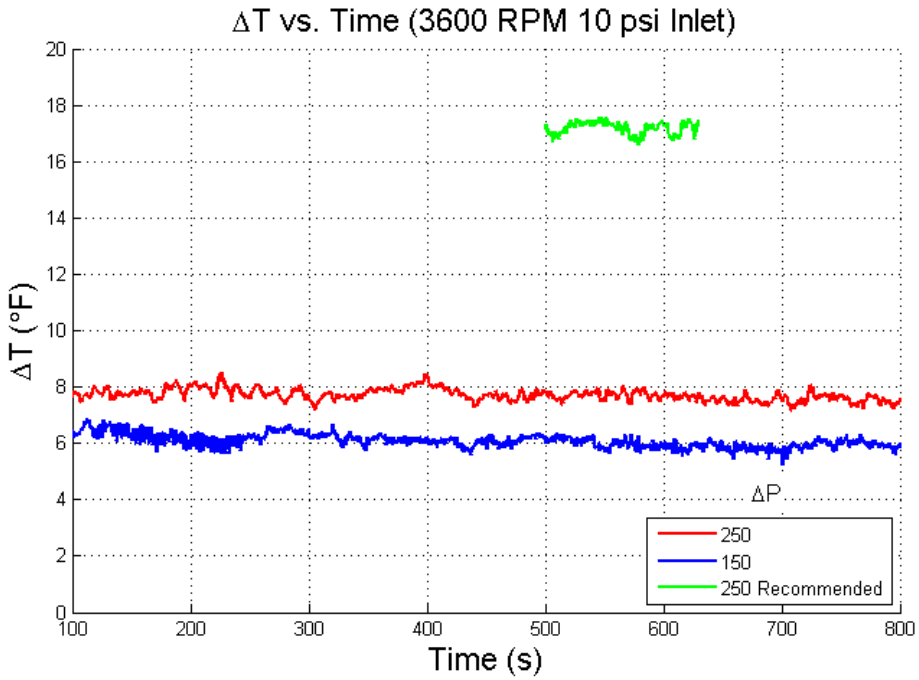

Figure 5.40 ΔT vs. Time

To fully understand the result of heat added to the system through the pumping process, a simple calculation was performed to examine the amount of heat that was added to the fluid. Continuing with the idea proposed by Räbiger, the following analysis was preformed. $\dot{Q}_{flush}$ describes the amount of heat added to by the liquid seal flush fluid where the differential temperature was taken between the seal flush entering the pump inlet and the exhaust temperature

$$\dot{Q}_{flush} = \dot{m}_{flush} c_l (T_{exh} - T_{flush})$$

The heat of compression required to compress the gas portion of the fluid is assumed to be isentropic, therefore the following Gibb's relation can be applied. It is also assumed that the air entering the pump inlet meets with the "hot" seal flush fluid and is thoroughly mixed. Therefore it is assumed that the air is at a uniform temperature with the seal flush fluid before the compression process starts. The isentropic process is calculated using absolute pressure and temperature values is described by

$$\frac{T_{exh}}{T_{flush}} = \left(\frac{P_{exh}}{P_{in}}\right)^{\frac{\kappa-1}{\kappa}}$$

The differential temperature found from the previous isentropic relation is then used to find the heat of compression

$$\dot{Q}_{HC} = \dot{m}_g c_g (T_{exh} - T_{flush})$$

This is the theoretical temperature rise of the gas for isentropic compression. However, the gas is cooled by being in contact with the seal flush fluid. This reduces the actual gas temperature to be equal to the seal flush fluid at the pump exhaust, reducing the actual amount of energy added to the gas.

Table 5.4 shows the values used to calculate the amount of heat added to the system while using the liquid recirculation. At first glance it appears that the pump is operating more efficient at the lower flush rate. However, both the gas mass flow rate and the differential pressure rise are lower. Table 5.5 presents the ratios of various quantities for the two cases. The high flush rate produces 24.2% more heat added to the fluid flush. The mass flow rate is 8.4% larger and the differential pressure is 6.4% larger. The larger differential pressure produces a 2.6% larger differential temperature calculated by the isentropic Gibb's relation, resulting in a larger heat of compression. The higher flow rate and larger differential pressure for the 250 case compensates for the larger $\dot{Q}_{HC}$.

Slight differences in the steady state operating points provide a near match to the proportionality shown by the pump. The majority of heat being introduced to the liquid from the heat of compression is 80.3%, 75.5%, and 78.6% of the total energy for the 250, 150, and 250R conditions respectively. This shows that the same amount of heat is added to the fluid between the "250" and "250 Recommended" trial, is constant and it can be concluded that the seal flow has a significant effect on pump performance. The second result from Table 5.4 shows that the $\dot{m}_g$ is lower for the reduced seal flush flow. There is a slightly smaller differential pressure across the pump for the reduced fluid flush flow so any change of mass flow rate should be higher due to the reduced differential pressure. Since the $\dot{m}_g$ is lower with the reduced flush fluid the final result is a loss of mass flow rate with reduced seal flush flow.

Table 5.4 Tabulated Values Used for Calculating Heat Generation

Trial (ΔP)	T_{in} (°C)	T_{flush} (°K)	T_{exh} (°K)	ΔT_{flush} (°K)	$T_{exh,gas}$ (°K)	ΔT_{gas} (°K)	P_{in} (kPa)	P_{Exh} (kPa)	$\dot{m}_{flush}$ (kg/s)	$\dot{m}_g$ (kg/s)	$\dot{Q}_{flush}$ (kW)	$\dot{Q}_{HC}$ (kW)
250	296.0	340.7	345.0	4.22	670.8	330.1	181.5	1943.2	1.3896	0.0181	24.6	6.0
150	298.0	323.9	327.1	3.26	557.4	233.5	182.5	1220.4	1.0886	0.0203	14.8	4.8
250R	297.1	347.9	357.6	9.65	669.8	321.9	185.9	1841.2	0.4884	0.0167	19.8	5.4

Table 5.5 Ratios to Compare Rate of Heat Transfer

$\frac{\Delta T_{gas,250}}{\Delta T_{gas,250R}}$	$\frac{\Delta T_{flush,250}}{\Delta T_{flush,250R}}$	$\frac{\Delta P_{250}}{\Delta P_{250R}}$	$\frac{\dot{m}_{flush,250}}{\dot{m}_{flush,250R}}$	$\frac{\dot{m}_{gas,250}}{\dot{m}_{gas,250R}}$	$\frac{\dot{Q}_{HC,250}}{\dot{Q}_{HC,250R}}$	$\frac{\dot{Q}_{flush,250}}{\dot{Q}_{flush,250R}}$
1.026	0.437	1.064	2.845	1.084	1.111	1.242

An energy balance was then applied to the system to find the power lost in the pumping process. Starting with the 1[rst] law of thermodynamics the energy balance is

$$\left(\dot{W}_{shaft} + \dot{Q}\right)_{out} - \left(\dot{W}_{shaft} + \dot{Q}\right)_{in} + \iint \left(h + \frac{V^2}{2} + gz\right) * \rho V \cdot dA + \frac{d}{dt}\iiint e_{C\forall}\rho \, d\forall = 0$$

Assuming a steady process, ΔKE=0, ΔPE=0, no shaft work out, and no external heat input the energy balance reduces to

$$\dot{W}_{shaft} = \iint h * \rho V \cdot dA + \dot{Q}_{out}$$

The final result is then

$$\dot{W}_{electric} = \left(\dot{m}_{flush} c_l + \dot{m}_g c_g\right)\Delta T_{flush} + \dot{Q}_{loss}$$

where

$$\dot{W}_{fluid} = \left(\dot{m}_{flush} c_l + \dot{m}_g c_g\right)\Delta T_{flush}$$

where $\dot{W}_{electric}$ is the electrical power supplied by the VFD and $\dot{Q}_{loss}$ is the amount of energy lost in the process. $\dot{W}_{electric}$ is interchangeable with the load examined in the steady state performance section.

Table 5.6 Energy Balance Tabulated Values

Trial (ΔP)	$\dot{W}_{electric}$ (kW)	$\dot{W}_{fluid}$ (kW)	$\dot{Q}_{loss}$ (kW)
250	28.709	24.628	4.081
150	19.089	14.909	4.18
250R	27.815	19.932	7.883

Table 5.7 Tabulated Fluid Work

Trial (ΔP)	$\dot{m}_{flush}C_{flush}\Delta T_{flush}$ (kW)	$\dot{m}_{gas}C_{gas}\Delta T_{flush}$ (kW)	Total Work (kW)
250	24.551	0.0771	24.628
150	14.842	0.066	14.909
250R	19.770	0.162	19.932

Table 5.6 and Table 5.7 show the results of the energy balance. Table 5.6 calculates the total heat lost in the pumping process. There is a constant value for the relationship between the 250 and 150 psi differential pressure which shows the proportional relationship between the differential pressure and the seal flush flow rate. Once the seal flush flow rate is reduced the losses increase. This accounts for the high temperature differential between the pump inlet and outlet. It also accounts for the faster temperature rise of the liquid recirculation system.

Table 5.7 shows the components of the total work done on the fluid. The gas heat of compression is transferred to the seal flush liquid and is calculated by subtracting the $\dot{m}_{gas}C_{gas}\Delta T_{flush}$ from $\dot{Q}_{HC}$. This is a result of the gas being cooled by the flush and exiting the pump at the exhaust temperature. This explains why $\dot{m}_{gas}C_{gas}\Delta T_{flush}$in

Table 5.7 is much lower than $\dot{Q}_{HC}$in Table 5.6. At the reduced flush rate ΔT_{flush} is larger, hence the amount of thermal energy in the gas is larger, reducing the amount of heat added to the fluid flush. There is still a sizable amount of heat generated in the pump which must be dissipated by the seal flush fluid. Adding a friction reducing agent to the liquid recirculation system is recommended to try and reduce the amount of heat generated by the seal flush fluid.

Figure 5.41 plots the exhaust temperature rise along with the seal flush rate. The plot shows how the fluid flush rate remains constant while the differential pressure is held constant.

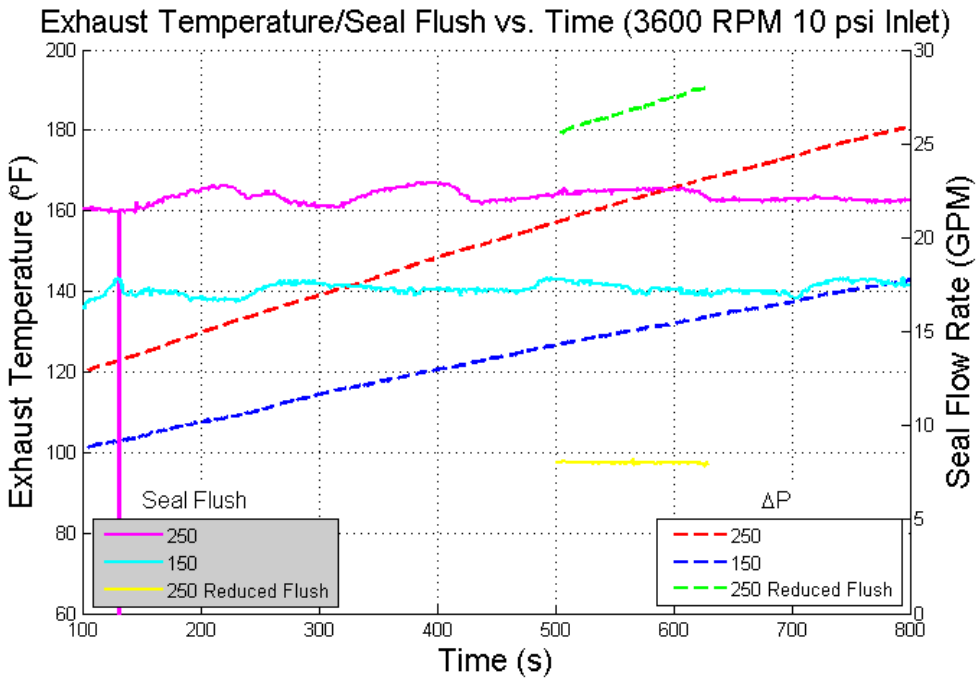

Figure 5.41 Exhaust and Seal Flush Temperature for Three Flow Conditions

Figure 5.42 and Figure 5.43 show the entire time the condition was analyzed. The information found is representative of the 250 and 150 differential pressure investigations. The time duration that was achieved for the "250 Recommended" condition was not long enough to present useful information in this form. This is due to the short amount of time before the exhaust temperature reached the maximum value.

Figure 5.42 shows that a differential pressure of 250 psi was held for the first 800 seconds. Between 800 and 1600 seconds that differential pressure was reduced until the exhaust temperature stabilized. The exhaust temperature did not stabilize until the differential pressure was reduced to 50 psi. At a differential pressure of 50 psi the temperature stopped rising but did not show any appreciable decrease in temperature from 1600 seconds to 3000 seconds. The system's inability to remove the heat from the knockout boot presents a limitation to the pump operation. Under long durations of 100% GVF operation, the absence of heat dissipation from exterior fluid entering the

system can lead to a catastrophic failure if the pump is not cooled from an external source. A radiator mounted on the seal flush line is recommended to supply the cooling required.

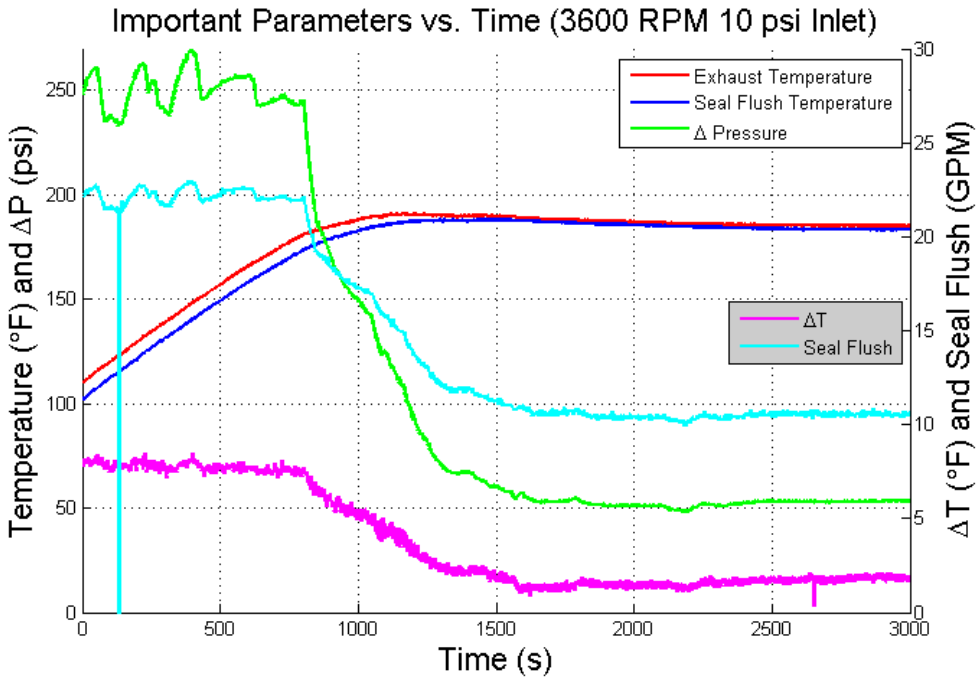

Figure 5.42 Important Parameters for 250 ΔP

Figure 5.43 presents the data from the trial run at 150 psi differential pressure. The results show that the temperature did not stabilize and reached the maximum operation temperature at ~1600 seconds. The lower differential pressure reduced the time that it took to reach the maximum operating temperature but did not show any signs of asymptoting at a stable temperature. This implies that above a critical differential pressure the heat being added to the system will continue to rise to the maximum pump temperature. If the pump temperature reaches the maximum operating temperature of 180 °F it is recommended that the differential pressure across the pump be reduced to 50 psi.

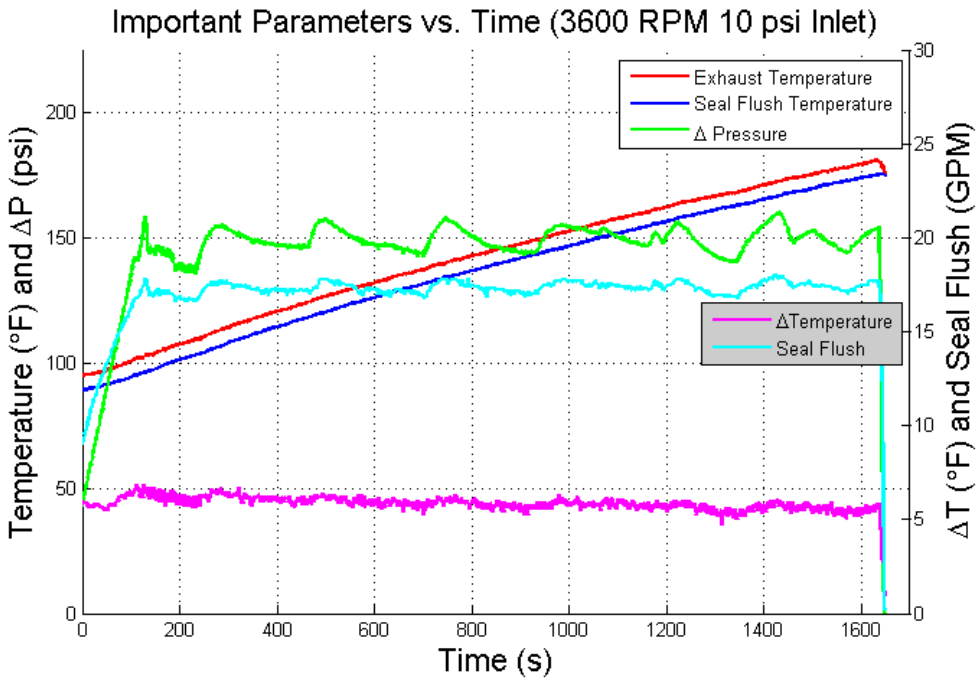

Figure 5.43 Important Parameters for 150 ΔP

Figure 5.44 shows how the total flow rate varies with the exhaust temperature of the mixture for 100% GVF flow with an inlet pressure of 10 psi and the previously analyzed differential pressure. The total flow rate decreases significantly as the temperature increases. Figure 5.45 shows the relationship of the seal flush flow rate as a function of differential pressure and GVF. The seal flush rate did not vary with temperature as shown in Figure 5.41. This indicates that the total volumetric flow rate reduction with temperature is due to reduced gas flow as shown in Figure 5.46. For all three cases a linear relationship exists between the exhaust temperature and the reduction in flow rate through the pump. This happens because of the location where the volumetric flow rate for the air is calculated. The volumetric flow rate of air entering the pump is calculated before the air is mixed with the hot seal flush fluid. The mixing of the cooler air with the hotter seal flush water expands the air and lowers the density. Assuming the pump's actual volumetric gas flow rate through the pump remains constant, the

mass flow rate will decrease as the pump temperature increases due to the heating of the gas resulting in a lower gas density. Since the gas volumetric flow rate presented in this investigation is calculated from the gas temperature and pressure entering the pump assembly, the pump inlet temperature is different than the pump temperature resulting in the reported flow rate changing.

Figure 5.44 includes the seal flush as part of the total fluid passing through the pump. Figure 5.46 does not include the seal flush fluid and while it retains the same slope, the position of the curves shifts. Figure 5.46 supplements Figure 5.45 and explains how the shift is possible. Figure 5.45 is a plot of the seal flush rate as a function of differential pressure and GVF. Regardless of the GVF, the seal flush rate is held constant and fully depends on the differential pressure. The fluid recirculation loop injects a prescribed amount of fluid per differential pressure and explains how the curves can shift while retaining the original shape.

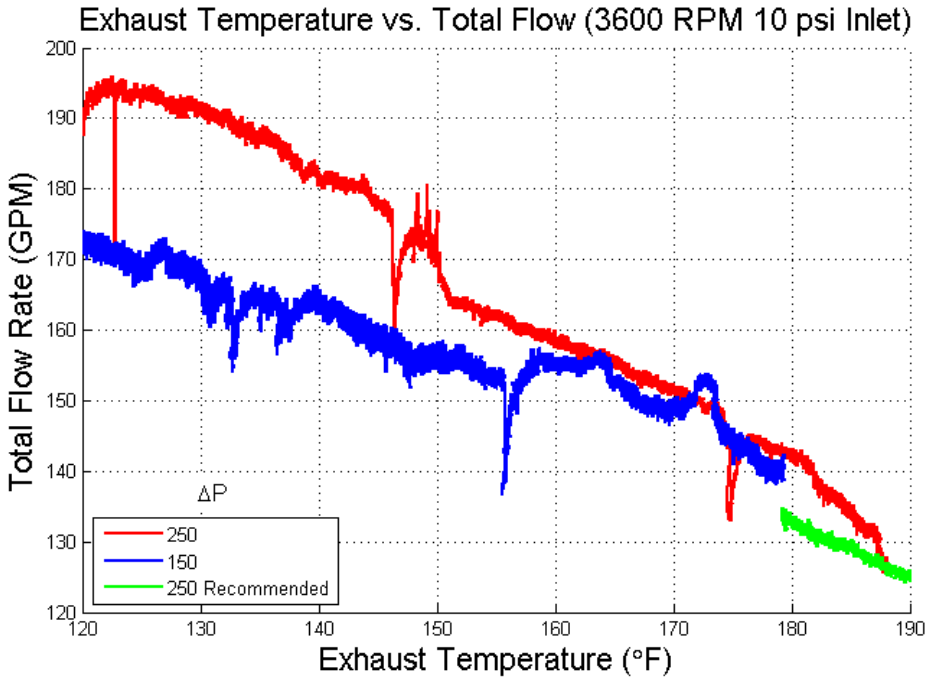

Figure 5.44 Exhaust Temperature vs. Total Flow for 100% GVF

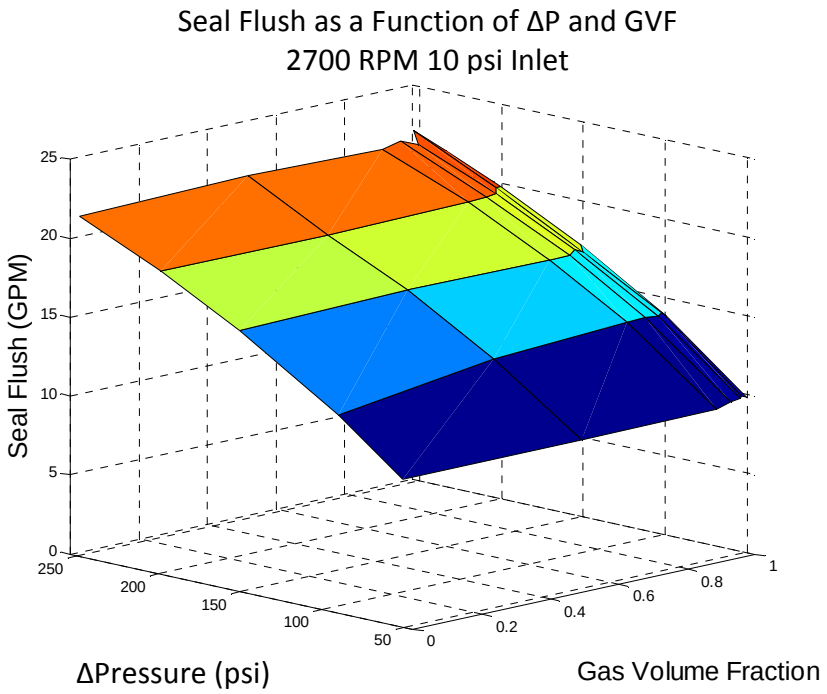

Figure 5.45 Seal Flush as a Function of ΔP and GVF

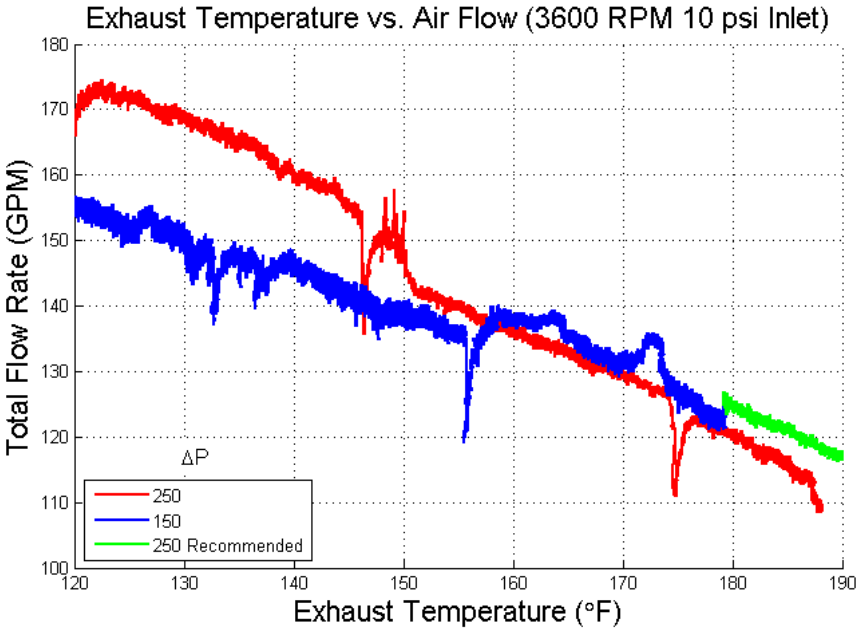

Figure 5.46 Exhaust Temperature vs. Air Flow for 100% GVF

The spikes and noise found in Figure 5.45 and Figure 5.46 are due to the PID loop holding the inlet pressure constant as well as a manual control that keeps a constant differential pressure. As these two parameters change and are adjusted back to the prescribed condition, the flow rate of the fluid passing through the pump can vary slightly. The manual adjustment to hold a constant differential pressure can also describe the oscillations in the differential pressure in Figure 5.42 and Figure 5.43.

To show how dramatic the pump performance varies between high and low temperature operation, Figure 5.47 shows the volumetric efficiency vs. differential pressure for 100% GVF. "High" and "Low" temperatures could be considered ambiguous but due to the dynamic performance of the pump and the constant addition of heat from the liquid recirculation system, the "Low" temperature can only be held for a short time while the "High" temperature is limited by the maximum operating temperature. "Low" temperature is characterized as below 120 °F while "High" temperature is between 170 and 180 °F.

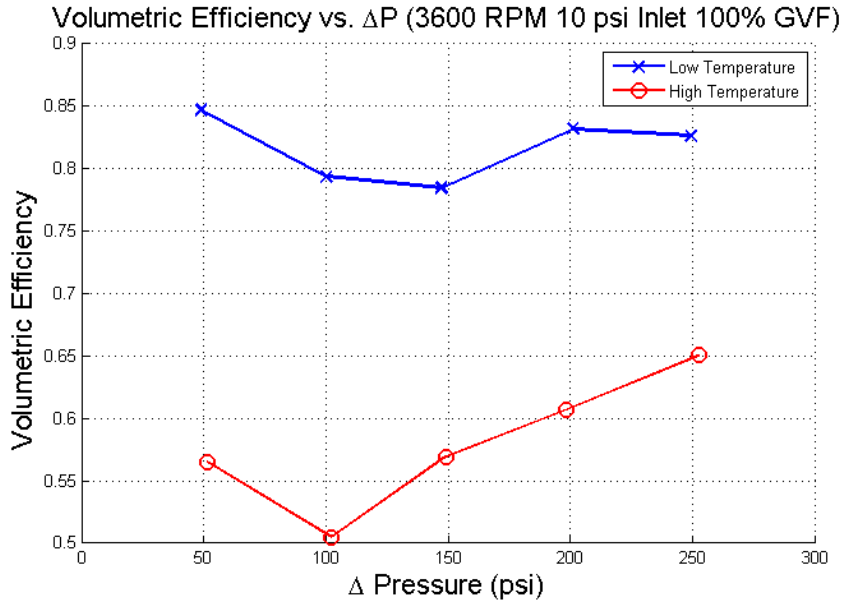

Figure 5.47 Volumetric Efficiency vs. ΔP (High and Low Temperature)

As previously discussed and shown in Figure 5.45 and Figure 5.46, the volumetric flow rate through the pump is reduced as the temperature rises. Therefore, because of the working principle of the positive displacement pump, the volumetric capacity of the pump holds constant and the volumetric efficiency goes down as the temperature rises. Without a way to hold a constant inlet temperature the steady performance of the pump cannot be perfectly characterized. The temperature profile described in Section 5.1.5 can affect the performance of the pump across the entire matrix used to investigate the pump performance. This means that by allowing the inlet temperature to increase over time, due to the rising seal flow temperature, the pump cannot be fully characterized. The current investigation reduced the possibility of these errors caused by this phenomenon by ensuring that the temperature distribution of each pump speed/inlet condition followed the pattern described in Section 5.1.5. Future work should include a method to maintain the seal flush temperature constant. A more precise characterization of the pump's dependence on operating conditions can be made.

6. CONCLUSIONS AND RECOMMENDATIONS

The main objective of this thesis was to characterize the performance of a twin-screw pump implementing a liquid recirculation system running at high GVFs. The initial investigation explored the behavior of the twin-screw pump under multiple running speeds and inlet pressures. The secondary investigation explored the effect of the liquid recirculation circuit on the pump's operating temperature at 100% GVF. The experimental results gave a more detailed understanding of the steady state performance of the pump as well as an in depth look at the liquid recirculation circuit designed to improve pump performance while operating at high GVFs. The use of the liquid recirculation loop gives the twin-screw pump the ability to operate at high GVFs relative to the assembly control volume but the actual GVF across the pump is much lower.

Section 6.1 summarizes the results from the steady state pump performance characteristics. Section 6.2 summarizes the results from the liquid recirculation loop's effect on pump performance while operating at 100% GVF, 3600 RPM, and the 10 psi inlet condition. The following sections will also include specific recommendations for further characterization of the steady state pump performance and recommendations to improve the effectiveness of the liquid recirculation circuit.

6.1 Steady State Pump Performance

The experimental investigation of the steady state pump performance concluded with a performance map generated for all of the parameters varied during the pump operation. In all of the cases the increase of differential pressure and the operation above 90% GVF resulted in a decrease of total flow and volumetric efficiency. A maximum volumetric efficiency occurs between 0 and 90% GVF. This represents the

results typically seen in the operation of twin-screw pumps. Between the two inlet pressures, the 10 psi inlet had better volumetric efficiency while the 50 psi inlet showed greater mechanical efficiency. The operating temperature of the pump increases with an increase of differential pressure and GVF, which reflects previous publications. This phenomenon directly relates to the amount and temperature of external fluid entering the pump assembly.

As the pumping process heats the liquid in the recirculation knockout boot the external fluid can sufficiently absorb the heat added to the system under certain conditions. This is only possible under a critical GVF. The critical GVF for this investigation is 95% GVF. Above this GVF there is not enough external liquid available to cool the liquid in the recirculation loop. When this occurs the heat added to the system cannot be sufficiently removed and the temperature of the pump operation continually rises until the maximum operating temperature is reached and the pump must be shut down before any damage occurs to the pump internals.

While it was hypothesized by previous publications that increasing the pump speed should increase the volumetric efficiency, the current investigation shows comparable volumetric efficiency between 2700 and 3600 RPM indicating that there is a maximum pump speed that does not result in the increase of volumetric efficiency. The increase in pump speed does have an increase of total flow rate through the pump but operates at a similar volumetric efficiency. Comparing the full speed and the half speed volumetric efficiency showed massive improvement. At half speed the pump was unable to overcome the slip required to move any appreciable volume of fluid and was rendered inoperable at differential above 150 psi.

To ensure the results obtained at the multiphase pump lab are consistent, the following recommendations and test standards are presented:

- Hold the seal flush temperature constant
- Use the dual control volume assumption to quantify results if a liquid recirculation loop is incorporated
- Remove bypass valve for low differential pressures
- Reduce the amount of vertical piping in the system to dissipate pressure oscillations
- Install a system of air control valves similar to the water system where different control valves can meter different ranges of gas flow. This ensures a more consistent inlet pressure reading

While the seal flush temperature and the liquid recirculation loop recommendations have been described in detail, it is imperative to use consistent temperatures during continued investigation. This ensures that any dynamic changes in temperature is kept to a minimum and leads to more consistent results. The results of the temperature evaluations provide the basis that an increase of the pump temperature reduces the volumetric flow rate. The cause of the heat rise is primarily due to the continual heat rise of the seal flush fluid. Stabilizing the flush temperature will lead to more consistent performance results. The bypass valve is unique to the Leistritz system and made running at low differential pressure impossible. Its purpose is to act as a safety device in case the inlet pressure is higher than the outlet pressure, thus allowing the fluid to bypass the pump. By reducing the amount of vertical piping in the system, the associated “slug” flow required to evacuate the liquid up vertical columns could reduce the pressure oscillations seen during pump operations.

6.2 Liquid Recirculation Effect on Pump Performance

The experimental investigation conducted on the liquid recirculation loop's effect on the twin-screw pump performance concluded that modifications to the recirculation loop must be implemented to sustain operation at extreme GVF operation. The particular GVF studied in this investigation focused on the worst case scenario where the pump operates at 100% GVF for an extended period of time.

The three conditions investigated showed conclusive results that consistently demonstrated that the rise of pump's operating temperature depends on the differential pressure across the pump. It is also conclusive that the amount of heat added to the system through the pumping process is stored in the liquid knockout boot. The heat accumulated in the knockout boot continues to build during continued operation and leads to a continuously rising pump operation temperature. At 250 psi differential pressure the time required to reach the maximum operating temperature was significantly less than the time required to reach the maximum temperature at 150 psi. The 150 psi differential pressure showed no signs of asymptoting at a steady temperature. Once the pump was operating at the maximum temperature, the differential pressure had to be lowered to ~50 psi to stabilize the operating temperature. The third condition was conducted at 250 psi differential pressure but reduced the volumetric flow rate of the seal flush fluid. The resulting change had no effect on the temperature rise of the pump. The differential temperature between the inlet and exhaust for the pump rose considerably between the high and low seal flush rates. This indicates that the same amount of heat is being added to the fluid passing through the pump to raise the exhaust temperature consistently between the two cases.

A correlation was found between the flow rate through the pump and the exhaust temperature. For all three cases there is a linear relationship between the exhaust temperature and the reduction in flow rate through the pump. The volumetric flow rate of air entering the pump is reduced as the temperature rises due to the change of density between the location of the pump inlet and the location where the volumetric flow rate is calculated. The effect of volumetric flow rate changing as the temperature changes can be applied to the entire investigation including the steady state operation. Without a way to hold a constant temperature the steady state performance of the pump cannot be adequately characterized.

To ensure that the results obtained at the multiphase pump lab are consistent the following recommendations and test standard are presented:

- Conduct the heat rise investigation with a radiator designed to remove the heat of recirculation
- Conduct the heat rise investigation at different pump speeds
- Investigate the most extreme condition that the pump can operate at a stable condition under the recommended maximum pump temperature

It is necessary to investigate further the use of the liquid recirculation system applied to the twin-screw pump application. Previous publications and research conducted on twin-screw pumps show that for high GVF operation liquid injection is necessary to retain the volumetric efficiency required to move appropriate amounts of gas in the field application. The heat addition to the liquid stored in the recirculation circuit becomes more important parameter as the duration of high GVF operation increases. For long periods of operation above the critical GVF for the external fluid to cool the recirculation fluid sufficiently there must be a way to remove the heat added to the system through the pumping process. It is also necessary for pump manufacturers to develop pumps specifically designed for high GVF operation compared to retrofitting

current twin screw pumps with the liquid recirculation system. In the case where a radiator is applied to the liquid recirculation system the maximum operating temperature can be reduced and stabilized to a much lower temperature. This would allow the pump manufacturer to reduce the clearances without risking pump damage and develop better internal geometry specially designed for high GVF operation.

It was shown that the majority of heat added to the system is primarily due to the liquid being re-circulated, as opposed to the heat of compression for the air. It is recommended that future investigations look at chemical friction reducing agents to reduce the amount of heat added to the system through the pumping process. While this may theoretically reduce the amount of heat added to the system, it does not seem to remove the root problem of the stored energy in the knockout boot. The addition of a friction reducing agent may be enough to prolong the duration that it takes for the pump to reach a maximum operating temperature and increase the running time at extreme GVFs but may not completely solve the heat rise issue.

From the results presented it appears the best pump performance can be attained when the pump's operating temperature is as low as possible. The final conclusion leads to a way of removing the heat stored in the liquid recirculation circuit. By passing the seal flush fluid through a heat exchanger, the heat added to the system through pumping can be removed before the fluid enters the pump suction, therefore removing the issue of a constant heat rise over time. This solution would also create a more consistent temperature distribution across the entire operating range of the pump and would possibly create more consistent results for the steady state operation.

It would also be advantageous to initiate investigations to see how the pump speed affects the temperature rise. There could be a maximum operating speed where the heat added through the knockout boot would be naturally dissipated. Reduction to the critical running speed may allow steady operation at high differential pressures without

a complete pump shutdown. This additional recommendation goes along with finding the most extreme steady operating case. While the 95% GVF limit was seen in the current investigation, it is proposed that the limit could be different depending on the inlet temperature for both the multiphase fluid and the seal flush fluid. Consistent measurements must be made to reduce the chance of variability in the pump operation caused by a temperature dependent transient phenomenon.

6.3 Final Conclusion

It was shown that the use of a liquid recirculation circuit can and does allow a twin-screw pump to operate at extreme GVFs for a set amount of time. It is necessary for future research to investigate the temperature rise associated with pumping the fluid. To increase the amount of time the pump can be operated at extreme GVFs it will be necessary to either remove the heat added to the system through the pumping process or if possible reduce the amount of heat generated through the use of a friction reducing agent. The later may indicate a temporary solution while a heat exchanger that can reduce the temperature of the seal flush liquid seems to provide a more permanent solution. By adding the friction reducing agent the viscosity of the fluid is increased. The increase of viscosity reduces the turbulence in the fluid and this effect is what reduces the amount of heat generated. A secondary effect of adding the friction reducing agent such as guar gel was shown by Xu to increase the volumetric performance of the pump.

The effect of the heat being added to the system and stored in the recirculation system has an effect on the overall functionality of the pump. To completely characterize the pump operation and ensure that the measurements recorded during the steady state pump operation, it is imperative to stabilize the inlet conditions of the pump across the entire range of operating parameters.

REFERENCES

[1] Hardeveld, W., 2008, "Multiphase Pumps –Future Needs for the Oil and Gas Industry," presentation given at the 2004 EMBT Conference, Hannover, Germany.

[2] Rohlfing, G., 2008, "The Research & Development Path of the Multiphase Pump Technology," paper presented at the 2004 EMBT Conference, Hannover, Germany.

[3] Shippen, M., and Scott, S., 2002, "Multiphase Pumping as an Alternative to Conventional Separation, Pumping, and Compression," paper presented at the 2002 34th Annual PSIG Meeting, Portland, Oregon.

[4] FMC Technologies, 2007, "Sheel Perdido," [Brochure], Houston, Texas, FMC Technologies.

[5] Heyl, B., 2008, "Multiphase Pumping," presentation given at the 24th International Pump Users Symposium, Houston, Texas, (April 2, 2008).

[6] Bratland, O., 2010, "Pipe Flow 2 Multi-Phase Flow Assurance," http://www.drbratland.com.

[7] Karassik, I. J., 1976, *Pump Manual* 3rd Ed*,* McGraw-Hill, New York.

[8] Leistritz Corp, 2010, "Twin Screw Multiphase Pumps," [Brochure], Allendale, New Jersey, Leistritz Corp.

[9] Vetter, G., Wincek, M., 1993, "Performance Prediction of Twin Screw Pumps for Two-Phase Gas/Liquid Flow," Pumping Machinery*,* **154**, pp. 331-340.

[10] Vetter, G., Wirth, W., Korner, H., and Pregler, S., 2000, "Multiphase Pumping with Twin-Screw Pumps- Understand and Model Hydrodynamics and Hydroabrasive Wear," *Proceedings of the 17th International Pump Users Symposium*, Houston, Texas.

[11] Martin, A. M., 2003, "Multiphase Twin-screw Pump Modeling for the Oil and Gas Industry." Ph.D. dissertation, Texas A&M University, College Station, Texas.

[12] Chan, E., 2006, "Wet-Gas Compression in Twin-Screw Multiphase Pumps." M.S. Thesis, Texas A&M University, College Station, Texas.

[13] Xu, J., 2008, "Modeling of Wet Gas Compression in Twin-Screw Multiphase Pump," Ph.D. dissertation, Texas A&M University, College Station, Texas.

[14] Räbiger, K. E., 2009, "Fluid Dynamic and Thermodynamic Behavior of Multiphase Screw Pumps Handling Gas-liquid Mixtures with Very High Gas Volume Fractions." Ph.D. dissertation, University of Glamorgan, Germany.

[15] Bornemann Pumps, 2006, “Bornemann Multiphase Boosting,” [Brochure], Obernkirchen, Germany, Bornemann Pumps.

[16] Rohlfing, G., and Muller-Link, D., 2006, “Twin-Screw Rotors-2nd Generation for Increased Efficiency,” Paper presented at the 8th Multiphase Pump User Roundtable, Calgary, Alberta, Canada.

APPENDIX A

SAMPLE GVF CALCULATION

Gas Volume Fraction Calculations

Inputs

Air Inlet Pressure = P1 (psi) - Transducer Output – 111.29 psi

Pump Inlet Pressure = P2 (psi) – Transducer Output – 30.1664 psi

Air Inlet Temperature = T1 (^{o}F) – 81.95 ^{o}F

Pump Inlet Pressure = T2 (^{o}F) – 76.47 ^{o}F

Flowmeter Air Reading = F1 , F2(Pulses/Second) – 509 Pulses/Second (K-Factor – 2385,3695)

Flowmeter Water Reading = F3,F4,F5,F6 (Pulses/Second) – 462 Pulses/Second (K-Factor -47.5,116, 911,10600)

Calculations

1. Density of Air Inlet = {(P1 + 14.7) *6894.75}/[287.05* (T1+459.67)*5*0.111111] = P1/RT1= 10.05 kg/m^3

   Pressure Conversion -> psi to Pascal

   Temperature Conversion -> F to K

2. Density of Pump Inlet = (P2 + 14.7) *6894.75}/[287.05* (T2+459.67)*5*0.111111] = P2/RT2 = 3.618 kg/m^3

   Pressure Conversion -> psi to Pascal

   Temperature Conversion -> F to K

   Gas Constant = 287.05 J/Kg-K

3. $m^{3/}$Min_Air = (((F1*60)/2385)*0.0283168466)+ (F2*60)/3695); = 0.362598 $m^{3/}$min

   Flow Conversion -> Cubic feet to m^3

4. m_air = $m^{3/}$Min_Air * Density of Air Inlet = 3.644 Kg/min

5. Volume Flow Rate Air (GPM) = (mass_air)/(Density)= (m_air/Density of Pump Inlet)* 264.172052358 = 266 GPM

   Flow Conversion -> m^3 to Gallons

6. Volume Flow Rate Water (GPM) Q = (F3*60)/47.5) +(F4*60)/116.5) +(F5*60)/911) +(F6*60)/10603) = 30.428 GPM

GVF = Volume Flow Rate Air (GPM) /(Volume Flow Rate Water (GPM) + Volume Flow Rate Air (GPM))

89.86 %

APPENDIX B

LEISTRITZ PUMP SCHEMATIC

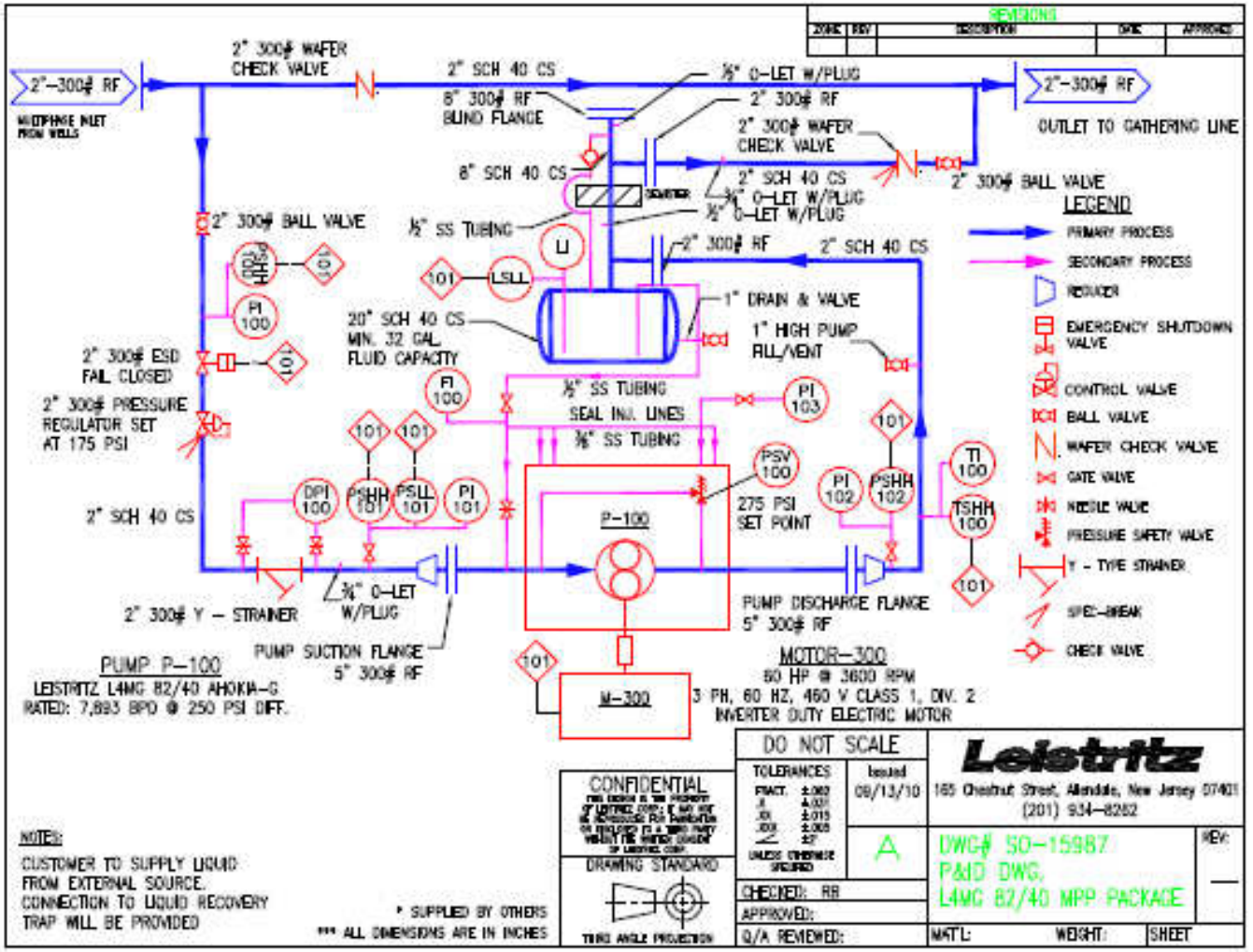

APPENDIX C

TYPICAL UNCERTAINTY ANALYSIS

Mass flow rate of air entering the lab for Q_{air} = 15 ACFM, air pressure = 10 psi, and the air temperature is 75°F

$$W_{\dot{m},air} = \sqrt{\left(W_q\left(\frac{P}{T}\right)\right)^2 + \left(Wp\left(\frac{Q}{T}\right)\right)^2 + \left(W_T\left(\frac{P}{T^2}Q\right)\right)^2}$$

$$W_{air} = 0.001483\ \left[\frac{kg}{s}\right]$$

The calculated total horsepower for Q_{flow} = 220 GPM, P_{in}= 10 psi, and P_{out} = 110 psi

$$W_{HP,Total} = \sqrt{\left(W_Q(P_{out} - P_{in})\right)^2 + \left(-W_{P_{in}}Q_{flow}\right)^2 + \left(W_{P_{out}}Q_{flow}\right)^2}$$

$$W_{HP,Total} = 1.368\ [Hp]$$

The calculated gas horsepower for Q_{gas} = 15 ACVF, P_{in} = 10 psi, and ΔP = 100 psi

$$W_{HP,Air} = \sqrt{\left(W_{P_{in}}\left(Q_{gas} * \frac{ln\left(1+\frac{\Delta P}{P_{in}}\right)}{\frac{\Delta P}{-P_{in}}}\right)\right)^2 + \left(W_{\Delta P}\left(Q_{gas} * \frac{\ln\left(1+\frac{\Delta P}{P_{in}}\right)}{\frac{1}{P_{in}}}\right)\right)^2 + \left(W_{gas}P_{in} * \ln\left(1+\frac{\Delta P}{P_{in}}\right)\right)^2}$$

$$W_{HP,Air} = 1.1054\ [Hp]$$

The uncertainty of HP_{net} is then, 2.473 found by adding the $W_{HP,Air}$ and $W_{HP,Total}$ together.

The mechanical efficiency for HP_{net} at the previous conditions is

$$W_{\eta_{mech}} = \sqrt{\left(W_{HP_{net}}\frac{1}{HP_{VFD}}\right)^2 + \left(W_{HP_{VFD}}\frac{HP_{net}}{-HP_{VFD}{}^2}\right)^2}$$

$$W_{\eta_{mech}} = 0.1355\ \%$$

APPENDIX D

SUPPLEMENTARY PLOTS

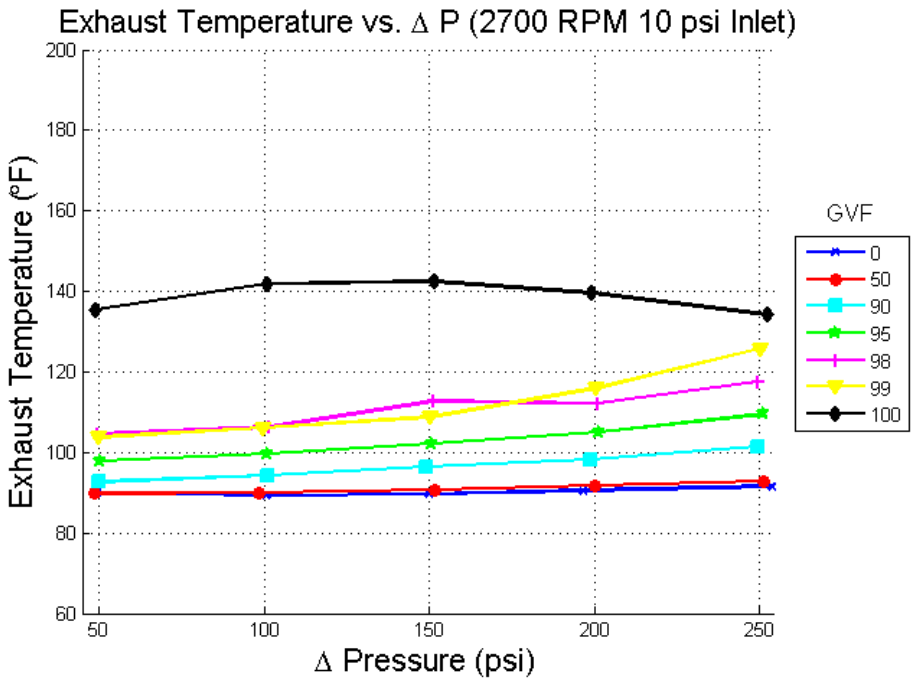

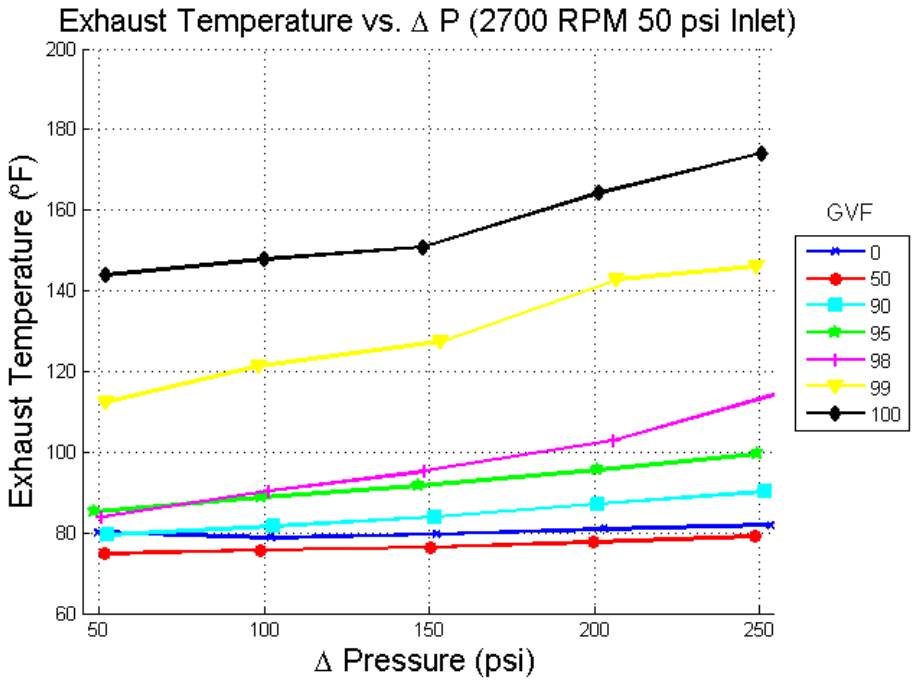

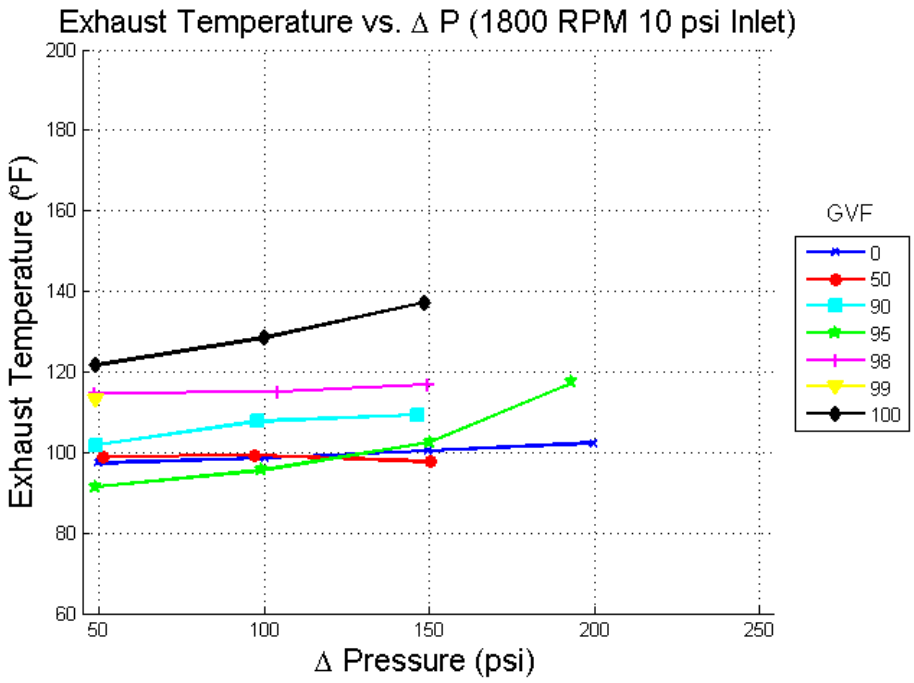
Exhaust Temperature vs. Δ P (1800 RPM 10 psi Inlet)
Exhaust Temperature (°F)
Δ Pressure (psi)
GVF
0
50
90
95
98
99
100

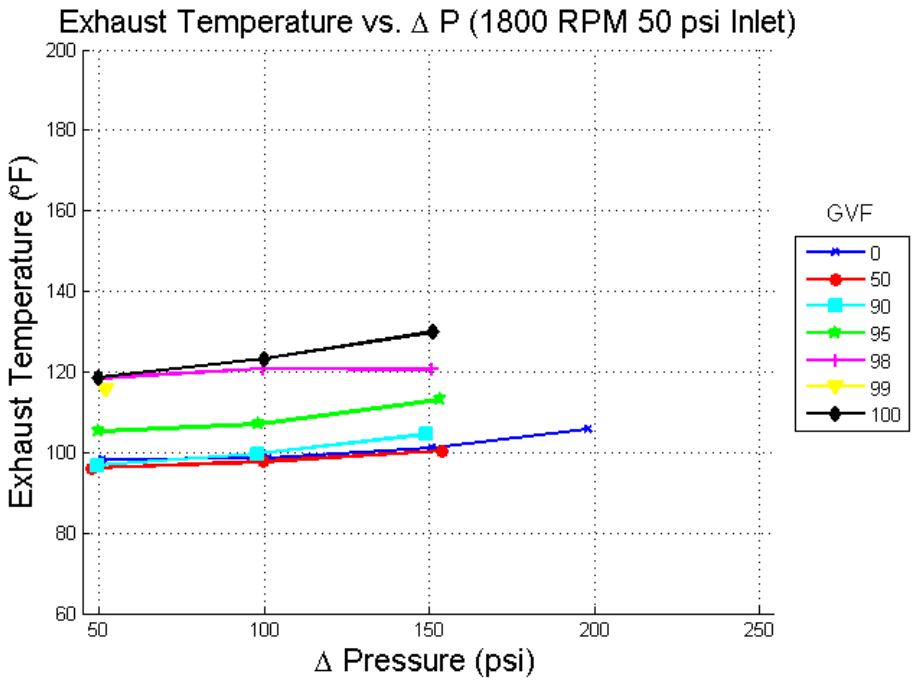
Exhaust Temperature vs. Δ P (1800 RPM 50 psi Inlet)
Exhaust Temperature (°F)
Δ Pressure (psi)
GVF
0
50
90
95
98
99
100

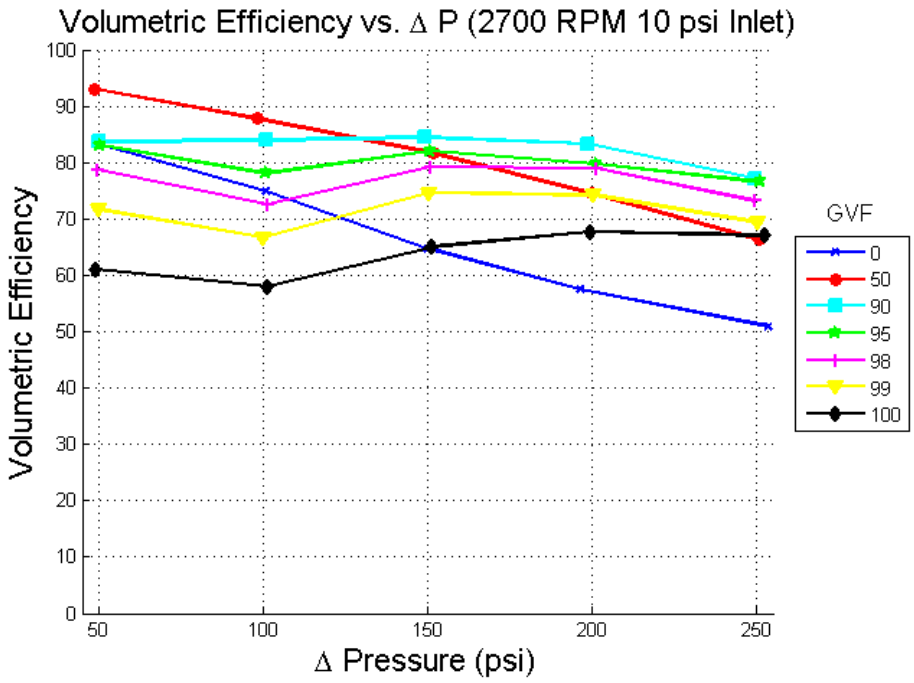
Volumetric Efficiency vs. Δ P (2700 RPM 10 psi Inlet)
Volumetric Efficiency
Δ Pressure (psi)
GVF
0
50
90
95
98
99
100

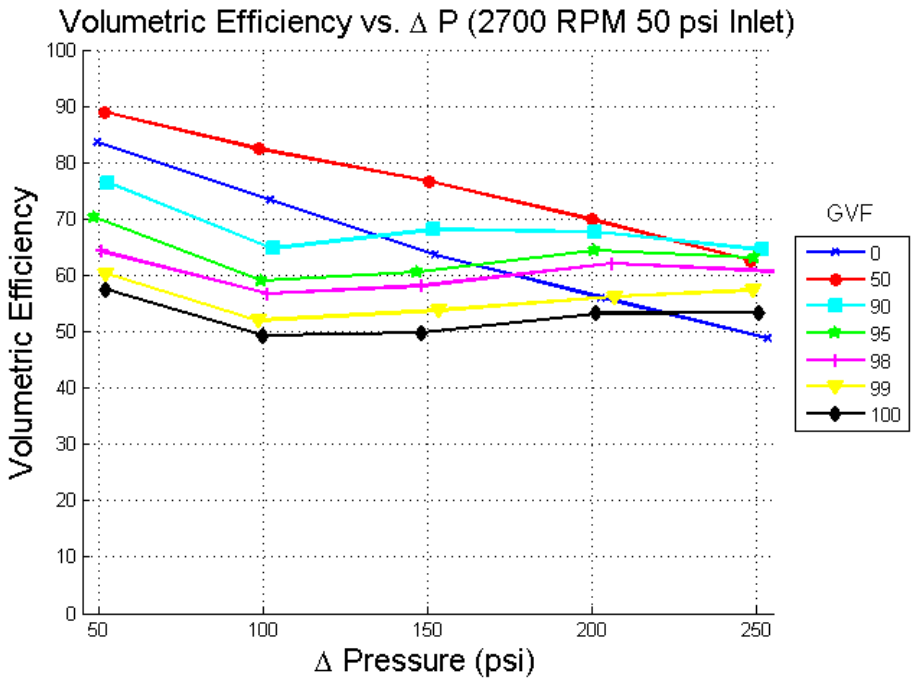
Volumetric Efficiency vs. Δ P (2700 RPM 50 psi Inlet)
Volumetric Efficiency
Δ Pressure (psi)
GVF
0
50
90
95
98
99
100

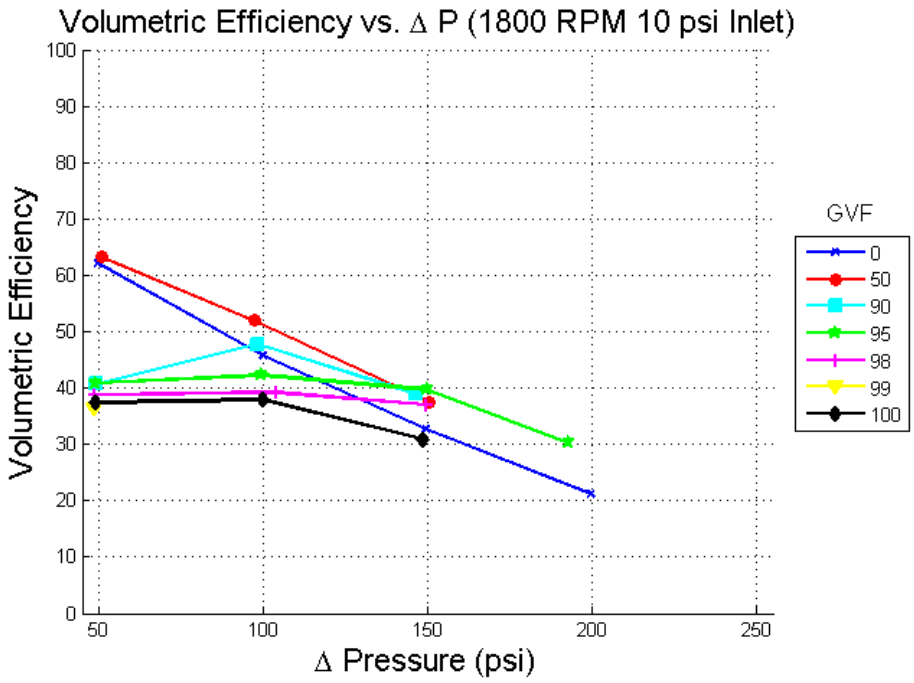
Volumetric Efficiency vs. Δ P (1800 RPM 10 psi Inlet)
Volumetric Efficiency
Δ Pressure (psi)
GVF
0
50
90
95
98
99
100

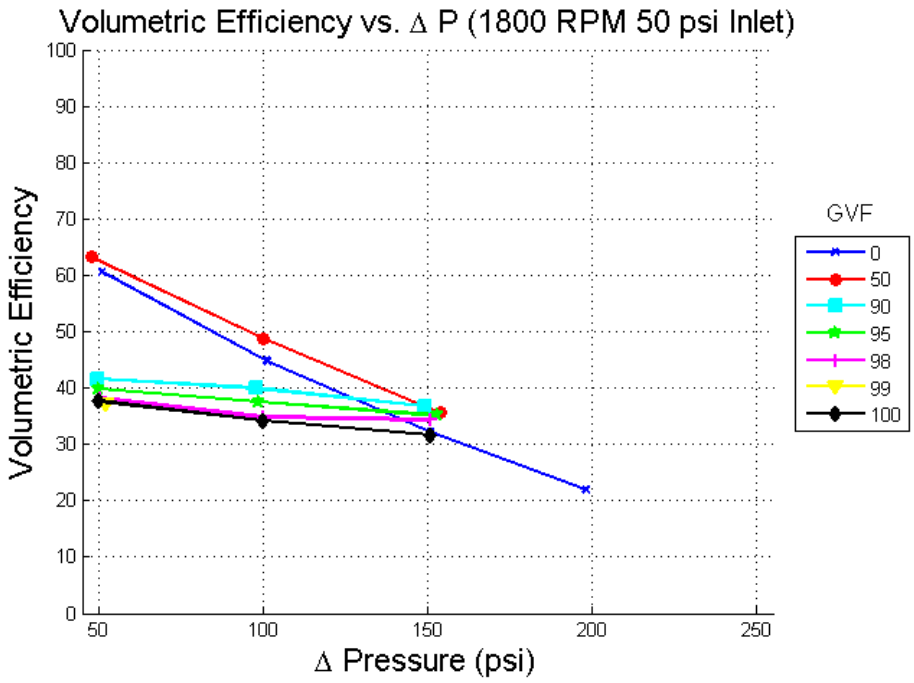
Volumetric Efficiency vs. Δ P (1800 RPM 50 psi Inlet)
Volumetric Efficiency
Δ Pressure (psi)
GVF
0
50
90
95
98
99
100

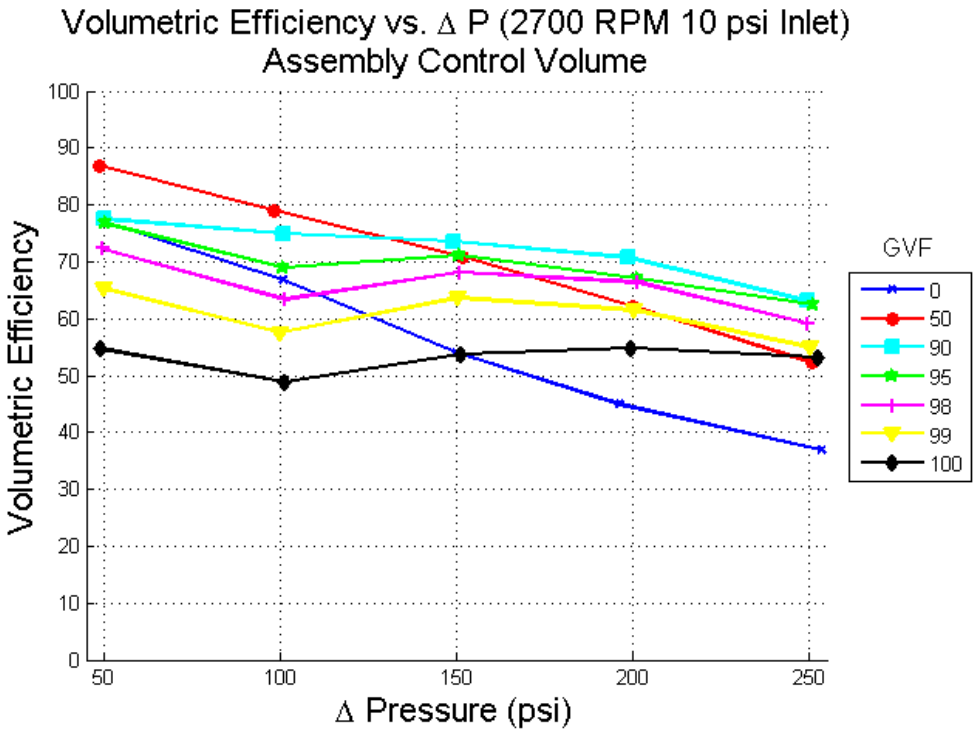
Volumetric Efficiency vs. Δ P (2700 RPM 10 psi Inlet)
Assembly Control Volume
Volumetric Efficiency
Δ Pressure (psi)
GVF
0
50
90
95
98
99
100

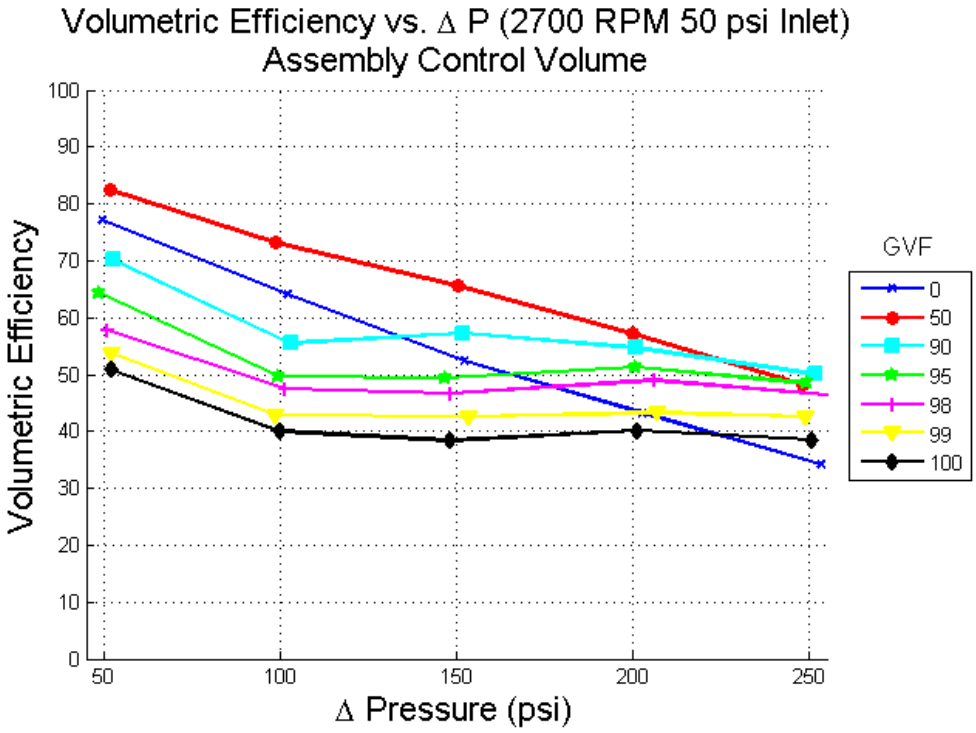
Volumetric Efficiency vs. Δ P (2700 RPM 50 psi Inlet)
Assembly Control Volume
Volumetric Efficiency
Δ Pressure (psi)
GVF
0
50
90
95
98
99
100

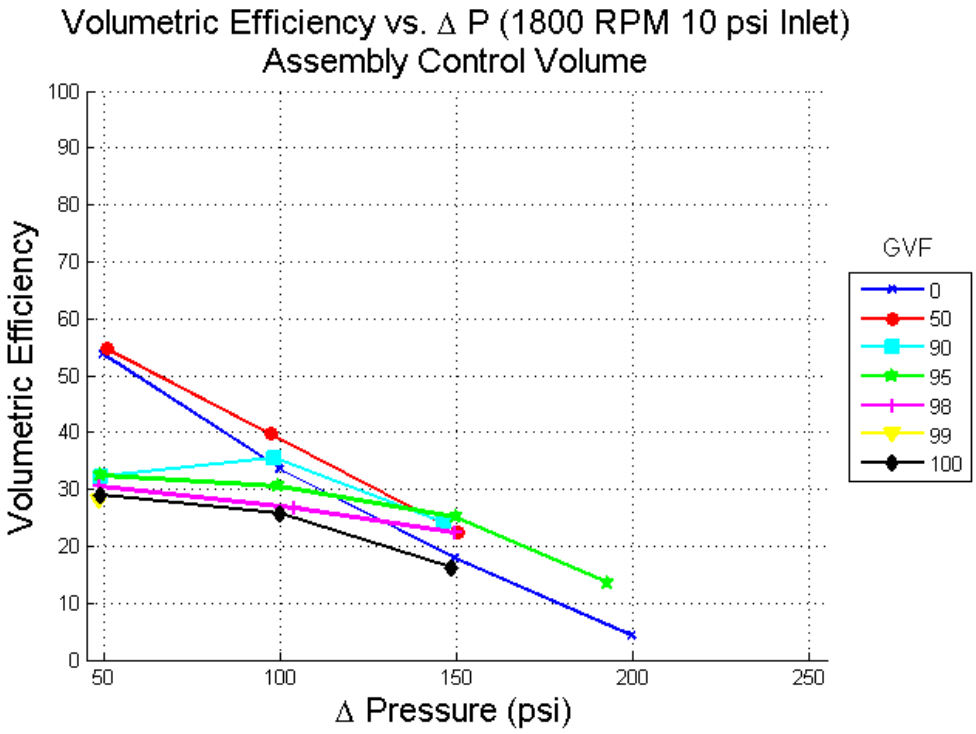
Volumetric Efficiency vs. Δ P (1800 RPM 10 psi Inlet)
Assembly Control Volume
Volumetric Efficiency
Δ Pressure (psi)
GVF
0
50
90
95
98
99
100

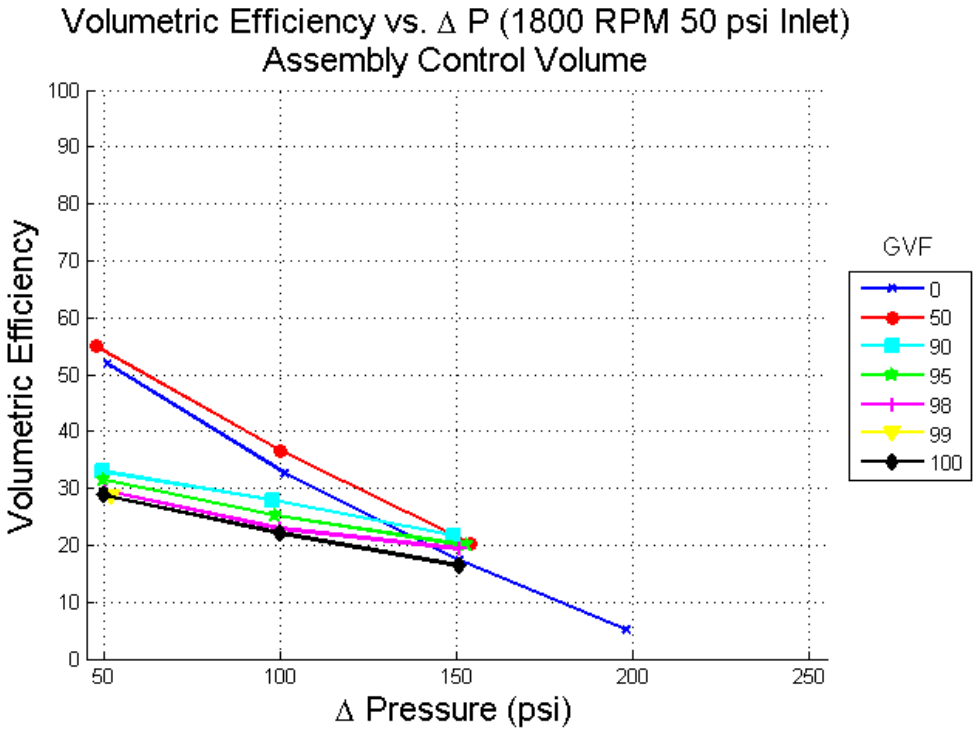
Volumetric Efficiency vs. Δ P (1800 RPM 50 psi Inlet)
Assembly Control Volume
Volumetric Efficiency
Δ Pressure (psi)
GVF
0
50
90
95
98
99
100

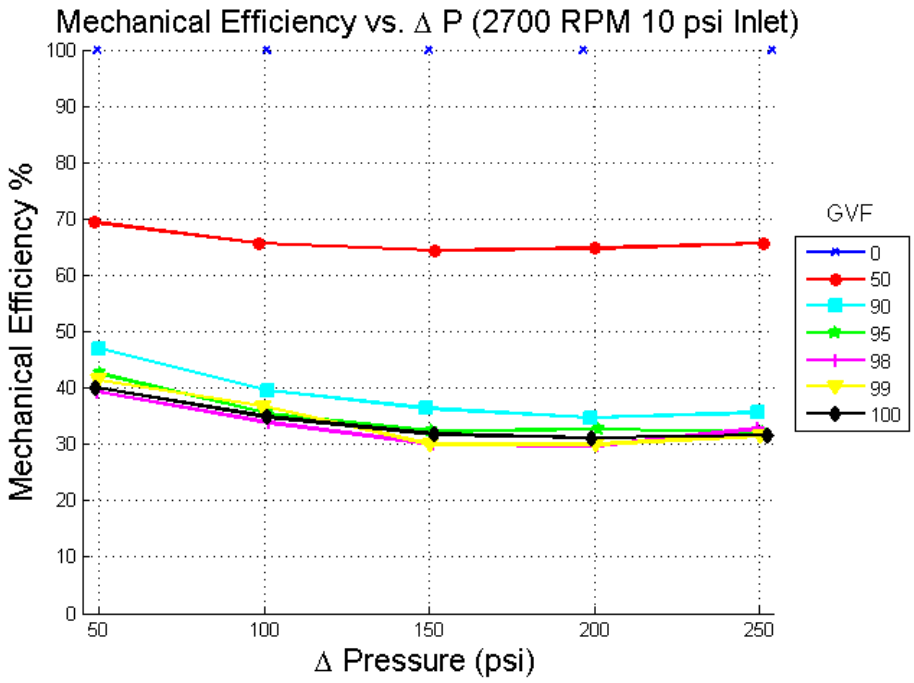
Mechanical Efficiency vs. Δ P (2700 RPM 10 psi Inlet)
Mechanical Efficiency %
Δ Pressure (psi)
GVF
0
50
90
95
98
99
100

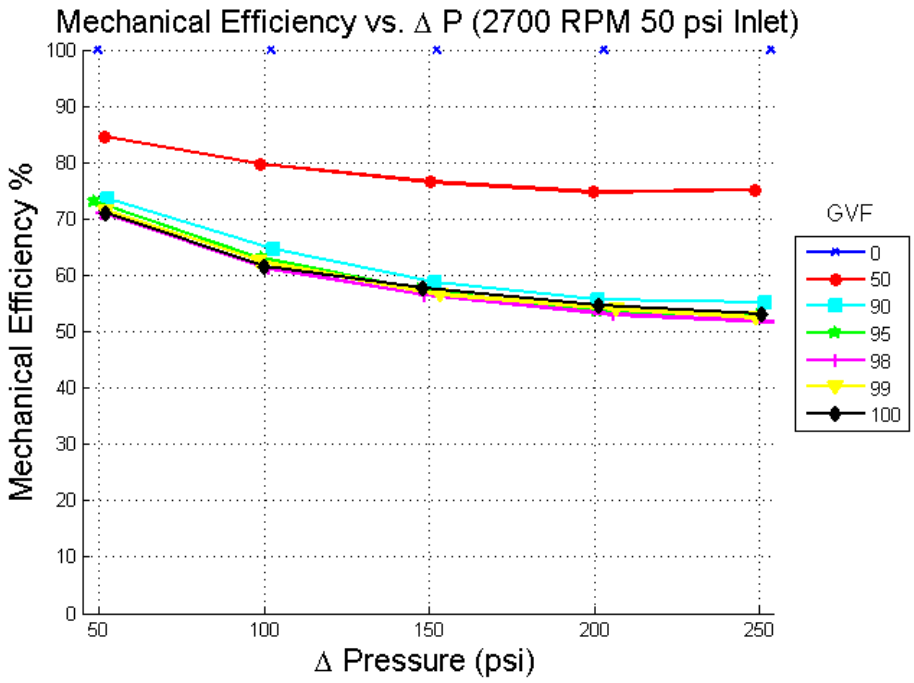
Mechanical Efficiency vs. Δ P (2700 RPM 50 psi Inlet)
Mechanical Efficiency %
Δ Pressure (psi)
GVF
0
50
90
95
98
99
100

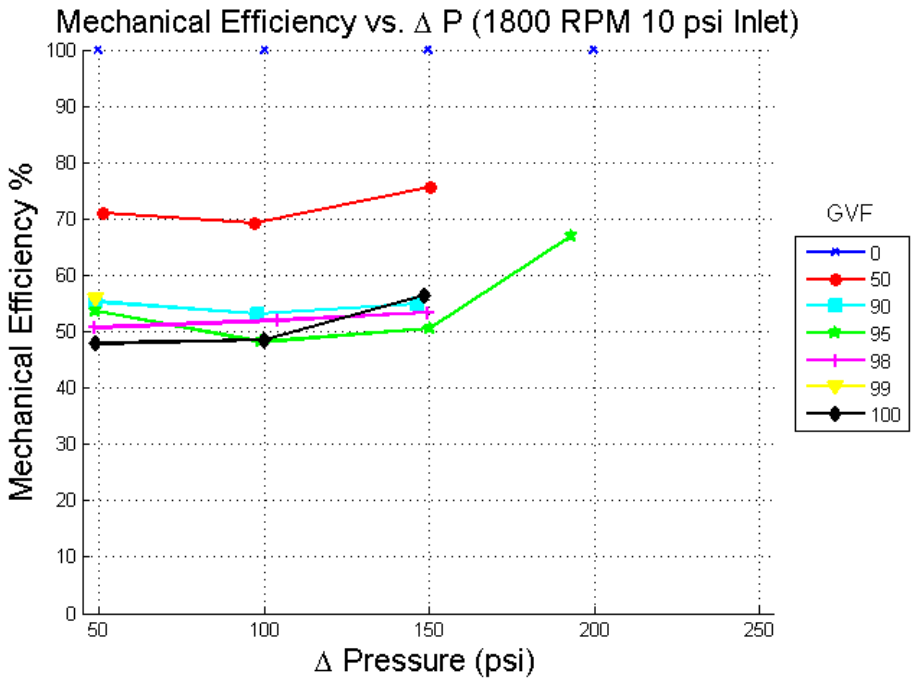
Mechanical Efficiency vs. Δ P (1800 RPM 10 psi Inlet)
Mechanical Efficiency %
Δ Pressure (psi)
GVF
0
50
90
95
98
99
100

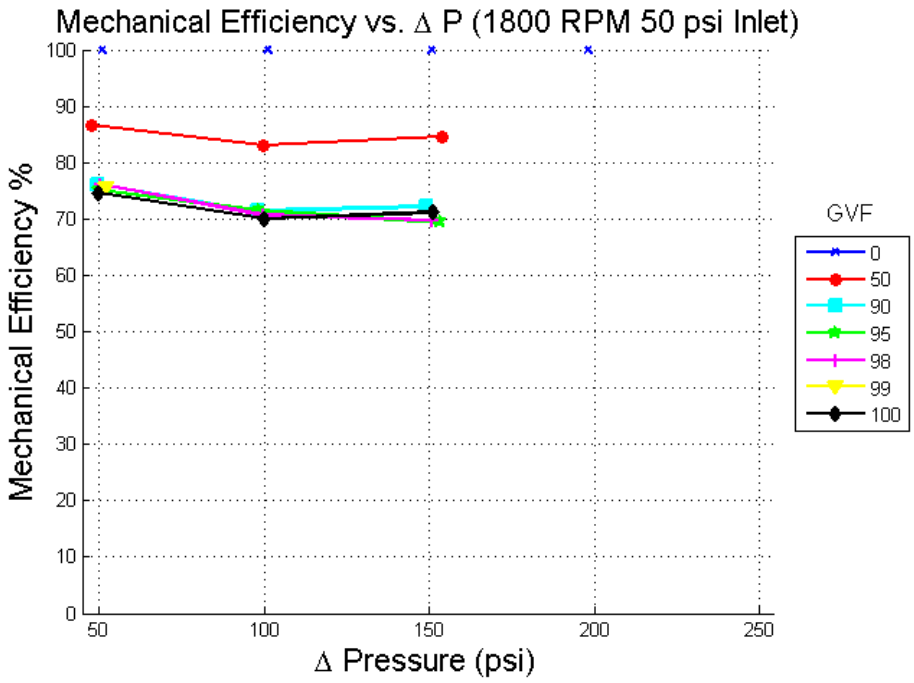
Mechanical Efficiency vs. Δ P (1800 RPM 50 psi Inlet)
Mechanical Efficiency %
Δ Pressure (psi)
GVF
0
50
90
95
98
99
100

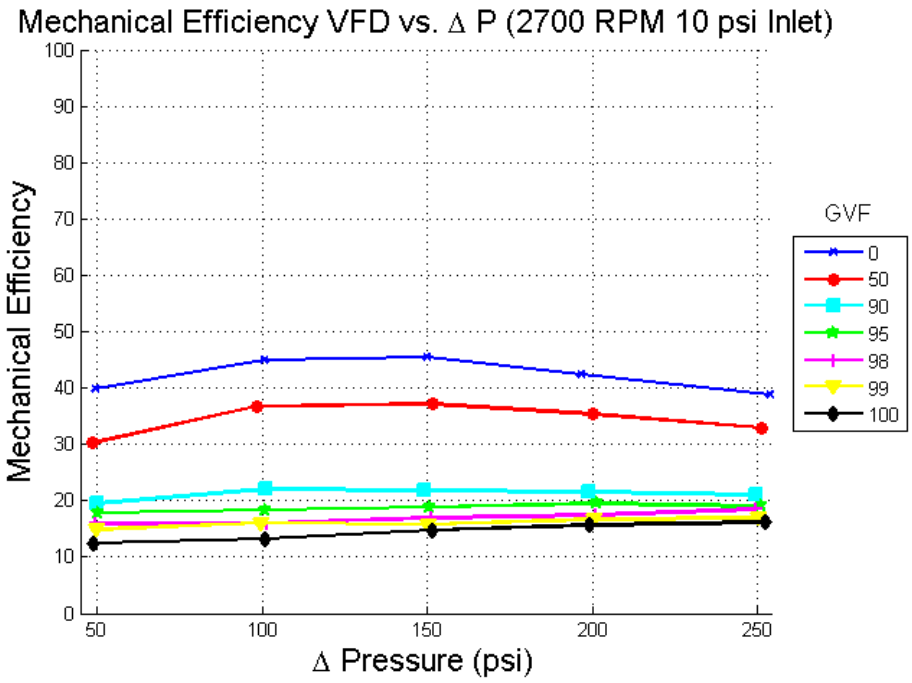
Mechanical Efficiency VFD vs. Δ P (2700 RPM 10 psi Inlet)
Mechanical Efficiency
Δ Pressure (psi)
GVF
0
50
90
95
98
99
100

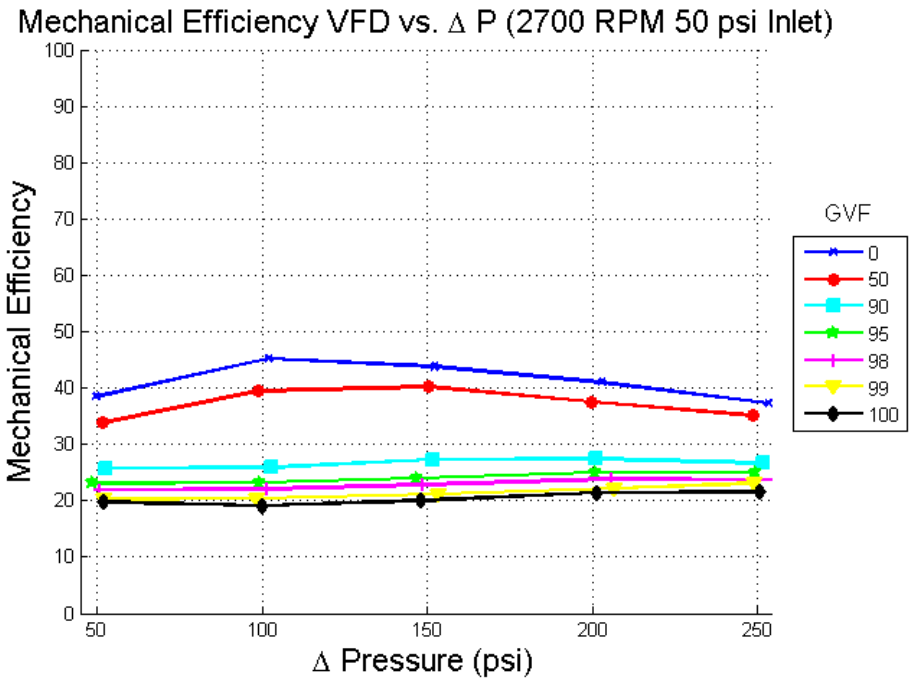
Mechanical Efficiency VFD vs. Δ P (2700 RPM 50 psi Inlet)
Mechanical Efficiency
Δ Pressure (psi)
GVF
0
50
90
95
98
99
100

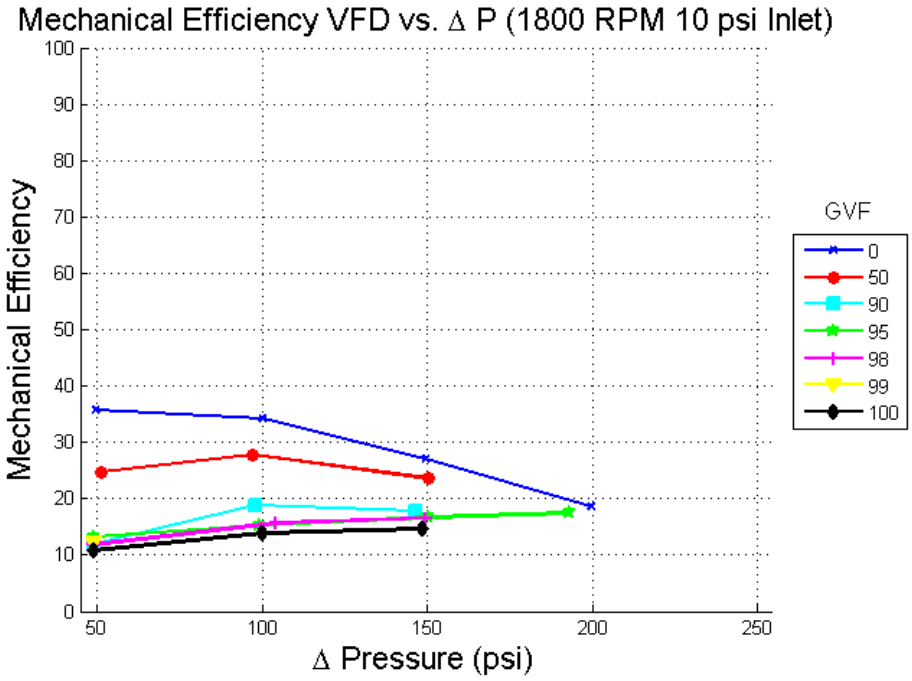
Mechanical Efficiency VFD vs. Δ P (1800 RPM 10 psi Inlet)
Mechanical Efficiency
Δ Pressure (psi)
GVF
0
50
90
95
98
99
100

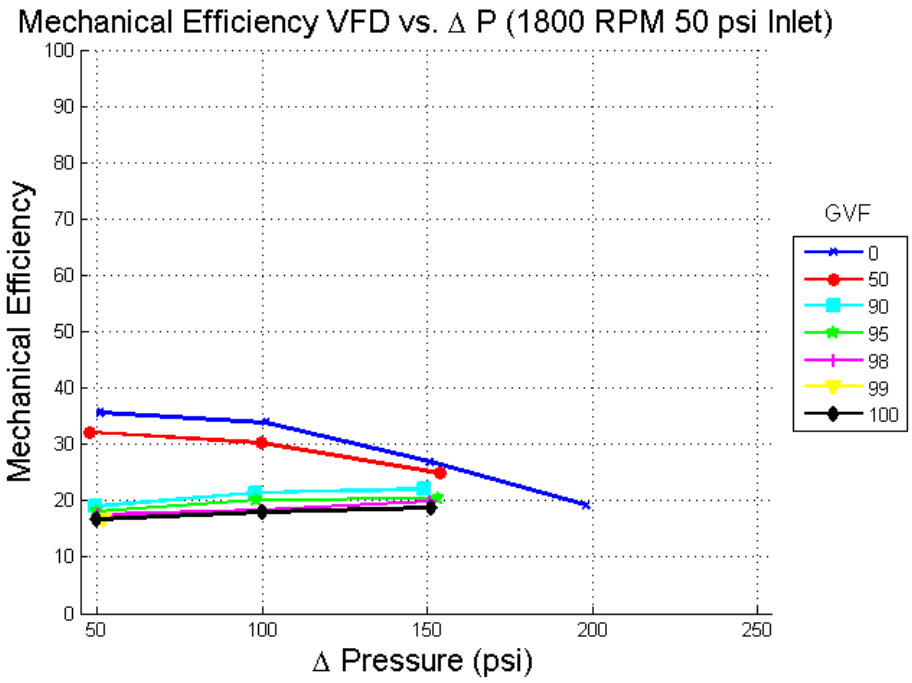
Mechanical Efficiency VFD vs. Δ P (1800 RPM 50 psi Inlet)
Mechanical Efficiency
Δ Pressure (psi)
GVF
0
50
90
95
98
99
100

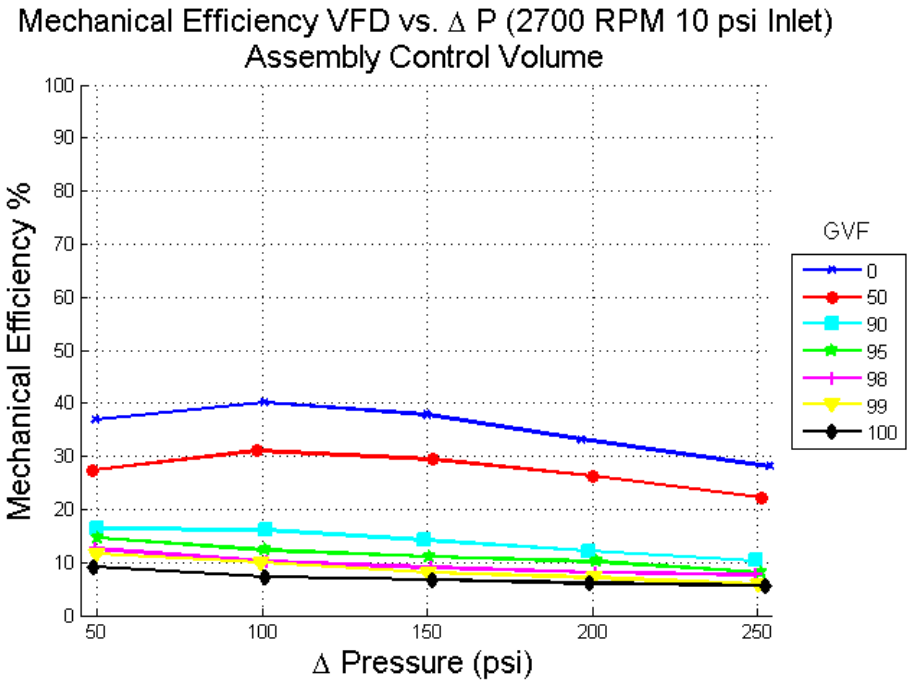
Mechanical Efficiency VFD vs. Δ P (2700 RPM 10 psi Inlet)
Assembly Control Volume
Mechanical Efficiency %
Δ Pressure (psi)
GVF
0
50
90
95
98
99
100

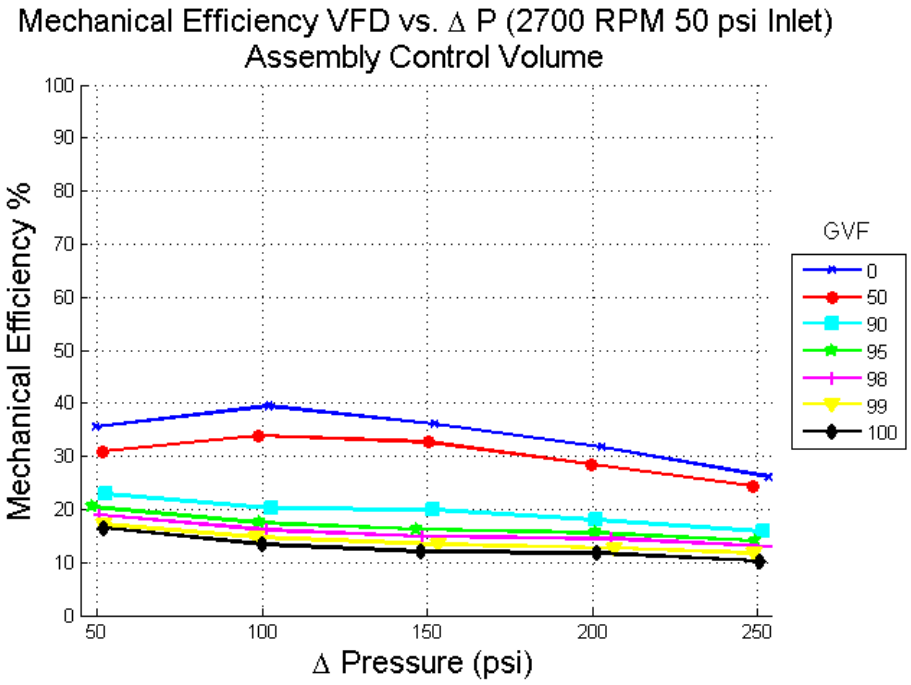
Mechanical Efficiency VFD vs. Δ P (2700 RPM 50 psi Inlet)
Assembly Control Volume
Mechanical Efficiency %
Δ Pressure (psi)
GVF
0
50
90
95
98
99
100

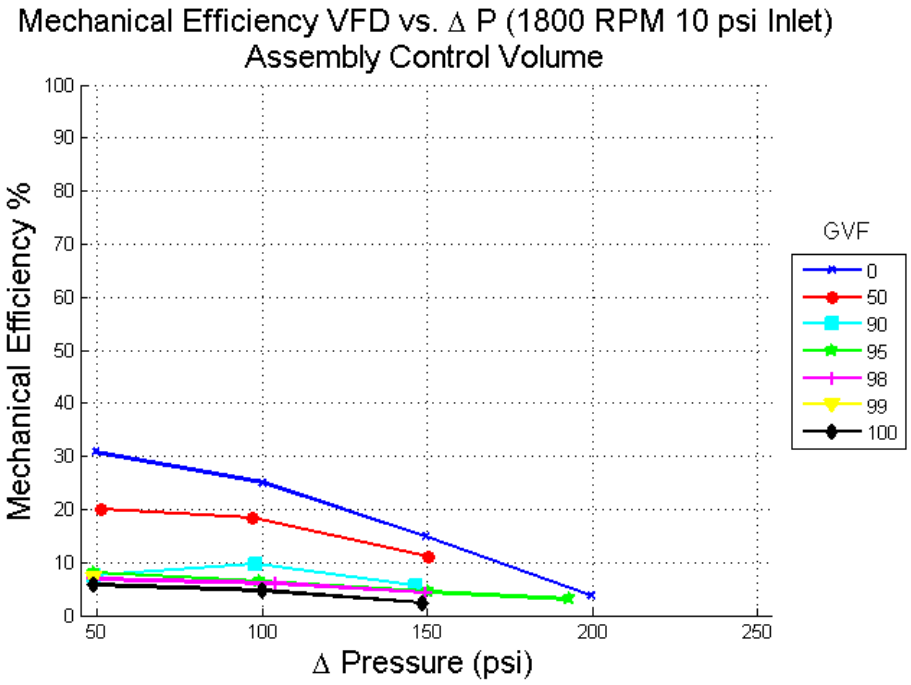
Mechanical Efficiency VFD vs. Δ P (1800 RPM 10 psi Inlet)
Assembly Control Volume
Mechanical Efficiency %
Δ Pressure (psi)
GVF
0
50
90
95
98
99
100

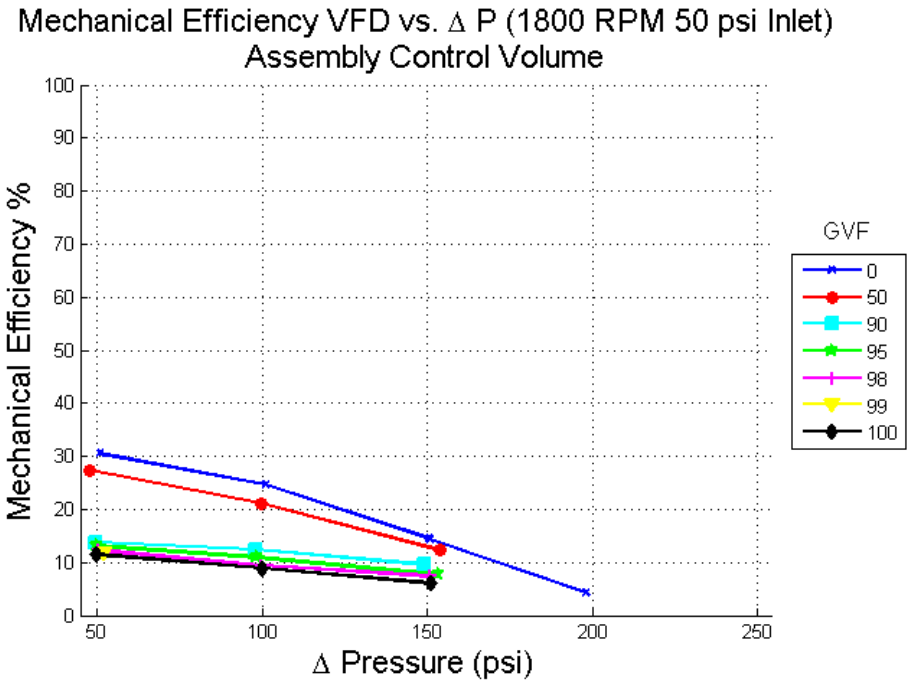
Mechanical Efficiency VFD vs. Δ P (1800 RPM 50 psi Inlet)
Assembly Control Volume
Mechanical Efficiency %
Δ Pressure (psi)
GVF
0
50
90
95
98
99
100

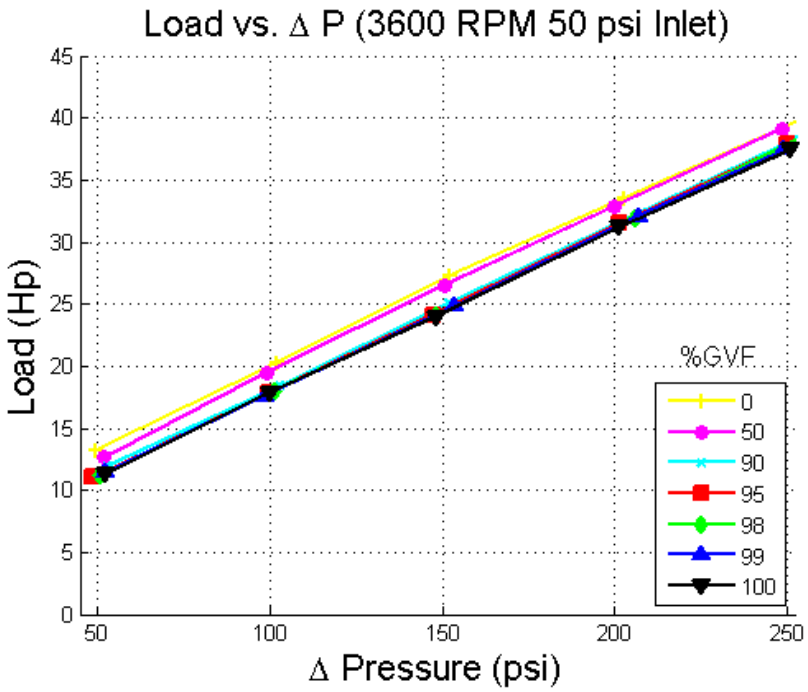
Load vs. Δ P (3600 RPM 50 psi Inlet)
Load (Hp)
Δ Pressure (psi)
%GVF
0
50
90
95
98
99
100
0
5
10
15
20
25
30
35
40
45
50
100
150
200
250

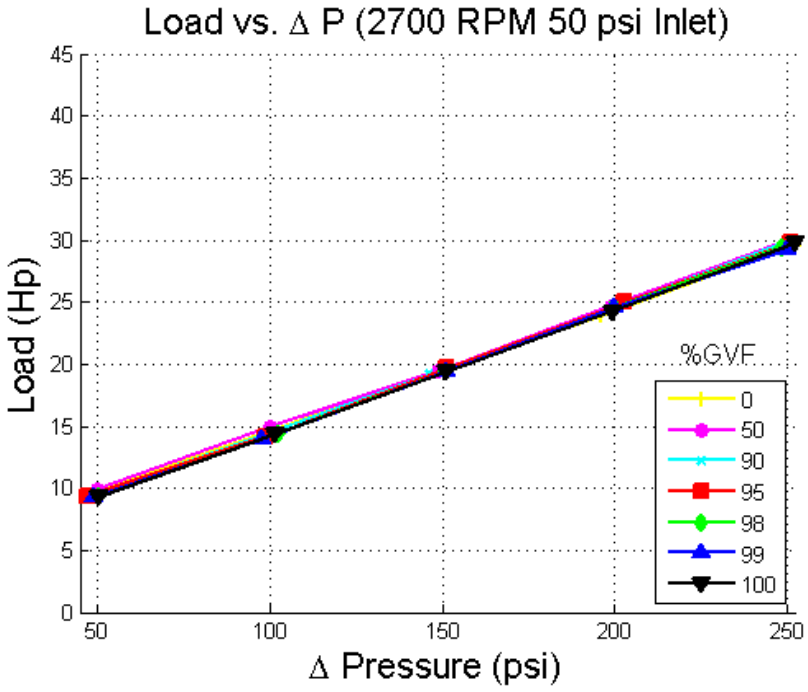
Load vs. Δ P (2700 RPM 50 psi Inlet)
Load (Hp)
Δ Pressure (psi)
%GVF
0
50
90
95
98
99
100
0
5
10
15
20
25
30
35
40
45
50
100
150
200
250

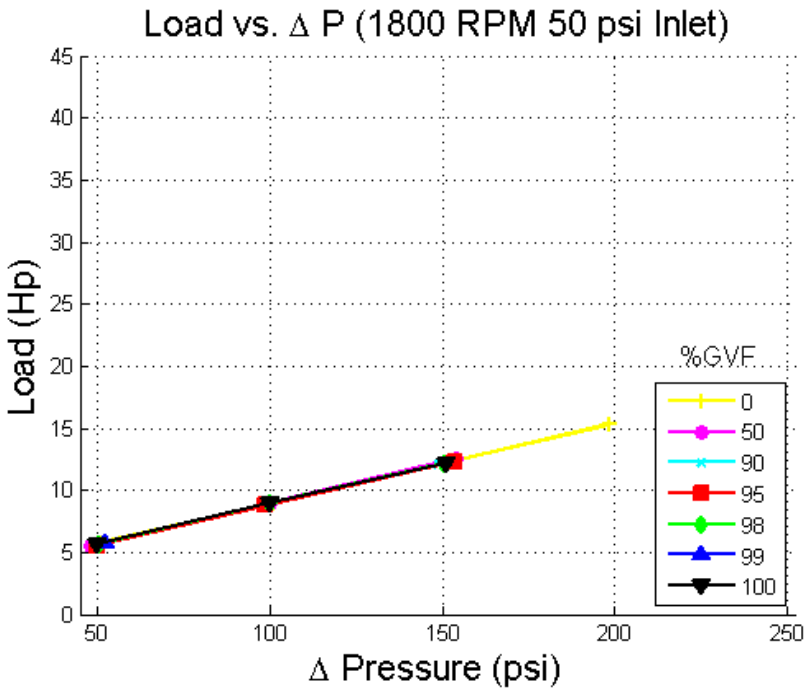
Load vs. Δ P (1800 RPM 50 psi Inlet)
Load (Hp)
Δ Pressure (psi)
%GVF
0
50
90
95
98
99
100

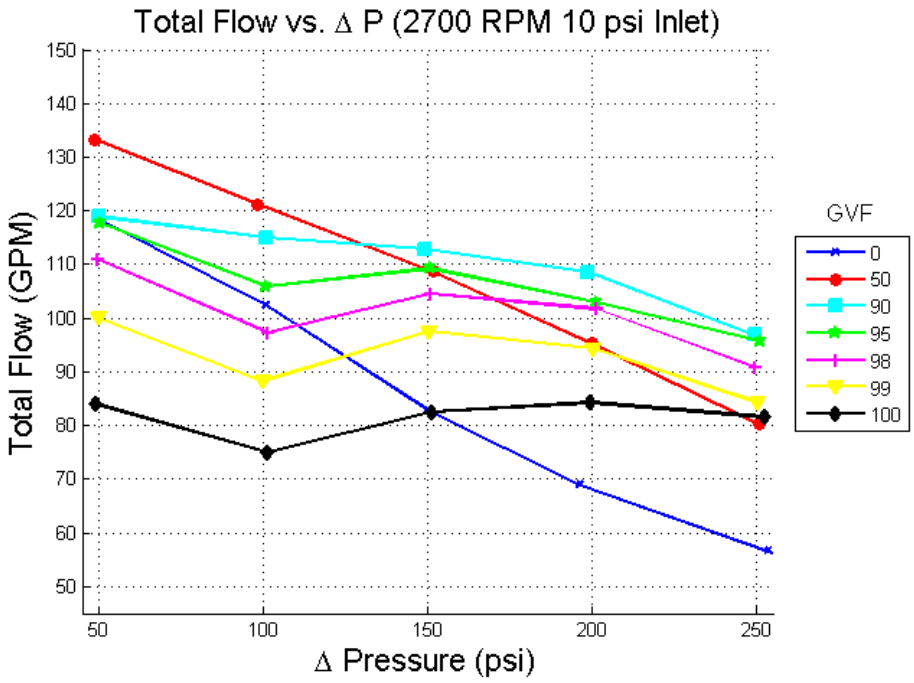
Total Flow vs. Δ P (2700 RPM 10 psi Inlet)
Total Flow (GPM)
Δ Pressure (psi)
GVF
0
50
90
95
98
99
100

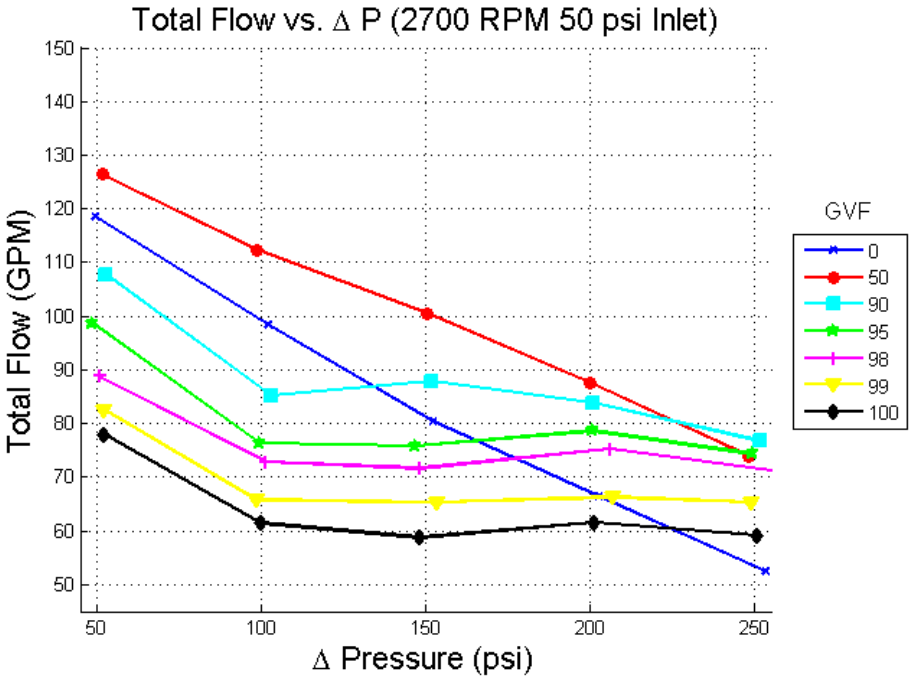
Total Flow vs. Δ P (2700 RPM 50 psi Inlet)
Total Flow (GPM)
Δ Pressure (psi)
GVF
0
50
90
95
98
99
100

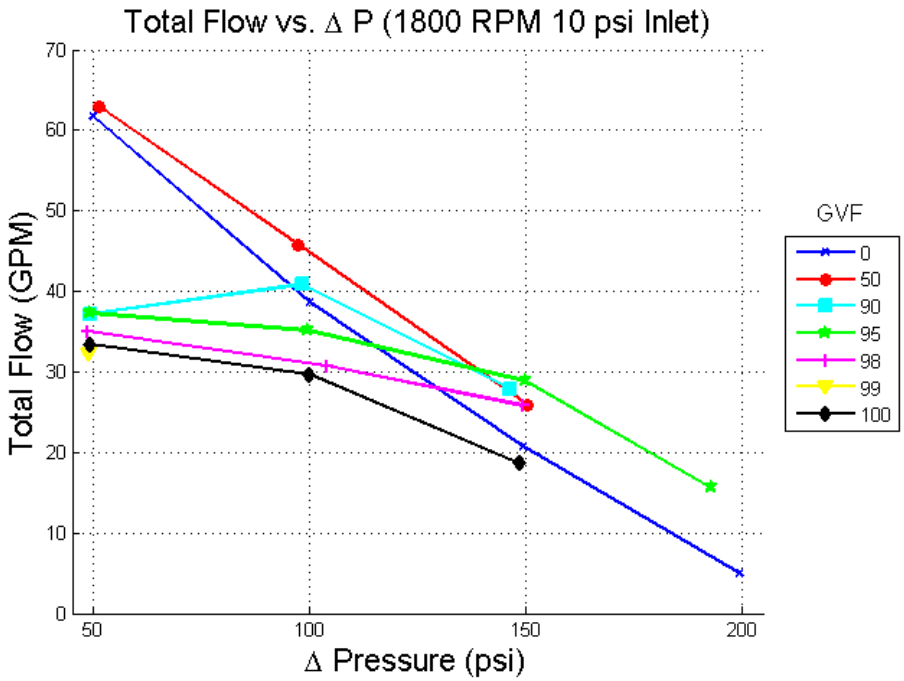
Total Flow vs. Δ P (1800 RPM 10 psi Inlet)
Total Flow (GPM)
Δ Pressure (psi)
GVF
0
50
90
95
98
99
100

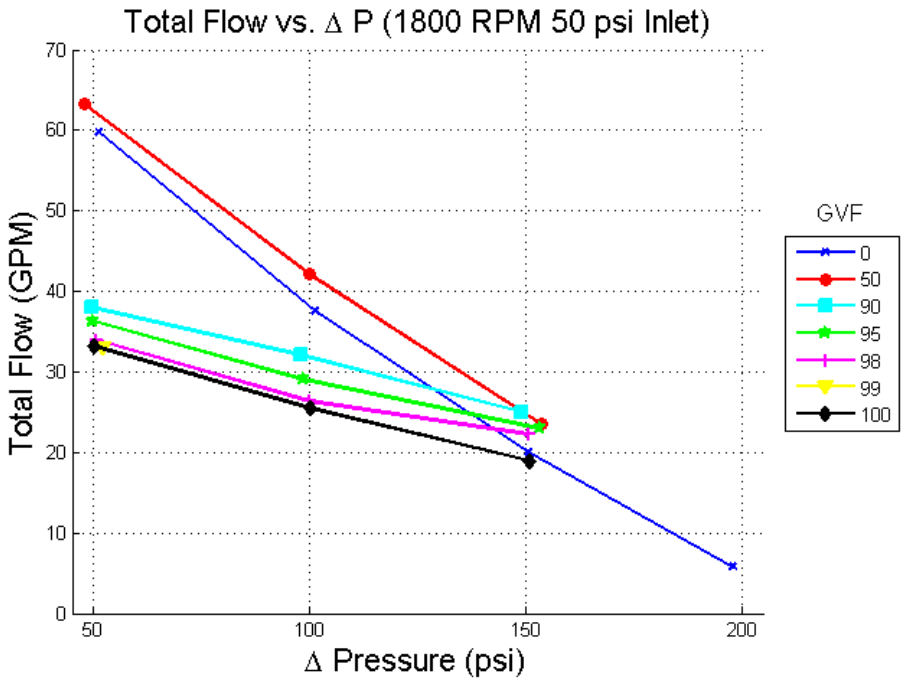
Total Flow vs. Δ P (1800 RPM 50 psi Inlet)
Total Flow (GPM)
Δ Pressure (psi)
GVF
0
50
90
95
98
99
100
0
10
20
30
40
50
60
70
50
100
150
200

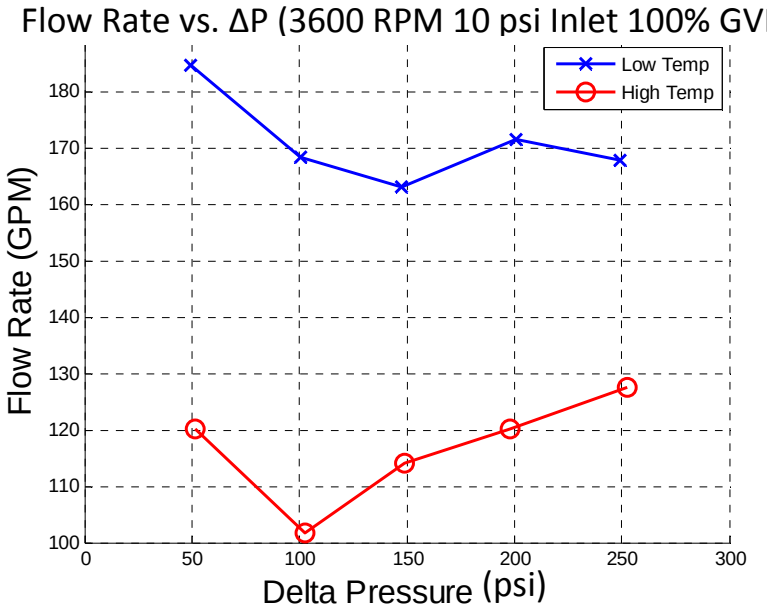
Flow Rate vs. ΔP (3600 RPM 10 psi Inlet 100% GVF)
Low Temp
High Temp
Flow Rate (GPM)
Delta Pressure (psi)
100
110
120
130
140
150
160
170
180
0
50
100
150
200
250
300

Effective Flow Rate vs. ΔP (3600 RPM 10 psi Inlet 100% GVF)

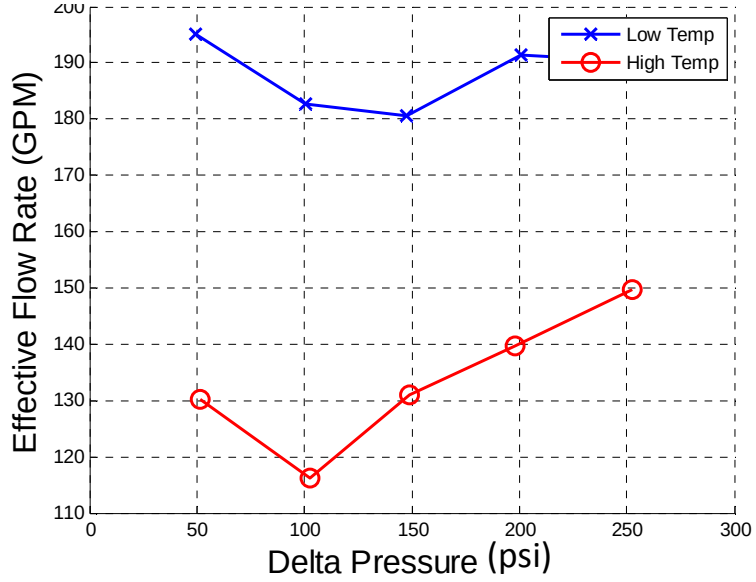

Effective Volumetric Efficiency vs. ΔP (3600 RPM 10 psi Inlet 100% GVF)

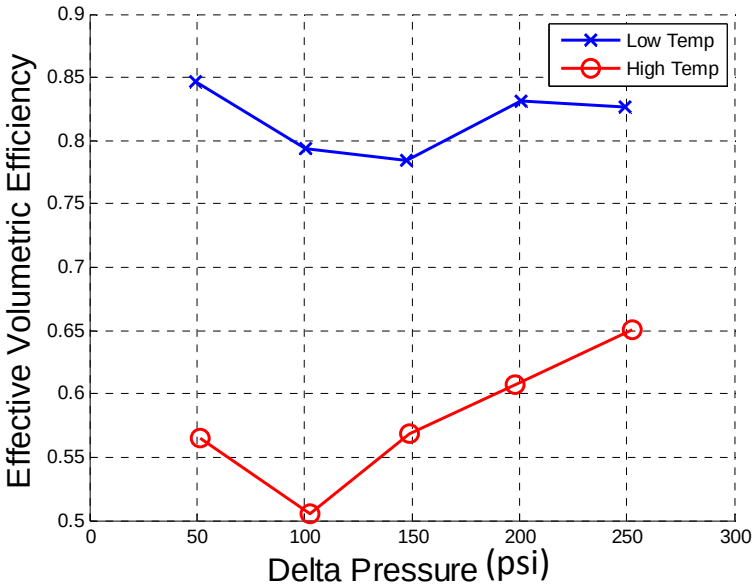

Mechanical Efficiency vs. ΔP (3600 RPM 10 psi Inlet 100% GVF)

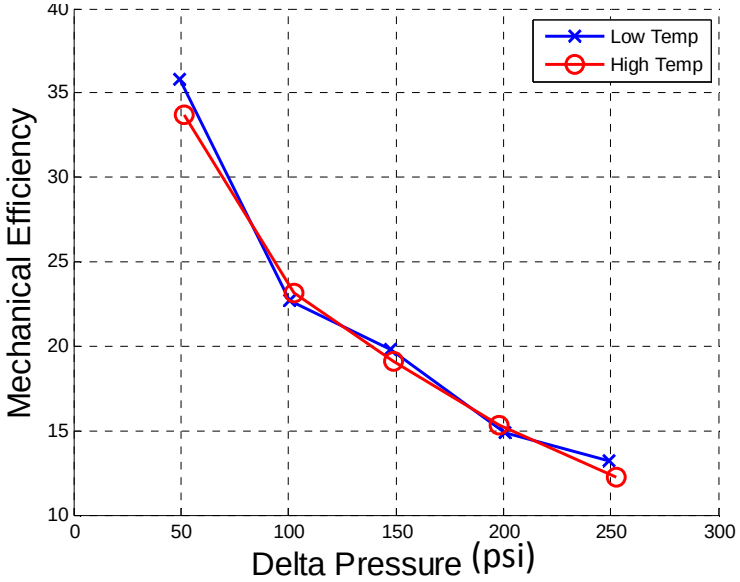

Effective Mechanical Efficiency vs. ΔP (3600 RPM 10 psi Inlet 100% GVF)

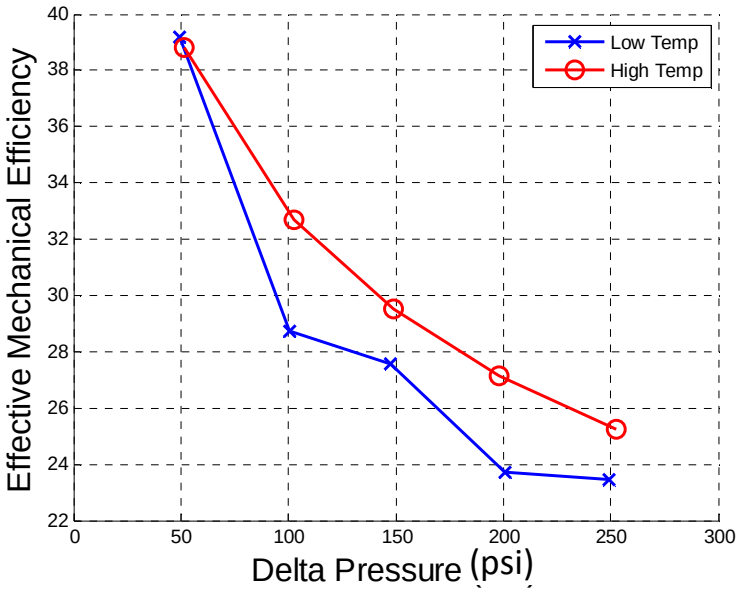

Effective Gas Volume Fraction vs. ΔP (3600 RPM 10 psi Inlet 100% GVF)

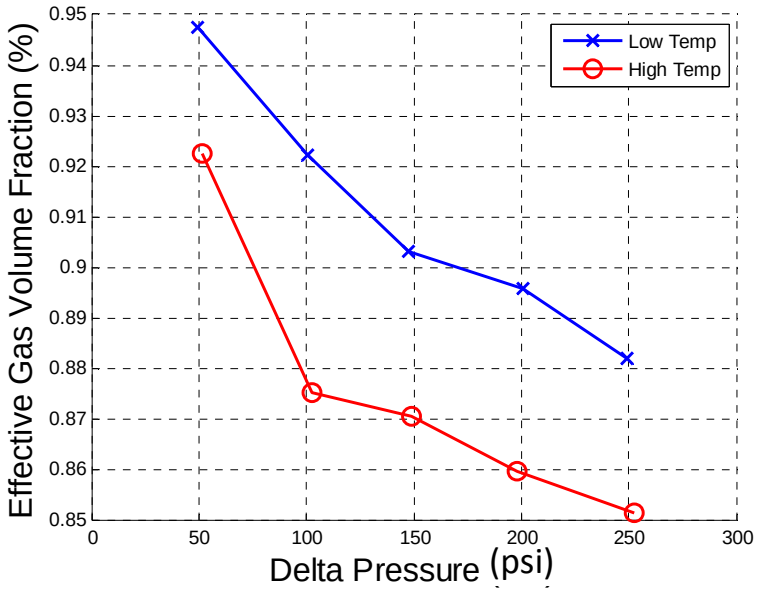

Seal Flow Rate vs. ΔP (3600 RPM 10 psi Inlet 100% GVF)

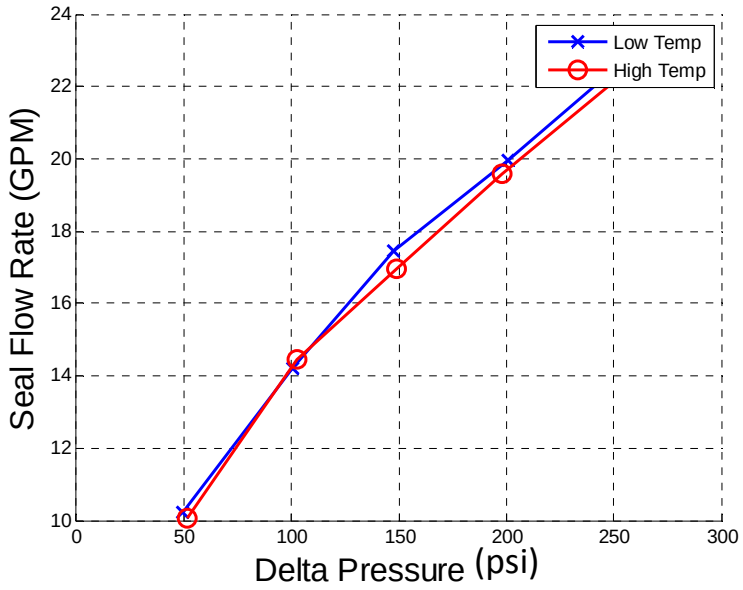

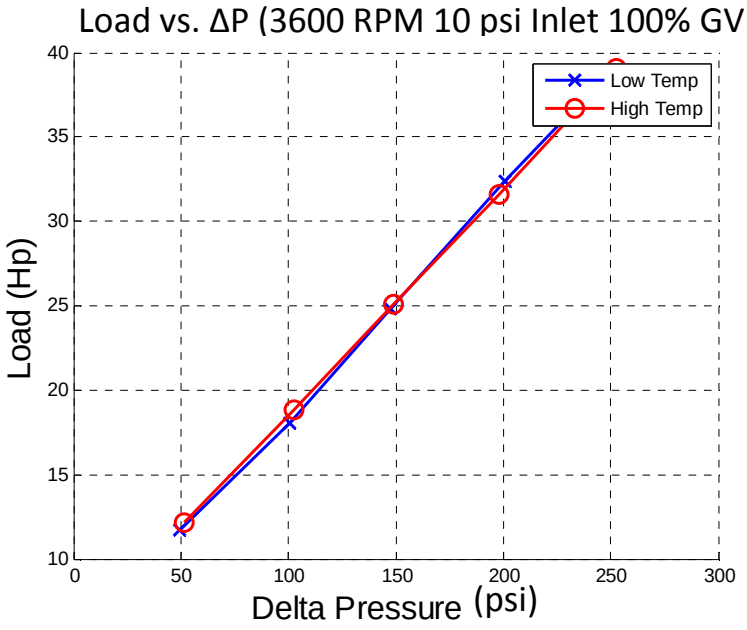
Load vs. ΔP (3600 RPM 10 psi Inlet 100% GVF)
Low Temp
High Temp
Load (Hp)
Delta Pressure (psi)
40
35
30
25
20
15
10
0
50
100
150
200
250
300

VITA

Ryan Daniel Kroupa
Texas A&M University
Department of Mechanical Engineering
3123 TAMU
College Station, TX 77843-3123

Education

Texas A&M University, College Station, Texas
Master of Science, Mechanical Engineering, May 2011

University of Wisconsin – Milwaukee, Milwaukee, Wisconsin
Bachelor of Science, Mechanical Engineering, December 2008